Internal connectivity and topological roles of nodes in functional brain networks

Elisa Ryyppö

School of Science

Thesis submitted for examination for the degree of Master of Science in Technology.

Espoo 14.07.2018

Thesis supervisor:

Prof. Jari Saramäki

Thesis advisor:

D.Sc. (Tech.) Onerva Korhonen

Aalto University
School of Science

AALTO UNIVERSITY
SCHOOL OF SCIENCE

ABSTRACT OF THE
MASTER'S THESIS

Author: Elisa Ryyppö

Title: Internal connectivity and topological roles of nodes in functional brain networks

Date: 14.07.2018 Language: English Number of pages: 7+77

Department of Computer Science

Professorship: SCI0132 Computational Science

Supervisor: Prof. Jari Saramäki

Advisor: D.Sc. (Tech.) Onerva Korhonen

Many real-life phenomena consist of a number of interacting elements and can thus be modeled as a complex network. The human brain is an example of such a system where the neuronal information processing of the brain is characterized by interaction and information exchange between different brain regions.
In this Thesis, we examine functional brain networks estimated from functional magnetic resonance imaging (fMRI) data. When defining network nodes, the small measurement units, voxels, are grouped to larger entities that represent supposedly functionally homogeneous brain regions referred to as Regions of Interest (ROIs). Despite their assumed homogeneity, it has been demonstrated that the voxels within a ROI exhibit spatially and temporally varying correlation structure. This gives rise to a concept referred to as internal connectivity.
On the larger scale, the ROIs form a brain network where each ROI has its role in the structure of the network topology, *i.e.*, a topological role. Topological roles have been suggested to be indicative of the node's functional specialization. On the other hand, it has been argued that internal connectivity may relate to the mechanisms the ROI uses to interact with its neighbors in the functional brain network. This Thesis combines these two ideas. To this end, we aim to predict the ROI's topological role from its internal connectivity features. We find that using internal connectivity features as model variables increases the classification accuracy in comparison to a baseline classifier.
These results suggest that there is a relationship between internal connectivity and the ROI's topological role. This link provides a basis for faster and more computationally efficient topological role estimation. Further, it helps to better understand the mechanisms brain regions use to interact with each other. Both of these factors importantly increase our knowledge on brain function under different tasks and circumstances.

Keywords: Functional brain networks, node definitions, connectivity, topological roles, fMRI

AALTO-YLIOPISTO
PERUSTIETEIDEN KORKEAKOULU

DIPLOMITYÖN
TIIVISTELMÄ

Tekijä: Elisa Ryyppö

Työn nimi: Solmujen sisäinen konnektiviteetti ja topologiset roolit toiminnallisissa aivoverkoissa

Päivämäärä: 14.07.2018 Kieli: Englanti Sivumäärä: 7+77

Department of Computer Science

Professuuri: SCI0132 Laskennallinen tiede

Työn valvoja: Prof. Jari Saramäki

Työn ohjaaja: TkT Onerva Korhonen

Monet todellisen maailman ilmiöt koostuvat useista vuorovaikutuksessa olevista elementeistä, ja niitä voidaan mallintaa kompleksisina verkostoina. Ihmisaivot ovat esimerkki tällaisesta järjestelmästä, jossa aivojen hermosolutason tiedonkäsittely perustuu aivoalueiden väliseen vuorovaikutukseen ja tiedonvaihtoon.
Diplomityössäni tutkin toiminnallisesta magneettikuvausdatasta rakennettuja toiminnallisia aivoverkkoja. Verkon solmuja määritettäessä pienet mittauselementit, vokselit, ryhmitellään isommiksi kokonaisuuksiksi, jotka edustavat toiminnallisesti yhtenäisiksi oletettuja aivoalueita (engl. Region of Interest, ROI). On kuitenkin osoitettu, että oletetusta yhtenäisyydestään huolimatta ROIden sisällä on monimuotoisia sekä paikallisesti että ajallisesti vaihtelevia korrelaatiorakenteita. Tästä syntyy sisäisen konnektiviteetin käsite, joka kuvaa ROI:n sisäistä korrelaatiorakennetta ja sen vaihtelua.
Laajemmassa mittakaavassa ROI:t muodostavat aivoverkon, jossa jokaisella ROI:lla on verkon rakenteessa oma roolinsa, n.s. topologinen rooli. Topologisten roolien ajatellaan liittyvän ROI:den toiminnalliseen erikoistumiseen. On myös esitetty, että sisäinen konnektiviteetti liittyy niihin mekanismeihin, joiden avulla ROI vuorovaikuttaa naapureidensa kanssa toiminnallisessa aivoverkossa. Tämä diplomityö yhdistää nämä kaksi ajatusta: ROI:n topologista roolia pyritään ennustamaan sen sisäisen konnektiviteetin tekijöiden avulla. Tulokset osoittavat, että sisäisen konnektiviteetin tekijät parantavat ennustustarkkuutta verrattuna valistuneeseen arvaukseen perustuvaan pohjatasoluokittimeen.
Tulokset osoittavat, että ROI:n sisäisen konnetiviteetin ja topologisten roolien välillä on yhteys. Tämä yhteys tarjoaa pohjan topologisten roolien nopeammalle ja laskennallisesti tehokkaammalle määrittämiselle ja lisää ymmärrystä niistä mekanismeista, joita ROI:t käyttävät vuorovaikuttaakseen toistensa kanssa. Nämä tekijät lisäävät tietoa aivojen toiminnasta eri tilanteissa ja tehtävissä.

Avainsanat: toiminnalliset aivoverkot, solmumääritelmät, konnektiviteetti, topologiset roolit, toiminnallinen magneettikuvantaminen

Preface

My journey towards this Thesis began almost five years ago when I first came to Aalto to pursue the degree of Master of Science (Technology). During these years I have had the pleasure to become a part of two great research groups: Brain and Mind Laboratory at the Department of Neuroscience and Biomedical Engineering and Complex Systems group at the Department of Computer Science. In both groups I have gotten to work with amazing scientists that have taught me many valuable lessons not only about science but also about life.

I would like to thank my Thesis advisor Onerva Korhonen and my supervisor Professor Jari Saramäki for their support, help and feedback during the data analysis and writing process of this Thesis. Moreover, I'd like to acknowledge the help from Onerva Korhonen, Professor Jari Saramäki, Enrico Glerean and Professor Elvira Brattico in the analysis process carried out as a part of our earlier work that formed a good basis for this Thesis.

In addition, I wish to thank everyone that has been a part of my academic journey since I first entered the world of data, neuroscience and networks. I want to show special appreciation for Enrico Glerean for guidance in my transition from neuroscienctist to becoming a data scientist and for Onerva Korhonen for guiding me towards the world of network science. I want to also thank my first supervisors Mareike Bacha-Trams, Professor Iiro Jääskeläinen, Professor Mikko Sams, and everyone else at Brain and Mind Laboratory for all the great brain related opportunities I got during the years. Moreover, I am grateful to Onerva Korhonen, Professor Jari Saramäki, and the whole Complex Systems group for teaching me everything I know about networks.

Finally, I wish to thank my family and friends for all the support you have given me during the years.

Espoo, 09.06.2018

Elisa Ryyppö

Contents

Abbreviations

ROI	Region of Interest
MRI	Magnetic Resonance Imaging
fMRI	functional Magnetic Resonance Imaging
BOLD	Blood Oxygenation Level Dependent signal
HRF	Hemodynamic Response Function
PCC	Pearson correlation coefficient
LDA	Linear Discriminant Analysis

1 Introduction

Our everyday lives consist of many complex systems formed by many interacting elements. Network science is a discipline that aims to model these systems of interacting components as networks where different entities are represented as nodes and the relationships between them as edges (Newman 2010). Real-world networks exhibit many non-random structures and properties the characterization of which may help in understanding the function of the underlying systems. Networks are typically characterized by network properties. These properties typically provide information on different scales ranging from single nodes till the whole network (Newman 2010). Depending on the connectivity patterns, the nodes have different roles in the network referred to as topological roles (Guimera et al. 2005b, Guimera et al. 2005a). Nodes can, for example, be hubs that are central to the general network connectivity or connector nodes that join different neighborhoods together. In many real-world networks these topological roles of nodes may be indicative of the node's functional specialization (Harriger et al. 2012, Olesen et al. 2007).

Examining and comparing network structures gives us powerful tools to uncover patterns, relationships, and differences which would not be visible by looking at the sole components alone. The development of the field has greatly profited from more accurate data collection methods as well as by computational and methodological advances in the algorithms and tools used to analyze the network data (Bassett et al. 2017). In the past decades, methods of network science have been utilized with great results in many different fields ranging from social science to network security and from epidemic modeling to bioinformatics.

Throughout the history humans have had an ever-lasting interest in understanding the functioning of the mind, reasoning, and emotion. Early on, it was established that the brain was the home of such cognitive functions (Bear et al. 2007). This lead to a quest for understanding its functioning mechanisms and to emergence of a field today known as neuroscience. Past decades have seen a fast development in neuroimaging methods which have provided tools to increase our knowledge on the structure and function of the brain. Traditionally neuroscience examined the brain through finding brain regions responsible for different tasks often referred to as localization of brain activation (Friston 2011, Wig et al. 2011). However, it later became evident that localizing a function to a single region was rather difficult (Friston 2011) and that the functioning mechanisms of the brain were interactive rather than regionally independent by nature.

Network neuroscience is a branch of neuroscience that aims to understand the functional role of the interactions and models the human brain as a set of interconnected and interacting components, *i.e.* a complex network (Bassett et al. 2017, Muldoon et al. 2016). The brain is a complex information processing entity and its function is based on transmitting signals between neurons that are connected by synapses (Bear et al. 2007). These neurons and groups of neurons form hierarchical structures where the connections between neurons are aggregated to form connections between brain regions. With the rich structure of connectivity between the neurons and the brain regions, it is a natural choice to model the brain as a network instead

of the traditional approach of examining activation patterns independent of each other. It has, for example, been suggested that the underlying connectivity is related to the individual differences in brain activity through differential recruitment of brain areas (Chan et al. 2017). This indicates the large role that the connectivity and the underlying brain network have in the overall brain functioning.

Brain connectivity can be divided into structural, functional and effective connectivity depending on the research questions and on the types of data that the estimates are based on (Sporns et al. 2004). Brain connectivity exists on multiple spatial and temporal scales ranging from the level of one neuron to the level of inter-subject brain networks and from fast task-related connectivity changes to long-term structural changes (Betzel et al. 2017). The kind of spatial and temporal scales that are examined are chosen according to the kind of information that we wish to extract. This choice is also affected by the limitations posed by the spatial and temporal resolution of the imaging modalities. In addition to these temporal and spatial scales, the network properties of brain networks can also be examined on multiple topological scales focusing on the microscopic, mesoscopic or macroscopic network properties (Betzel et al. 2017).

The concept of modeling the brain as a network comes with many methodological challenges starting from the question of defining the nodes and edges. This is a non-trivial but essential task as the node definitions have been shown to have a considerable effect on the network properties of the generated networks (Wang et al. 2009, Zalesky et al. 2010). These definitions importantly depend also on the chosen scale of examination. It has been suggested that interesting brain connectivity patterns often originate on a scale larger than single measuring units (Wig et al. 2011, Shen et al. 2013). Therefore, it may be necessary to group these small units together into larger groups. This implies that each one of the final nodes may consist of multiple measurement units. For the node to be well-defined, these subunits within a node are assumed to perform similar dynamics and should, therefore, conform to assumptions of functional homogeneity (Korhonen et al. 2017). However, it has also been shown that the relationships between these within-node units may show rich spatial and temporal variation (Korhonen et al. 2017, Ryyppö et al. in press), giving rise to connectivity patterns also within a node. These connectivity patterns are referred to as internal connectivity. Examining internal connectivity may help us not only to validate the homogeneity assumptions but also to uncover interesting information on the temporally and spatially varying mechanisms of interaction.

While internal connectivity is a property of the node itself, the node is also part of a network that can be studied using the methodology of network science. As a part of the network, each node expresses a combination of different network properties which may be used to understand the organization of brain networks on different scales. Similarly to other real-world networks, brain networks exhibit rich and non-random network structure where different nodes have varying roles in the network topology (for examples see van den Heuvel et al. 2011, van den Heuvel et al. 2013, Bassett et al. 2013, Bassett et al. 2017). This network structure and different roles in it have been suggested to be related to many important information processing features of the human brain such as the balance between integration and segregation of

information (Sporns 2013, Tononi et al. 1994, Friston 1994). Therefore, studying these topological roles may help reveal the differing roles brain regions have in the over-all brain functioning and information processing.

Both the internal connectivity and the topological roles of nodes have, therefore, been suggested to be related to important features and mechanisms that underlie the interactions and structure of brain networks. This Thesis combines these ideas and examines the relationship between internal connectivity and topological roles in functional brain networks estimated from functional magnetic resonance imaging (fMRI) data. This constitutes studying networks on the level of brain regions and on relatively fast time scales. We start by introducing the methodological challenge of even defining what the nodes and edges should depict and examine in more detail the kinds of assumptions that different kinds of node and edge definition schemes may imply. Next we study the internal connectivity and the topological roles of nodes in networks built with different node definition methods. Finally, we examine the link between these properties by attempting to predict the topological role of a node from its internal connectivity features. We hypothesize that the node's topological role and internal connectivity are related due to the different mechanisms and patterns that a node uses to connect to its neighbors. We find that internal connectivity features indeed increase the predictive accuracy of topological role classification indicating that there exists a relationship between internal connectivity and the topological roles of nodes.

This Thesis aims to make both neurophysiologically and methodologically meaningful observations on the internal connectivity and topological roles of network nodes and their relationship. Therefore, these methods can broaden our knowledge on the topological roles of brain regions in the network and, therefore, also help us better understand the underlying functional roles. Functional roles relate to many important activities of the brain. Thus, understanding the functional roles can facilitate understanding the role of the network structure in brain function as a whole. This is valuable for the field of neuroscience but also has many direct clinical applications as altered topological and functional roles may relate to the root causes behind many neurological and psychiatric diseases or disorders. The relationship between the internal connectivity patterns and topological roles may allow for more direct estimates and characterization of the functional roles in brain networks.

2 Background

2.1 Networks and network topologies

2.1.1 Representing networks

Many real-life phenomena consist of entities that are interacting or interconnected. A network is a representation of such a system where entities are represented by nodes or vertices and their relationships are represented by edges or links (Newman 2010). Examples of networks range from abstract networks such as a social network to concrete physical networks such cities connected by the road network. Network science studies such network systems. What follows will be based on the book Newman 2010.

In order to be able to store and study the network information, we need to first define a mathematical representation of the network. The first step is labeling the involved entities or nodes with unique labels for unambiguous identification. The common notation dubs the number of nodes as n. Sometimes there may be some data directly associated with the nodes such as personal information in social networks or information on the location or size of brain regions in brain networks.

In addition to this node-wise data, the essence of networks makes it also necessary to store information on the relationships of nodes. Two nodes that have a relationship are connected by an edge and considered network neighbors. There are multiple ways of representing the edges of the network such as edge lists, adjacency matrices and adjacency lists.

Edge lists consist of lists of node pairs where the connected pairs are listed and any pair that is not on the list is considered not connected. Potentially the best know mathematical network representation is the adjacency matrix, a $n \times n$ square matrix where the element A_{ij} shows the relationship between nodes i and j. Sometimes, instead of using and storing the whole adjacency matrix, it is more favorable to use an adjacency list, a list of n sublists where the ith list contains all the nodes connected to node i.

Each representation type poses its own advantages and disadvantages. For example adjacency matrices allow for many convenient computational procedures such as easy and fast indexing but at the same time they may cause wasteful memory consumption for sparse networks with only a few links. Which representation to choose depends on the network size and sparsity but also on the algorithms we use for processing and the memory constraints for the storage.

2.1.2 Different types of networks

The huge variety of networks present in the real world implies a need for flexibly defining many different types of networks. The network type is usually defined by the phenomena being modeled and represented. For example some phenomena such as molecular excitatory and inhibitory interaction are directed by nature and some interactions naturally contain an intensity measure. In some more complex cases also the limitations of the network estimation methods may have their effect on the

network type produced. This Thesis focuses on undirected weighted networks that may contain self-links and studies also some properties associated with dynamically changing temporal networks. Next sections introduce the types of graphs that are most central for the topic of this Thesis.

Simple graphs and multigraphs

At a most simple form, networks consist of maximum one link between a node pair and no links between a node and itself. This is referred to as a *simple graph* and its counterpart is a *multigraph* that can contain *self-edges* or *multi-edges*, i.e. edges between a node and itself, or multiple edges between the same pair of nodes (Newman 2010).

Weighted and unweighted networks

The interaction or relationship between nodes may be considered to exist or not exist implying a binary adjacency matrix. However, the relationship may also contain some intensity measure that can be stored in the adjacency matrix making it contain also values differing from zero and one. This intensity measure conveys application-specific information such as the number of text messages per day between two people in a social network or the level of co-expression in a gene expression network. These networks are referred to as *unweighted* and *weighted networks* respectively. The line between a multigraph or a weighted network may not always be clear in the light of the adjacency matrix if the values are integers. However, the distinction is normally rather clear considering the phenomena being represented.

Directed and undirected networks

In the most simple networks, when nodes i and j are connected, the relationship runs both ways so that i interacts towards j but also j towards i. However, in some applications the relationship may be unidirectional so that the interaction effect flows only towards one direction such as in a case where there is a link from one web page to another or a flight from one city to another but the link or flight to the other direction may not exist. This property gives rise to differentiation between *undirected networks* with only mutual interaction links and *directed networks* where also unidirectional links may exist (Newman 2010). This is visible in the asymmetry of the adjacency matrix.

Temporal networks

So far, we have discussed the basic concepts of static networks that are merely a snapshot of the network connectivity at a certain time. Some real-life networks remain static in their structure over long periods of time whereas some networks undergo fast dynamic changes even on short time scales. These kinds of networks that experience changes or altering edge activations over time are called *temporal networks* (Holme et al. 2012). Temporal networks can be represented by a series of adjacency matrices

sampled at some known intervals in time. This method constitutes a challenge of defining an appropriate sampling interval keeping in mind the typical time scales of the modeled phenomena as well as the potential limitations of the computational estimation methods used. In some applications this challenge can be addressed by rather representing the temporal network and its active links as a list of interactions between nodes and their associated time stamps.

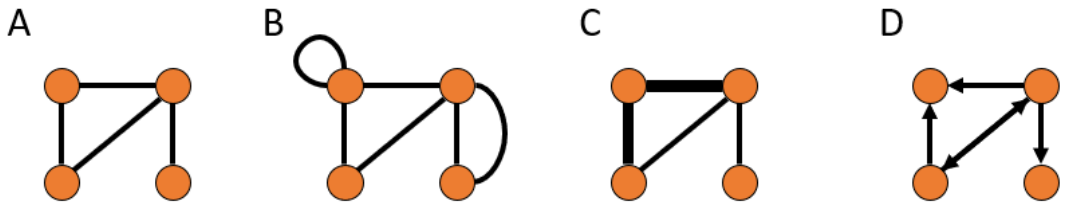

Figure 1: A) Simple, undirected network B) Multigraph C) Weighted, undirected graph. D) Directed graph

2.1.3 Local and global network properties

Once the network has been constructed, the next step in studying it is characterizing the network properties and structure and the patterns they exhibit. Network properties range from small scale properties associated with the node and its connectivity in its immediate neighborhood to large scale properties associated with the whole network or the node's global role. These are often referred to as local and global network properties. There are countless measures for different network properties each conveying meaningful information about the network and its structure. However, this section focuses on the properties that are necessary for understanding the methodology used in this Thesis.

Node degree

Each node has a set of other nodes that it is connected to referred to as neighbors. The *degree* of a node is a property that indicates the number of a node's neighbors and it can be computed as a sum of the nonzero elements on the adjacency matrix row associated with the node i (Newman 2010). For an unweighted undirected graph, this is as follows:

$$k_i = \sum_{j=1}^{n} A_{ij}, \tag{1}$$

where k_i is the degree of the node i, n the total number of nodes in the network, and A_{ij} the adjacency matrix element representing the link between nodes i and j.

Node strength

The degree only counts the number of neighbors ignoring the intensity of the relationships. However, in the context of weighted networks this intensity of the relationship may also be crucial for the studied phenomena. The *strength* of a node takes also into account the weight of the links adjacent of a node counting the total weight of the node's connections. Similarly to the degree, the strength s_i of the node i can be computed as a row sum of the weighted adjacency matrix.

Network properties on the global level

Many of these local network property measures can be aggregated over all nodes in order to form global network measures. For example, the mean degree gives an idea of the overall connectivity patterns of the network. Also, networks may have characteristic distribution shapes when it comes to local property distributions. For example, degree distributions have been shown to differ between different kinds of model networks (Newman 2010).

In addition to the local measure aggregates, global network properties include measures of a node's role in the overall network. This includes, for example, some centrality measures such as betweenness centrality that measures the fraction of the shortest paths that a node lies on (Newman 2010).

Some global measures originate on the whole network level. For example, the *density* measures the fraction of links that exist in the network out of all possible links that could exist.

2.1.4 Mesoscopic-level network properties

Both local and global network properties convey important information on the network structure and topology. However, many interesting patterns happen on a level somewhere in between of the immediate local neighborhood and the global level of the whole network (Betzel et al. 2017). This is often referred to as a component and community structure.

Connected components

A *connected component* is a collection of nodes that are all connected so that any one node can be reached by following a set of links from another node in that component (Newman 2010). Some networks are fragmented into more than one component in which case only the nodes in the same component can be reached and there are no connections to other components.

Communities

In addition to connected components, many real life networks exhibit a *community structure* (Girvan et al. 2002). While there is no consensus on the exact definition, a *community* or a *module* is usually considered to be a group of nodes that is more densely interconnected than connected to other nodes that do not belong to the same

community (Fortunato 2010). Therefore, there are more intracommunity links than there are intercommunity links. However, also intercommunity links exists which differentiates communities from connected components. Thus, communities are less well defined than connected components and the community structure is not always clear from just observing the network. Sometimes a community assignment might be inherent from the application and the meta data associated with the nodes but often the community structure has to be detected from the network connectivity using different algorithms targeted at modularity detection in static networks (Girvan et al. 2002, Fortunato 2010) or temporal networks (Mucha et al. 2010). The algorithms used in this Thesis are presented in detail in the methods section.

Network properties on the community level

The community level gives rise to new network properties that can be used to characterize the node's role in regards to the community structure. *Within-module degree* depicts the number of links a node has to the other nodes within its community whereas *between-module degree* shows the number of links to nodes in other modules. Similarly we could define within-module and between-module strength when dealing with weighted networks. In addition there are different measures associated with the distribution of node's links among the different modules (Guimera et al. 2005b).

Different network properties convey information on different network characteristics depending on their level of scope and on the quantity they measure. Different property measures are needed depending on the questions that we wish to answer.

2.1.5 Topological roles of nodes

Different topological roles

Many real-world networks exhibit a rich, non-random structure with different nodes carrying out different tasks and roles. A node's function in the network is largely defined by its connectivity patterns (Guimera et al. 2005b, Guimera et al. 2005a). For example, the node's topology has been suggested to be related to the node's functional specialization such as its tendency to collect signals or emit signals onto target regions in a signalling network (Harriger et al. 2012) or its role as a specialist, generalist or a supergeneralist in an ecological pollination network (Olesen et al. 2007). This gives rise to an interest to examine the node's topological role, *i.e.*, the node's role in the connectivity of the network.

Hubness is one of the central concepts in defining a node's role in the network. While there is no one universal definition for hubness, it is generally thought that *hubs* are network nodes with high degree or high centrality (van den Heuvel et al. 2013, Bullmore et al. 2009, Göttlich et al. 2017). In addition to this global definition of hubs, it is also possible to define hubs in relation to the module structure of the network (Bullmore et al. 2009, Guimera et al. 2005c). Some complex networks have been shown to contain nodes that are not hubs in the global sense when considering all nodes in the network but may still be considered hubs in their own module (Guimera

et al. 2005c). The exact definition of a hub, therefore, varies among different fields and applications.

Even the nodes that are considered hubs may have varying roles and connectivity profiles in the network, especially in relation to their roles in the module structure or to their temporal and spatial behavior. Therefore, it is possible to divide the hub nodes into sub-groups that further characterize their connectivity patterns and properties. When considering the node's role in relation to its module, one of the commonly used divisions is between connector and non-connector hubs. In this framework, the connector hubs have many links to nodes in other communities while non-connector hubs exhibit high connectivity mainly within their own module (Chan et al. 2017). Similar phenomena has also been dubbed as provincial or local hubs and connector hubs (Guimera et al. 2005b, Guimera et al. 2005a).

In addition to these module-role-based hub subdivisions, also more temporally and spatially oriented hub sub-roles have been suggested. The date and party hub framework describes the different characteristic interaction patterns of hubs. Party hubs typically interact with many of their neighbors simultaneously, whereas date hubs interact with different neighbors at different times and locations (Han et al. 2004). The party-hub-date-hub framework is also to some extent related to the connector-non-connector framework as some combinations of these classes are often more common than others (Agarwal et al. 2010). In this Thesis we keep our focus on non-temporally measured topological roles and, therefore, do not handle party hubs and date hubs in more detail.

Hubs are thought to have an important role in the integration of the network for example by combining and processing information from many different functionally specialized nodes (Göttlich et al. 2017, van den Heuvel et al. 2013). Therefore, hubs have been suggested to be important for the network connectivity and their removal risks leading to a fragmented network and network dysfunction (Bullmore et al. 2009, van den Heuvel et al. 2013). Within the connector and non-connector hub framework, connector hubs have been suggested to have a broader role in information integration whereas non-connector hubs are thought to have an important role in their own module's functional specialization (Chan et al. 2017). Party hubs are typically thought to act as local coordinators whereas date hubs perform more global connector functions (Agarwal et al. 2010).

In addition to hubness, also other types of topological roles may be defined and studied. Some networks exhibit a core-periphery structure which implies a division of nodes into a densely connected core and sparsely connected periphery (Holme 2005, Zhang et al. 2015, Bassett et al. 2013). In some real-world networks the hub nodes have been shown to be more densely interconnected than what would be expected based solely on their high degree. These densely connected hub nodes are said to form a rich club giving rise to a phenomena referred to as rich club organization or rich club ordering of the network (Colizza et al. 2006, Harriger et al. 2012, van den Heuvel et al. 2011).

When examining the topological roles of nodes, this Thesis focuses on hubness related to the nodes role in the module structure and especially the division between provincial hubs and connector hubs. The framework used is presented in more detail

in the methods section.

Defining and detecting topological roles

Topological roles are typically defined by a combination of one or more network topological properties that measure the node's connectivity and its distribution over communities or temporal and spatial scales. In accordance with the focus of this Thesis, this section focuses on the topological roles related to the module structure.

In order to define a node's topological role in terms of the module structure, the nodes have to first be divided into modules by running a module detection algorithm such as Infomap (Chan et al. 2017), simulated annealing (Guimera et al. 2005b, Guimera et al. 2005a) or the Louvain method (Meunier et al. 2009).

Once the modules have been detected, different measures are computed to quantify the level of connectivity and the distributedness of the links among the communities (Guimera et al. 2005b, Guimera et al. 2005a). Examples of such measures are the within-module degree and the participation coefficient which will be discussed in more detail in the Methods section.

The combination of these measures is then used to divide the measure space into subregions, each of which corresponds to a different topological role. In many studies, the division of the space has been realized through thresholding the space in a decision-tree-like fashion, for example requiring a certain level of within-module degree for a node to be considered a hub node (Guimera et al. 2005b, Guimera et al. 2005a, Chan et al. 2017). The used thresholds have typically been heuristic (Guimera et al. 2005b, Guimera et al. 2005a) or based on medians or different percentiles of the values among nodes (Chan et al. 2017).

The thresholding is often done globally by applying the same threshold to all of the nodes in the network (Guimera et al. 2005b, Guimera et al. 2005a, Power et al. 2013). However, the functional characteristics of some real-world networks may give rise to modules in which nodes in general exhibit higher level of topological measures than nodes in other modules. In these kinds of networks, global thresholding of topological properties risks finding hubs only in certain modules. It has been suggested that it may be helpful to rather use a local thresholding scheme where the thresholds are defined for each module individually (Chan et al. 2017). This facilitates finding an appropriate scale for detecting different roles in all the modules.

Once the space spanned by the topological properties has been thresholded, the nodes in the network can be classified into different topological role categories by examining the values of their topological properties and following a decision tree-like decision logic. Different numbers and definitions of the topological role classes have been used in different studies. The detailed definitions used in this Thesis are presented in the Methods section.

2.2 Understanding and measuring the brain

2.2.1 Basics of neuroscience

The brain and the nervous system have been studied by many different disciplines in the course of history and many scientists have attempted to decode the structure and functioning of the nervous system on different scales. The interpretations on the role of the brain have evolved throughout the history. Egyptians tossed the brain away after death as unessential and Aristotle suggested it to be merely a cooler of the blood overheated by the real center of intellect, the heart (Bear et al. 2007). However, already the ancient Greek philosopher Hippocrates acknowledged the brain as the center of sensation and intelligence providing a base for the modern interpretation of the brain as a home of cognition, emotion, sensing and action. Since then the brain and its functioning mechanisms have been of great interest among the scientific community. Some of the early explanations for the functioning mechanism included hydraulic interpretations where for example limb movements could be explained by fluid-mechanical changes in the brain. However, by the turn of the 19th century, this notion was replaced by the idea that nerves conduct electrical signals between brain and the other parts of the body (Bear et al. 2007). The electric and wired nature of the brain and nervous system functioning was established and this notion holds still today.

Neuroscience as a term and as its own independent field of science is a rather recent development with the key neuroscientific associations officially founded only in the 1970s (Bear et al. 2007). Since then it has been a growing field with active and evolving research ranging from molecular and cellular neuroscience of examining the chemical and cell-level mechanisms to systems, behavioral and cognitive neuroscience of studying the neural mechanisms of more complex sensory and behavioral patterns as well as cognitive functions (Bear et al. 2007).

The methods used to study the brain have varied across time from deducing the function from structure while dissecting the brain to examining the effect of lesions to the behavior (Bear et al. 2007). In the past decades, the fast development of medical imaging has lead to methods that enable us to noninvasively image and measure the brain and its functioning. Many different methods have been developed, each of which makes use of a different physical phenomena. For example electroencephalography (EEG) and magnetoencephalography (MEG) measure the electric signaling of the brain and the magnetic fields induced by these electric currents respectively. Each method has its advantages related to the temporal and spatial resolution as well as price and usability. This Thesis focuses on magnetic resonance imaging (MRI) and functional magnetic resonance imaging (fMRI) that make use of the variation of magnetic properties between different tissue types and blood oxygenation conditions. MRI and fMRI are presented in more detail in the Sections 2.2.2 and 2.2.3.

Also the studied research questions have developed together with the interpretation of the brain and the imaging methods. Historically much of the neuroscientific research consisted of making anatomical observations on the structure of the brain and trying to draw conclusions on its effect to the brain function. By the end of 18th century, localizing the general patterns of the gyri and sulci on the cortex gave rise to the

idea of different functions being localized to different parts of the brain (Bear et al. 2007). Consensus was not reached immediately but during the years different studies gathered evidence supporting the role of some brain areas in certain tasks or behavioral and sensory functions. Some of the early influential studies by Paul Broca and Carl Wernicke showed that lesions in certain brain regions indeed were linked to certain specific disabilities and impairments (Bear et al. 2007, Friston 2011). These studies strengthened the idea of functional localization which implies attributing a function to a specific cortical area (Friston 2011). Similarly the brain function was thought to be segregated so that each cortical area had its own functional specialization that was anatomically segregated on the cortex (Friston 2011). This idea of localizing functions on the cortex and finding out the functional specializations has been a key research question in neuroscience since then, leading to search of individual brain regions that would activate during a certain task or a stimuli. In recent years neuroscientific community has adopted also other approaches such as modeling the brain as a network of interacting elements rather than as independent areal activations. This network approach in neuroscience will be discussed in more detail in section 2.3.

2.2.2 Magnetic Resonance Imaging

Magnetic Resonance Imaging (MRI) is a well known noninvasive imaging modality used in the biological and medical context to estimate the structure of tissues and organs. The possibilities range from full body scans to detailed imaging of small organs. However, the focus of this Thesis is on the brain and, therefore, the examples will be drawn from the neuroscientific context.

MRI makes use of a strong magnetic field, e.g. 3 Tesla, and radio frequency pulses that are used to excite the nuclei of hydrogen atoms (Logothetis 2008, Huettel et al. 2004). Hydrogen atoms are a convenient substance in MRI as they are abundant in the bodily tissues and the hydrogen content varies between different tissue types. Like many nuclei, hydrogen nuclei possess a property referred to as the magnetic moment. The strong external magnetic field used in MRI makes these magnetic moments align with the external field. This alignment is then disturbed by exciting the nuclei by radio frequency pulses. After the pulses, the magnetic moments will attempt to realign with the external magnetic field, a process referred to as relaxation, and emit a signal that can be measured by a radio frequency receiver coil (Logothetis 2008).

This measured signal can be used to deduct the hydrogen content at different locations within the imaged object. With differing hydrogen contents in different tissue types, this allows us to form an image that contrasts different tissue types as gray pixels of different intensity and gives us an estimate of the structure of the tissue or organ, such as the brain.

The brain, like other organs and tissues, is ultimately a three-dimensional construct. Therefore, to get a 3D image of the brain, we sample multiple 2D slices and join them together for a final 3D representation of the whole brain volume. The 2D pixels of the slices are present in the volume as voxels, the dimensions of which are

defined by the spatial resolution of the 2D pixels and the number and distance of the imaging slices. A voxel is typically about 55 mm^3 in volume, which implies that ultimately we are imaging groups of about 5.5 million neurons (Logothetis 2008). By MRI we obtain a good spatial resolution but the temporal resolution is usually rather poor: it takes several minutes to sample the whole 3D brain volume. Due to this and the property of targeting hydrogen nuclei, MRI gives us only a static estimate of the anatomical structure of an individual's brain.

2.2.3 Functional Magnetic Resonance Imaging

As discussed in Section 2.2.2, MRI only provides us with a static image of brain structure. Therefore, MRI can only reveal long term structural changes. While these changes have also been studied to get insights into brain development and changes in disease and health, a large number of brain imaging studies aims to estimate brain function and activity which change much faster than the time scales of MRI. Functional Magnetic Resonance Imaging (fMRI) is a variant of MRI methods that aims at measuring brain activation on shorter time scales (Logothetis 2008, Huettel et al. 2004). This consists of repeatedly sampling 3D volumes of the brain to form a time series of brain images. When moving from MRI to fMRI, the time needed for sampling the whole brain volume is reduced from several minutes to a few seconds, the typical intervals being about 1-3 seconds. This sampling interval is referred to as repetition time (TR). In the recent years there have been studies on new pulse sequences that would be able to increase the temporal resolution of fMRI even to the very small value of 25 ms (Chang et al. 2013).

Instead of measuring the relaxation of hydrogen nuclei, fMRI measures some other variant that is related to the changes happening during neuronal activation. There are multiple functional variants but the most typical variant of fMRI makes use of pulse sequences sensitive to changes in the blood oxygenation level (Logothetis 2008). Therefore, the signal measured by fMRI is referred to as Blood Oxygenation Level Dependent (BOLD) signal (Logothetis 2008, Huettel et al. 2004). Measuring the oxygenation level of blood can be thought of as an indirect measure of brain activity: in regions with increased activity, the metabolism of neurons is enhanced which causes augmented oxygen consumption. Thus, the regions with changes in their BOLD signal can be thought to exhibit changes in their oxygen consumption and also in their level of activation. However, this intuitive relationship is not this straight forward (for more thorought discussion refer to Logothetis 2008).

The BOLD signal is not an absolute measure of activation but rather a measure of change which implies that the relative changes in the signal are of interest instead of examining its absolute value. At activation, we observe a change in the BOLD signal characterized by a hemodynamic response function. The BOLD signal is also a rather slow signal that has been estimated to peak several seconds, *i.e.*, 5-10 seconds, after the start of the response (Handwerker et al. 2012, Lindquist et al. 2009) which may make studying fast activation changes challenging. Additional challenges are posed by the large variation in the shape of the HRF: different individuals and brain regions have been shown to exhibit differing HRF shapes and even for the

same individual and brain region, the shape can be significantly altered by pre-scan conditions (Handwerker et al. 2012). The BOLD signal is usually also rather noisy making efficient preprocessing steps a necessity.

Finally, fMRI produces a series of 3D brain volumes and therefore, ultimately constitutes a 4D representation of the brain both with spatial information encoded in the voxel location in the 3D volumes and temporal information in the BOLD signal changes in time. Therefore, fMRI data are a 4D matrix from which we can separate for example single volumes or time series associated with a voxel. As discussed earlier, the temporal changes in the BOLD signal are of interest. Therefore, many analysis methods are based on extracting voxel-wise time series from the 4D data and examining their relationships between subjects, between voxels or with time series associated with experimental design of the tasks that the subject was performing during the scan.

2.3 Brain as a network

2.3.1 Network science's view on the brain

As discussed in Section 2.2.1, much of neuroscientific research has traditionally focused on localizing brain activation associated with a given task. This approach treats different brain areas as independent and disregards the interactions and relationships between regions. However, it was established early on that the connections between even distant brain regions made it difficult to attribute a function to only one brain region (Friston 2011). Indeed, the brain is ultimately a complex system of many interacting elements and its function is rather based on signaling between regions than on simple independent activations. Therefore, it is natural to represent the brain as a connected system of regions instead of as independent areas.

Network neuroscience is a multidisciplinary field that combines neuroscience and network science to study and model the brain and other neurobiological systems as complex networks (Bassett et al. 2017, Muldoon et al. 2016). Neuroscience provides the phenomena to be studied and the background for the neurocognitive interpretations of the results whereas network science contributes the mathematical and methodological tools for analysis. The development of the research area has greatly been facilitated in recent years by advances both in imaging techniques providing better and more detailed data as well as in computational techniques making it possible to analyze the resulting large networks (Bassett et al. 2017).

The brain and the nervous system are ultimately complex structures formed by millions of neurons that are interconnected by synapses and communicate through spikes of electric currents. These neurons form groups that are densely interconnected among themselves but also connected to the other groups for example through white matter tracts. In addition to these direct physical links, there is also less direct connectivity related to more abstract relationships between brain regions. This gives rise to three different types of brain connectivity referred to as structural, functional and effective connectivity. These different types of connectivity will be discussed in more detail in Section 2.3.3.

The above mentioned organization into neurons, brain regions, and groups of brain regions gives rise to spatially hierarchical organization that may be studied at different spatial resolutions. Different pairs or groups of neurons are firing at different times indicating that different connections are active but there are also longer term plastic changes in the connections that are altered through learning (Bear et al. 2007, Hebb 1949). This indicates the presence of properties that are temporally variant at different time intervals. The networks of the brain can be studied on multiple different scales ranging from local to global scale of network properties as discussed in Section 2.1.

These three factors together give rise to the three dimensions of examination that are present in network neuroscience: the analysis are located at a point among spatial, temporal and topological scale (Betzel et al. 2017). Spatial scales of examination range from cellular level until regional or even inter-subject level whereas temporal scales may constitute anything between instant signal dependent activation of connections to the long term evolutionary changes in the general connection patterns. Spatial and temporal scales are discussed in more detail in the next sections.

Topological scales refer to choosing the level of examining the network properties. As discussed in Section 2.1, some of the network properties such as the degree are local in nature as they are only associated with a node and its immediate neighborhood whereas some metrics such as the density characterize the whole network representing the global end of the topological scale. Between the local and global scale lies the meso-scale of network properties (Betzel et al. 2017). In fact the meso-scale can be rather viewed as a range of scales between the local and global extremes.

Brain networks exhibit many characteristic network structures and properties that show rich nonrandom topological attributes (Bassett et al. 2017). The organization of the brain is thought to be a manifestation of a balance between segregation and integration (Sporns 2013, Tononi et al. 1994, Friston 1994). Integration implies the ability to efficiently combine information from various brain regions whereas segregation consists of the organization into densely connected subregions with ability for specialized processing (Rubinov et al. 2010). Brain networks have many characteristic properties that are thought to be indicative of integration, segregation and their mutual existence. Brain networks exhibit high clustering implying high robustness to errors and short path lengths that have been suggested to be associated with high global efficiency of information transfer (Bullmore et al. 2009). Short paths lengths are thought to imply stronger potential for integration whereas high clustering gives promise for the existence of densely connected subregions typical for the idea of segregation (Rubinov et al. 2010).

These characteristics are often thought to be associated with the small-worldness property suggesting the brain network to be one. However, it has also been argued that the apparent small-worldness might be partly accounted for by the characteristics of data processing and the used small-worldness definitions (Papo et al. 2016). The brain is ultimately also a spatial network confined in the 3D space bordered by the skull. Therefore, it has also been suggested that this spatial embedding may explain the apparent high clustering and short path lengths even without the presence of the small-world property in the topological graph (Knoblauch et al. 2016).

For the network organization of the brain the meso-scale is also particularly interesting as many of the characteristic network structures and properties originate at this level. Brain networks have been shown to exhibit a community structure where the densely connected communities are linked to each other through hub nodes (Bassett et al. 2017, van den Heuvel et al. 2013). These hub nodes of different communities are often also densely interconnected implying the existence of a core-periphery structure (Bassett et al. 2013) or a rich-club (van den Heuvel et al. 2011). Core-periphery structure is manifested in the fact that the hubs form a densely connected core to which the peripheral nodes are connected while links between two peripheral nodes are rare. Brain networks also exhibit hierarchical organization where communities can be further fragmented into various smaller subcommunities.

Studying these network characteristics and their differences between tasks or between disease and health may give us important tools for understanding the neurocognitive mechanisms in their full complexity. The network approach is able to account for the brain as a whole instead of considering only independent regions which helps reveal characteristics that would otherwise go undetected. Network neuroscience is a growing discipline with a lot of promise for the future.

2.3.2 Node definitions

In many application areas of network science, it is immediately rather evident what the nodes of the network should be. For example, in social networks it is natural that nodes should represent people, whereas in the road network different cities should act as nodes. However, in network neuroscience the mere question of node definition has been a major challenge and no consensus has been reached in the network neuroscience community. Nevertheless, the way that the nodes are defined has been shown to have an effect on the network properties of the generated network (Wang et al. 2009, Zalesky et al. 2010) implying the importance of an accurate node definition strategy.

Node definitions on different spatial scales

As discussed in Section 2.3.1, the brain can be modeled on many different spatial scales ranging from the microscopic level of individual neurons to the macroscopic level of brain regions. The spatial scale of the study has a significant effect on the type of node definitions that need to be used. In order to study the brain network on the microscopic level, the nodes should depict individual neurons and their synapses. These kinds of studies have been carried out on non-vertebrates with simple nervous systems such as the *C. Elegans* worm (White et al. 1986). However, in the human brain the number of neurons is measured on the scale of 10^{11} (Herculano-Houzel 2009) imposing computational complications on studying the whole brain on the microscopic level. In addition, noninvasive imaging modalities have a limited spatial resolution making it impossible to image single neurons. Due to these constraints posed by the limitations of noninvasive imaging modalities and computational methods, obtaining a single-cell-level network representation of the entire human brain is currently non-feasible. Therefore, network neuroscientific research of the human brain is currently

confined to examine networks at the mesoscopic and macroscopic levels. This Thesis focuses on brain networks estimated from fMRI data where the smallest imaging unit constitutes a voxel of typically about 5.5 million neurons (Logothetis 2008). The mesoscopic scale of fMRI brain networks involves studying networks al the voxel level whereas the macroscopic level implies grouping voxels together into larger regions using some node definition strategy.

Typical node definitions strategies

When studying fMRI brain networks at the mesoscopic level, no specific node definition strategy is required: the smallest imaging unit available in the data set constitutes one node. However, as discussed in Section 2.3.2, studying macroscopic brain networks requires some strategy for grouping the small measurement voxels into larger groups.

Some of the most typical strategies include using predefined Regions of Interest (ROIs) or grouping the voxels into ROIs in a data-driven way. The predefined ROI approach consists of partitioning the brain into regions that are defined prior to the experiment independently of the current data set at hand. Some ROI parcellations are based on the brain anatomy (for examples see Desikan et al. 2006, Stanley et al. 2013, Tzourio-Mazoyer et al. 2002) while some aim to cover different combinations of anatomical, functional or connectivity profiles (for examples see Fan et al. 2016). Data-driven ways include starting at the voxel level and grouping voxels into data-driven ROIs by their functional connectivity. The groupings can be found for example by using different clustering algorithms (for examples see Craddock et al. 2012, Shen et al. 2013) or boundary mapping methods that rely on abrupt changes in functional connectivity patterns (Wig et al. 2014, Gordon et al. 2014). Many studies suggesting data-driven definition strategies have also published a corresponding example parcellation that is available online to be used as predefined ROIs for further experiments.

It has also been suggested that ROIs should be defined as spheres placed at the center of regions (Wig et al. 2011). That way only the core of the regions will be taken into account and the method is less affected by the potentially unclear borders between neighboring regions. These center coordinates may be taken from existing parcellations or they may be estimated by peaks of task localizers or historical activation studies (Wig et al. 2011). Another possibility is defining components using independent component analysis (ICA) that maximizes the independence of the signals of different components (Kiviniemi et al. 2003). However, in this case it is open to debate whether each component constitutes a node or a network of its own.

Using predefined ROIs has been the most common approach in network neuroscientific studies and studies using data-driven parcellation strategies are still a minority. In this Thesis, we examine both some predefined ROI parcellations as well as a data-driven parcellation strategy that makes use of network community detection. The details of the used strategies and standard parcellations are included in the Methods section.

Choosing the level of examination

The voxel-level and ROI-level networks have been shown to differ in terms of many basic network properties which shows the importance of choosing the level of examination (Hayasaka et al. 2010). The choice between the voxel-level nodes and ROI-level nodes depends on the question at hand and each approach has its advantages and disadvantages. From the neuronal point of view voxel-level nodes may already be problematic as they are formed by arbitrarily grouping neurons into measurement voxels (Wig et al. 2011) and they may, therefore, be noisy depending on the real scale of functional groups of neurons. Depending on the imaging resolution used, voxel-level networks may become very large imposing computational challenges on the analysis and storage of the networks. In addition, one could argue that the connectivity patterns of interest rarely originate at the level of single voxels but rather at the regional level (Wig et al. 2011, Shen et al. 2013) implying that voxels may be redundant. This limits the interpretability of the results obtained from examining voxel-level networks.

ROI-level networks may help to increase our ability to interpret the results in the neuroscientific context. However, ROI-level brain network modeling is also sensitive to the way that the voxels are partitioned into ROIs and even small changes may risk distorting the results (Wig et al. 2011). ROI-level node definitions also rely on certain assumptions about the internal structure of the resulting nodes and violation of these assumptions may lead to large inaccuracies in the analysis. One of the key assumptions is that the ROIs should be functionally homogeneous, *i.e.*, share some common dynamics. This may not always hold true especially for predefined atlas-based ROIs (Craddock et al. 2012, Korhonen et al. 2017). The problems posed by the functional homogeneity assumption and the effects of its violations to the network extraction are the largest pitfall of the ROI-level approach. These assumptions on the internal structure are discussed in more detail in Sections 2.3.2 and 2.3.5.

Data-driven node definition strategies are often based on optimizing the similarity in the behavior or dynamics of the within-ROI voxels. Therefore, defining the used ROIs in a data-driven way, taking into account the data set being studied, helps avoid some of the problems associated with inaccurate assumptions on the internal structure. However, some of these methods may again result in regions that are hard to interpret.

Representing the signal of the node

As discussed in Section 2.2.3, fMRI data consist of a 4D matrix in which each measurement voxel has an associated time series of a BOLD signal. This time series is said to indirectly represent the neural activity of the voxel.

When using the voxel-level nodes, the signal of the node is again evident: the signal that represents the node is simply the signal of the smallest measurement unit, the voxel. However, when dealing with ROI-level nodes we find ourselves with a set of voxels each having its own associated BOLD time series. From the network point of view the node is considered as a single uniform entity which implies the

necessity of aggregating the voxel signals into one that represents the whole ROI, or of otherwise defining the ROI-wise connectivity from the voxel-level BOLD signals.

Potentially the most commonly used method is to average the BOLD time series of the within-ROI voxels into one ROI time series that is thought to represent the dynamics of the whole ROI (Stanley et al. 2013). The links between ROIs are then estimated from these ROI-level time series. However, this approach leads to loss of information and involves a risk that the resulting time course may not be truly representative of the ROI, especially if the ROI is not well-defined and comprises of multiple functional areas (Shen et al. 2013, Stanley et al. 2013). Therefore, this approach is sensitive to assumptions about the internal structure of the ROI and violation of these assumptions may make the ROI time series a rather inaccurate representation of the ROI, biasing the whole construction of the network. The assumptions are discussed in more detail in Section 2.3.5.

In order to avoid the problems of averaged ROI time series, voxel connectivity aggregation methods have been proposed. This consists of first estimating voxel-level links and then aggregating these links to quantify the level of between-ROI connectivity. For example, graph coarse-graining first forms a voxel-level connectivity network and then aggregates these connections according to a parcellation scheme by counting the number of voxel-level links between different ROIs and within a ROI (Kujala et al. 2016). This ROI representation method is presented in more detail in the Methods section.

2.3.3 Edge definitions

Once the nodes have been defined, the next step in the network construction is to define how the nodes are connected, i.e. to estimate the edges or links of the network. Similarly to node definitions, defining the edges is not a straightforward task.

Different types of brain connectivity

The brain is ultimately a complex system of brain regions that are physically connected to each other by white matter tracts. However, due to its complexity, there are also less direct relationships and similarities in the way different brain regions function together that go beyond just direct physical links. This gives rise to different types of connectivity in the human brain.

Most typically human brain connectivity is divided into structural, functional, and effective connectivity (Sporns et al. 2004). Like its name implies, structural connectivity consists of physical links between different brain regions (Sporns et al. 2004). Structural connectivity can be estimated for example *post mortem* by dissecting the brain but also using MRI of high-contrast rare earth ions or diffusion tensor imaging (DTI), a variant of MRI sequence that is sensitive to the direction of water diffusion in the brain (Sporns et al. 2005). As axons of the brain have a direction, structural brain connectivity forms a directed network. However, depending on the imaging modality the direction information may not always be available leading to examination of an undirected network.

Functional and effective connectivity do not correspond to any physical connections and they constitute more abstract networks of brain areas that function together. Functional connectivity is associated with similarity of activity of brain regions which is usually measured as temporal correlation or other descriptive measure of statistical dependence (Friston 1994, Friston 2011). As a symmetrical measure it forms undirected networks. Effective connectivity, on the other hand, aims at assessing the influence one brain region has on another (Friston 1994). Therefore, it attempts to estimate directions of interaction implying a causal relationship and leading to directed networks (Bullmore et al. 2009). These effective connectivity networks are often referred to as models that explain the observed dependencies (Friston 2011).

This Thesis focuses on functional connectivity so the discussion focuses on methods for estimating functional brain networks instead of structural or effective networks.

Quantifying an edge in functional brain networks

Usually edge estimation consists of computing some similarity metric between the node time series and redeeming the nodes with high enough similarity connected. Probably the most used definition of a link is the correlation between node time series either on the voxel or ROI level. The *Pearson correlation coefficient* (PCC) is among the most widely used methods among the network neuroscience community.

Using the mere Pearson correlation coefficient has been noted to result in links that are in fact a result of spurious correlations rather than of a direct interaction (Smith et al. 2011). *Partial correlation* of regressing out the signal of other nodes has been suggested more robust towards spurious correlations and therefore, it could help catch only the true direct links (Smith et al. 2011).

One key challenge with correlation based edge definitions is that they often require the relationship between the two time series to be linear or monotonous. *Mutual information* (MI) is a metric that measures the statistical dependence between signals and does not require it to be of a certain form (Smith et al. 2011).

Based on their simulation study Smith et al. 2011 suggest the partial correlation to be among the most powerful methods for edge estimation in functional brain networks. However, the choice of the edge definition measure should be made based on the requirements of the research question and the limitations of the data set. Some questions also require building networks dynamically in time windows in which case the temporal scales used limit the number of time points available for the edge estimation. This affects the choice of metric favoring methods that are relatively robust even for a smaller number of time points. This same constraint concerns also short scan sessions with limited number of time points.

This Thesis focuses on undirected weighted networks estimated using the Pearson correlation coefficient. While the PCC is not the most powerful edge estimation method (Smith et al. 2011), it has the advantage of being commonly used, conceptually simple and easy to interpret. Despite being a more powerful estimation metric, partial correlation often requires more points for enough statistical power and stability to be able to still regress out the signal from other nodes especially if

there are many nodes in the network (Smith et al. 2011, Bassett et al. 2017). The PCC, on the other hand, is still relatively robust also for shorter time series and a larger number of nodes, giving it an advantage for the study of this Thesis where some metrics are computed dynamically for relatively short time windows and the number of nodes may vary.

2.3.4 From the nodes and estimated edges to a network

Once we have chosen and computed a similarity measure between all possible node pairs in the network, we are left with a non-binary square matrix that will be symmetric in the case of functional connectivity. If there is no incentive to include any constraints on the network, this obtained similarity matrix may be used directly as an adjacency matrix (Kujala et al. 2016). This is often referred to as the full or unthresholded network and it constitutes a weighted network where all node pairs are connected. As the similarity measures get their maximum value between a node time series and itself, inherently this network contains the strongest links between a node and itself implying the existence of self-links. Often it may be useful to impose an additional constraint of not allowing self-links and setting the diagonal of the adjacency matrix to zero (Rubinov et al. 2010).

An adjacency matrix that originates directly from the similarity measure will also have many small values and potentially even negative entries. There is no consensus on the role of the negative correlations in functional brain networks. It has been suggested that negative correlations are less reliable and less stable than positive correlations (Shehzad et al. 2009, Tian et al. 2007) and that networks constructed from the negative-tail correlations show weaker and less consistent network structure than positive-tail correlation networks (Schwarz et al. 2011), giving evidence that it may be appropriate to discard negative correlations from the analysis. However, it has also been suggested that negative correlations have a neurobiological interpretation potentially related to antagonistic neural relationships (Wig et al. 2011).

The small values, on the other hand, imply weak links that are often considered to be mainly spurious correlations and noise between nodes that are not actually connected (Rubinov et al. 2010) or the connections are not thought to be physiologically relevant (Wig et al. 2011). When leaving low-correlation links in the network, computational problems may arise from the large number of entries (Kujala et al. 2016). In addition, many graph algorithms do not allow for negative edge weights. These factors, in the absence of consensus on their role, may often motivate leaving negative correlations and small values out for computational convenience.

Therefore, thresholding the adjacency matrix is often a viable choice. This consists of keeping only the strongest links in order to filter out the noise of the weak relationships (Kujala et al. 2016). The thresholding methods can be divided into global and local, the former ones being more typical in human neuroimaging studies (Alexander-Bloch et al. 2010). Once the strongest edges to be kept have been chosen, they can be included in the network either as binary edges of an unweighted network or the level of connectivity can be included proportionally to the edge estimation metric to form a weighted network. However, caution should be taken

when thresholding and binarizing networks. The weights have been suggested to likely contain neurobiologically relevant information that is lost when the networks are binarized (Wig et al. 2011). In addition, over-thresholding may risk biasing the underlying connectivity patterns (Wig et al. 2011).

Global thresholding

The most typical global thresholding methods include fixed and density-based thresholding. Fixed thresholding comprises choosing a fixed predefined threshold on the scale of the edge estimation metric and rejecting edges weaker than this threshold. Density-based thresholding, on the other hand, includes setting a predefined density threshold and including the corresponding number of the strongest edges (Kujala et al. 2016).

Each method requires certain assumptions that may be problematic especially when assessing differences in network properties across groups of subjects. For the meaningfulness of statistical comparisons, the networks of different subjects should have approximately the same number of edges. Further, they should be connected (Alexander-Bloch et al. 2010), *i.e.*, all nodes should be reachable from any other node through a path of edges. As the shape and mode of the connectivity metric distributions may differ between subjects, fixed thresholding may yield networks with a widely varying number of links and other network metrics (Hayasaka et al. 2010) which risks biasing the statistical comparisons. For example normalizing the subject-wise edge estimation metric distributions may help to balance this discrepancy.

Density-based thresholding guarantees a constant number of edges. However, it may sometimes leave some brain regions completely without connections or cause the network to fragment into more than one component especially for sparse, low-density networks (Alexander-Bloch et al. 2010, Kujala et al. 2016). Therefore, the degree of connectedness may vary between subjects and networks which also implies challenges in statistical comparisons and in the use of some graph algorithms.

Local thresholding

While global thresholding methods apply the same threshold to all of the edges in the network, local ones take into account the local neighborhood of the nodes allowing also weak edges in the neighborhoods where strong edges are not present. Local thresholding methods help to address these issues associated with number of edges and connectedness.

A maximum spanning tree (MST) may be used to make sure all nodes form one connected component (Alexander-Bloch et al. 2010, Alexander-Bloch et al. 2012, Glerean et al. 2016, Kujala et al. 2016). The connectedness ensured by including the MST helps avoid many computational problems of graph algorithms caused by isolated components and nodes (Kujala et al. 2016). The MST is built by iteratively adding the strongest link that is between nodes in two different connected components until all nodes are in the same component. The MST may still be enriched by adding more links until some predefined density is reached (Alexander-Bloch et al. 2010).

In addition to MST-based local thresholding, some studies have also used an even more strictly local scheme of including only a fixed fraction of each node's strongest neighbors and disregarding other links (Wang et al. 2016). This corresponds to thresholding each adjacency matrix row independently. However, this method may result in an unsymmetric adjacency matrix and, therefore, a directed network.

Independent of whether global or local thresholding is used, the value of the threshold is ultimately arbitrary. Therefore, examining the network and network properties across a range of thresholds has been encouraged (Rubinov et al. 2010, Power et al. 2011).

In this Thesis, both full unthresholded networks and density-thresholded networks are used. Some analysis requires all the nodes to form one connected component in which case the MST approach is used. The Methods section contains a more detailed description of the processing of the raw edge estimation metric matrices to obtain adjacency matrices for the different parts of the analysis.

2.3.5 Internal connectivity of a node

Unlike the nodes of many other networks, the ROIs of functional brain networks consist of various measurement units distributed in the 3D space that spans the brain. This characteristic gives rise to the concept of connectivity patterns also within a ROI, referred to as internal connectivity. This means that the voxel correlations within a ROI may exhibit rich spatially and temporally varying patterns (Korhonen et al. 2017, Ryyppö et al. in press).

As discussed in Section 2.3.2, the signal of a node is typically represented by averaging the signals of the voxels of the ROI. Averaging the signal has both advantages and disadvantages. Averaging may help to improve the signal-to-noise ratio (SNR), reduce computational cost, as well as battle multiple comparison problems in statistical testing (Korhonen et al. 2017, Gordon et al. 2014). However, we also risk losing information (Stanley et al. 2013) and if the ROI covers multiple functional regions, the final time series may not be representative of any of the real ROI dynamics (Shen et al. 2013). On the other hand, it has also been speculated that similarly to spatial smoothing, averaging the voxel signals within a ROI may help to amplify the shared components and suppress the individual voxel variation accounted largely to noise.

For the ROI to be well-defined and the ROI signal to be representative of the ROI dynamics, the voxels within a ROI should have similar behavior (Korhonen et al. 2017). Gordon et al. 2014 summarize the key assumptions that need to be fulfilled for a ROI parcellation to be accurate. The ROIs should be functionally homogeneous which may be measured by various alternative definitions. Functional homogeneity may imply a common functional connectivity pattern that spans through the entire ROI (Shen et al. 2013, Craddock et al. 2012), a high correlation coefficient between within-ROI voxel-pairs (Korhonen et al. 2017, Ryyppö et al. in press) or a similar functional profile of within-ROI voxels estimated through β-series of functional task contrasts (Thirion et al. 2006). These alternative definitions ultimately measure the

same phenomena but caution should be taken when comparing the results.

In addition to functional homogeneity, the resulting network structure should correspond to the known large scale cortical network structure of the brain (Power et al. 2011, Wig et al. 2011). Finally, the ROIs should also be consistent with the known cortical cytoarchitectonics and the network connectivity patterns should be reasonably consistent between individual subjects. This implies that despite the individual variability, it is possible to find a parcellation that is representative of the group-level tendencies (Gordon et al. 2014). In this Thesis we will focus on the assumption of homogeneity measured by within-ROI correlations and perform some comparisons of the inter-subject variation to validate the results.

Spatial consistency

Functional homogeneity of a ROI has previously been measured through spatial consistency which measures the amount of variation between the voxels in the ROI (Korhonen et al. 2017):

$$\phi_{spatial}(I) = \frac{1}{N_I(N_I-1)} \sum_{i,i' \in I} C(x_i(t), x_{i'}(t)), \tag{2}$$

where I is the set of voxels in the ROI, N_I the size of this set, *i.e.* the number of voxels, $x_i(t)$ and $x_{i'}(t)$ the time series of voxels i and i', and $C(x_i(t), x_{i'}(t))$ the PCC between these time series. Ultimately, this is the mean correlation between voxel pairs discarding the pairs of voxel and itself.

Theoretically, the range of consistency values is the same as for the correlation coefficient: between -1 and 1. However, a negative consistency would correspond to a situation with pairs of anti-synchronized and independent voxel signals which are unlikely and have not been observed in practice in the previous work (Korhonen et al. 2017, Ryyppö et al. in press). In general, spatial consistency values close to zero indicate low homogeneity and values close to 1 indicate high homogeneity. Later in this thesis we will refer to spatial consistency as static spatial consistency to mark the difference to the following consistency metrics.

While static spatial consistency measures the mean of the within-ROI correlation distribution, the overall shape of the distribution may also be of interest. Therefore, it may be meaningful to characterize the width of the distribution by a scatter functional. The width is measured by standard deviation of the within-ROI correlation distribution:

$$C_{SD}(I) = \sqrt{\frac{\sum_{i,i' \in I} \left(C(x_i(t), x_{i'}(t)) - \phi_{spatial}(I)\right)^2}{N_I(N_I-1)}}, \tag{3}$$

where $\phi_{spatial}(I)$ is the static spatial consistency, I the set of voxels in the ROI, N_I the size of this set i.e. the number of voxels, $x_i(t)$ and $x_{i'}(t)$ the time series of voxels i and i' and $C(x_i(t), x_{i'}(t))$ the PCC between these time series. Small values indicate a narrow distribution of within-ROI correlation where most voxel pairs within a ROI are either as highly or as weakly correlated. Large values, on the other hand,

indicate a large variance in the correlation values: while some within-ROI voxel pairs exhibit high correlation, there are also pairs that are only weakly correlated or even anti-correlated.

Spatiotemporal consistency

As discussed, in addition to the rich spatial structure within ROIs, the ROIs' internal structure has been demonstrated to vary in time (Ryyppö et al. in press) as well. These changes can be examined through the spatiotemporal consistency which measures the temporal variation of the spatial consistency in time windows (Ryyppö et al. in press):

$$\phi_{spatiotemporal}(I) = \frac{N_I(N_I - 1)}{2\sum_{t<t'} \frac{|\phi_{spatial}(I,t) - \phi_{spatial}(I,t')|}{\phi_{spatial}(I,t)}}, \tag{4}$$

where I is the set of voxels in the ROI, N_I the size of this set, *i.e.*, the number of voxels, and $\phi_{spatial}(I,t)$ and $\phi_{spatial}(I,t')$ are the spatial consistencies in time windows t and t'. Therefore, spatiotemporal consistency measures the inverse mean relative change in spatial consistency between all pairs of time windows. Small values of spatiotemporal consistency indicate a small relative change in time whereas large values indicate large relative variability. As a reverse of the mean relative change, spatiotemporal consistency is not confined to a certain range of values like the static spatial consistency. Therefore, the scale depends on the current data set and the scale should not be interpreted as absolute across data sets but the results should rather be considered relative to the other nodes in the same data set.

Computing spatiotemporal consistency requires a choice of a time window length and the amount of overlap between the time windows. Choosing the time window length and overlap is a non-trivial task that involves a trade-off between the number of time windows and their length. A longer time window provides more stable correlation estimates, increasing the robustness of the estimated consistency values and the network structure. However, longer time windows may risk missing some of the faster dynamic changes. Therefore, time windows must be long enough to reliably estimate the functional association but short enough to capture the temporal evolution of the network (Bassett et al. 2011). In addition, long time windows allow for fewer time windows along the duration of the scan which decreases the ability to estimate temporal variation (Bassett et al. 2011) and may, therefore, risk biasing the spatiotemporal consistency estimates. The number of time windows may be increased by increasing the overlap between time windows. However, for evaluating some changes in the network structure, a large overlap may be problematic. We have shown in our previous work that with a constant scan length, changing from 50% overlap and a small number of windows to a 1 TR shift and a large number of time windows qualitatively only changes the mode and location of the spatiotemporal consistency distribution while its shape remains qualitatively the same (Ryyppö et al. in press).

Self-link

Depending on the network extraction methods used, the level of internal connectivity of the ROI can also be quantified through the number or strength of within-ROI links observed in the voxel-level network underlying the ROI partition (Kujala et al. 2016). This property is referred to as self-link weight. The detailed definition depends on the exact link aggregation method. The computations carried out in this Thesis will be presented in more detail in the Methods section.

Interpretation and challenges related to internal connectivity

As discussed earlier, for a ROI to be well-defined, it needs to be functionally homogeneous with a high and stable consistency. However, it has been shown that the levels of consistency vary both between ROIs and within the same ROI over time (Korhonen et al. 2017, Ryyppö et al. in press). These changes have been suggested to have neurocognitive interpretations. For example regions exhibiting resting state functional connectivity are thought to be coactive, *i.e.*, both regions were activated simultaneously (Gordon et al. 2014). Therefore, when a ROI exhibits a high internal connectivity at a certain time, it could be deduced that the voxels within the ROI are coactive indicating that the ROI in itself would be activated and involved in the current task.

It has been suggested that low consistency may not always be an indication of a poorly defined ROI but it may also be indicative of the ROI and its voxels being idle during a certain task. Indeed, the functional homogeneity reflected in the local connectivity of a ROI may be linked to the neural activity in the region. This idea has also been investigated independently of the ROI framework by examining only the immediate neighborhood of each voxel and computing their regional homogeneity (ReHo) as a measure of activity (Zang et al. 2004, Jiang et al. 2016).

While high spatial consistency has been suggested to indicate that a ROI is well-defined, it has also been suggested that a wide correlation distribution within a ROI combined with a low spatial consistency value may indicate that the ROI consists of subregions that are internally highly correlated but weakly correlated with other subregions (Ryyppö et al. in press). It has been argued that these subregions may have an important role in the ROIs interactions with its different neighbors.

Many factors affect the homogeneity of a region. Consistency has been shown to be correlated with ROI size (Korhonen et al. 2017, Gordon et al. 2014) so the mere definition of ROIs and the imaging resolution of the fMRI data may affect the observed levels of consistency. Some regions such as subcortical regions suffer from poor signal-to-noise ratio in fMRI measurements due to their location deep in the brain (Glasser et al. 2016). For such regions the low homogeneity may also result from the low SNR instead of the ROIs being ill-defined (Gordon et al. 2014). However, some functional regions may also exhibit internal structure that explains low homogeneity. The topographic organization such as somatotopy of the somatosensory regions may be an example of such a structure (Gordon et al. 2014). It has also been hypothesized that division of an otherwise functionally uniform ROI to multiple subregions in some time windows may be due to the mechanisms it uses to connect

to its different neighbors at different times (Ryyppö et al. in press).

The challenges posed by the node definitions and their homogeneity assumptions have an effect on the acquired network structure (Wang et al. 2009, Zalesky et al. 2010). As brain networks are ultimately dynamic in nature, it has been suggested that it might not even be possible to find a static parcellation that would give an at-all-times accurate representation of the network nodes (Ryyppö et al. in press). Therefore, it has been advised that the internal connectivity and its variation over time should be taken into account when studying brain networks to account for the inaccuracy of the ROIs and their inhomogeneity (Ryyppö et al. in press).

3 Methods

3.1 Data

3.1.1 Subjects

An fMRI data set measured in-house at the AMI Centre (Aalto Neuroimaging, Aalto University, Espoo, Finland) was used in the analysis. The data set consisted of 13 subjects (7 female, 6 male, aged 28.70 $\pm$ 10.17 years, 12 right-handed, 1 left-handed). The data set was measured as a part of a music listening experiment comparing musicians and nonmusicians and has previously been analyzed by Alluri et al. 2015, Alluri et al. 2017, Burunat et al. 2015. The subjects included in this analysis were all considered nonmusician as they had not had any formal musical training.

An informed consent was signed by all participants at their arrival to the laboratory. The participants received a compensation for their participation and use of time. All experimental procedures carried out for this study, included in the broad research protocol called Tunteet, were approved by the Coordinating Ethics Committee of the Hospital District of Helsinki and Uusimaa (the approval number 388 315/13/03/00/11, obtained on March the 11th, 2012). All experimental procedures were conducted in agreement with the ethical principles of Declaration of Helsinki.

3.1.2 Data acquisition

The fMRI data were measured at the AMI Centre (Aalto Neuroimaging, Aalto University, Espoo, Finland) using a 3T MAGNETOM Skyra MRI scanner (Siemens Healthcare, Erlangen, Germany) with a standard 32-channel head-neck coil. The functional data was measured using a T2*-weighted whole-brain echo-planar imaging (EPI) sequence with the following parameters: TR = 2 s, 33 oblique slices, TE = 32 ms, flip angle 75 °, voxel size $2 \times 2 \times 2$ mm^3, FOV = 192×192 mm^2, matrix size 64×64. In addition an anatomical image of the subject's brain was acquired by measuring a T1-weighted image with the following parameters: 176 slices, FOV = 256×256 mm^2, matrix size = 256×256, slice thickness = 1 mm.

3.1.3 Stimuli

During the measurement the subjects listened to the Adios, Nonino tango piece by Astor Piazzolla as a musical stimulus. The total duration of the piece and the functional sequence was 8.13 minutes (244 samples). The subjects were instructed to fix their gaze in the center of the screen during the scan. The music was played from MRI-compatible headphones and the noise of the scanning gradients was isolated by foam.

3.1.4 Preprocessing

FSL software (www.fmrib.ox.ac.uk, version 5.0.9) and custom in-house MATLAB code pipeline (BRAMILApipeline v2.0, available at https://version400.aalto.fi/gitlab/BML/bramila) were used to preprocess the data. Standard preprocessing steps were followed in the process. The EPI slice time differences were corrected and head motion correction was performed using MCFLIRT. In order to deal with the inter-subject anatomy differences the volumes were coregistered to the Montreal Neurological Institute (MNI) 152 2 mm standard template. This was done in a two-step procedure that included registering the functional EPI volumes to the participant's anatomical image (9 degrees of freedom) and then registering the anatomical image to the standard MNI template (12 degrees of freedom). Scanner drift was corrected for by applying a 240-seconds long Savitzky-Golay filter (Çukur et al. 2013) and the BOLD time series was filtered with a Butterworth bandpass filter at 0.01-0.08 Hz. No spatial smoothing was applied as it has been shown to be problematic in the context of network and connectivity studies (Alakörkkö et al. 2017). For additional motion and artefact control, the BOLD signal was cleaned by regressing out 24 motion-related regressors as well as signal from the deep white matter, the ventricles and the cerebrospinal fluid (Power et al. 2012).

For computational efficiency, the data was downsampled from 2 mm resolution to 4 mm. Group masks were created by applying the analysis masks from all subjects in order to secure that only in mask voxels with meaningful signal were included. Also voxels with more than 70% of their signal explained by motion or signal from other tissues than the gray matter were excluded.

3.2 Network extraction

3.2.1 Edge definitions

The Pearson correlation coefficient (PCC) between time series was used as the edge estimation metric. As discussed in Section 2.3.3, the Pearson correlation coefficient is the most frequently used metric for functional connectivity estimation. It is also conceptually simple and easy to interpret. The PCC was computed as the sample Pearson correlation coefficient:

$$r = \frac{\sum_{t=1}^{T}(x_t - \bar{x})(y_t - \bar{y})}{\sqrt{\sum_{t=1}^{T}(x_t - \bar{x})^2}\sqrt{\sum_{t=1}^{T}(y_t - \bar{y})^2}}, \tag{5}$$

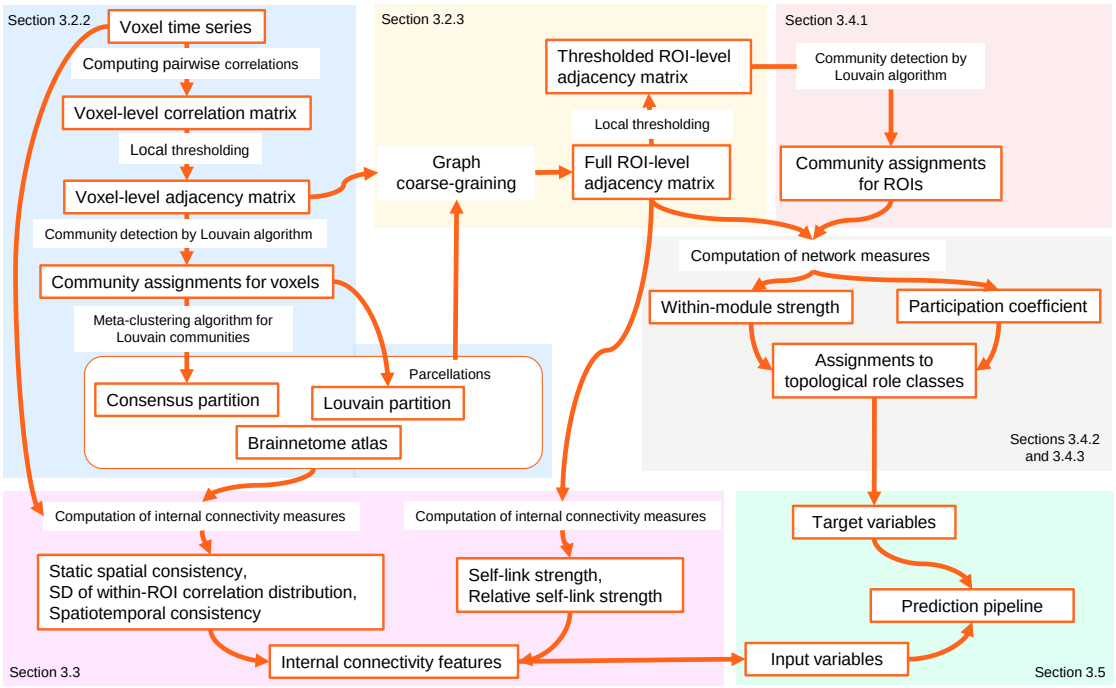

Figure 2: Flowchart of the analysis pipeline.

where T is the length of the time series, x_t and y_t are the node time series values at time t, and $\bar{x} = \frac{1}{T}\sum_{t=1}^{T} x_t$ and $\bar{y} = \frac{1}{T}\sum_{t=1}^{T} y_t$ are the sample means of the time series.

3.2.2 Node definitions

Data-driven Louvain partitioning

The network nodes were extracted following the framework introduced by Kujala et al. 2016 with some small adjustments. In order to acquire a set of data-driven nodes, a voxel-level network was formed by computing the Pearson correlation coefficient matrix between all possible voxel pairs. Given the group mask estimated as a part of the preprocessing, all in-mask voxels were included in the correlation matrix (see Section 3.1.4 for details on voxel exclusion criteria). This yielded one 23837×23837 matrix for each subject. These full correlation matrices were thresholded using a double layered thresholding scheme. First only 0.05% of the strongest neighbors of each node where included, the rest of the PCC were set to zero (Wang et al. 2016), and the matrix was made symmetrical by computing its sum with its transpose. Then the matrix was subjected to a local thresholding scheme where we first built a maximum spanning tree (MST) of the network and then added the strongest remaining links until a density of 0.01% was reached. This way the resulting network was guaranteed to be connected.

The nodes of this voxel-level network were then divided into modules using the Louvain algorithm (Blondel et al. 2008) in order to form subject-wise ROI partitions. The algorithm aims at maximizing modularity and its process consists of two phases

that are iterated until the modularity cannot be improved further. The first phase constitutes initialization by placing each node in its own community thus yielding N communities at first iteration. Each node i is then examined iteratively by looking at its neighbors and moving i to the community of its neighbor j that gives a maximum gain in modularity. If no community change yields a positive gain, the community assignment of i remains unchanged and the next node is taken under examination. The nodes' turns to be examined are iterated as long as some improvement in modularity is achieved. Once the local maxima is reached and the modularity can no longer be increased, the algorithm carries out the second phase of aggregating the network over the communities. A new network is formed with the communities from the first phase acting as nodes and the numbers of links between and within communities acting as link weights between these new nodes. The first phase is then repeated for this new network again until no further improvement in modularity can be achieved. These two phases are repeated until the modularity does not improve.

The algorithm is greedy and stochastic in nature which implies that the algorithm risks getting stuck at a local maxima while missing the global one. Therefore, we are not guaranteed to get the best result nor the same result every time. To avoid the local optima problem, the algorithm was repeated 50 times and the partition with the maximum modularity was chosen as the best partition. These subject-wise partitions were included in the analysis and will later be referred to as Louvain partitions.

Data-driven consensus partitioning

The obtained Louvain communities naturally differ between subjects. In order to achieve one comparable partition, a consensus partition was computed over the set of subjects and their iterations of the Louvain algorithm. This partition scheme aims at summarizing a set of partitions in a way that the final summary partition is maximally representative of the original set of partitions. Here a meta-clustering algorithm (MCLA) was used to compute the consensus partition (Strehl et al. 2002). The algorithm forms a new network from a set of subject-wise partitions with the detected communities acting as nodes. The connections between the communities are defined based on the similarity of voxels belonging to each community measured by the Jaccard index. The network partitioning algorithm METIS (Karypis et al. 1998) was then used to partition the network into meta-clusters and to assign each voxel-node into the meta-cluster to which it most consistently belongs. This yielded a final consensus partition with each voxel assigned to one community or parcel. These parcels of the consensus partition were then used as nodes of the final estimated functional brain network.

Brainnetome atlas

The Brainnetome atlas (Fan et al. 2016) was used as an alternative way of defining the nodes for comparison with the data-driven nodes. The Brainnetome nodes are based on structural and functional connectivity measured noninvasively with multimodal neuroimaging techniques. The atlas comprises a total of 246 nodes all of which were present in our subject population with good enough a signal quality

(see Section 3.1.4 for more details about voxel exclusion criteria). Out of these ROIs 210 covered the cerebral cortex while the remaining 36 ROIs were located in the subcortical gray matter. Cerebellum was not included in this atlas. After exclusion of some voxels (see Section 3.1.4) our final parcellation included ROIs of sizes in the range from 3 to 168 voxels (63.6 ± 33.4, mean $\pm$ STD, 60 median).

3.2.3 Network connectivity estimation through graph coarse-graining

The final network was formed by aggregating voxel-level connections over the partitions described in previous sections. This framework is referred to as graph coarse-graining (Kujala et al. 2016). The initial voxel-level network was built as described in Section 3.2.2. The voxel-level correlation matrix was estimated using the Pearson correlation coefficient and this network was thresholded by forming an MST and adding links until 0.01% density. The network was binarized so that no edge strengths were included.

The final network was formed by considering the ROI partitions described in Section 3.2.2 and counting the number of voxel-level links between each pair of ROIs and within a ROI. Thus, the weight of a link comprises the number of links between ROIs. This full untresholded network was then locally thresholded by building an MST and adding edges until the density of 2%. The remaining edges in this thresholded network were binarized to form an unweighted network. Both the full unthresholded network and the thresholded and binarized network were used in later analysis.

3.3 Internal connectivity

3.3.1 Static spatial consistency

The static functional homogeneity of the node was measured by static spatial consistency as introduced in Equation (2) (see Section 2.3.5 and Korhonen et al. 2017 for more details) and in addition the standard deviation of the within-ROI correlation distribution was computed following the Equation (3).

This yielded a spatial consistency estimates over the whole time series for each ROI of each subject.

3.3.2 Spatiotemporal consistency

Temporal variation of the functional homogeneity was measured through spatiotemporal consistency. In order to evaluate the spatiotemporal consistency of the nodes, the spatial consistency was computed in time windows. Time window length of 80 samples corresponding to 160 seconds of scan time was used. In the scope of this Thesis we do not compute any time window-wise network measures that would be sensitive to the amount of overlap. Therefore, we chose to use time windows with 1 repetition time (TR) shift yielding a total of 165 time windows. As discussed in Section 2.3.5, the choice of overlap did not qualitatively affect our spatiotemporal consistency results in our previous work (Ryyppö et al. in press). The time window

length was also previously validated for this data set and this choice of 80 samples corresponded to a window length where the consistency values of different subjects had saturated to an approximately constant level. A similar number of samples per time window has been used in earlier literature (Bassett et al. 2011, Bassett et al. 2013). The spatiotemporal consistency was then computed as shown in Equation (4) (see Section 2.3.5 and Ryyppö et al. in press for more details).

This measure is aggregated across time windows, so a value for each ROI of each subject was acquired.

3.3.3 Self-link weight

The Self-link weight of a node was computed as the number of voxel-level links within a ROI in the voxel-level network underlying the ROI partition. Here the same voxel-level network was used as for the consensus partition based node definitions (see Section 3.2.2). The voxel-level network was locally thresholded to the density of 0.01%. The self-link was then computed as

$$c_I = \frac{1}{2} \sum_{i \neq i' \in I} A(i, i'), \tag{6}$$

where I is the set of voxels belonging to a ROI and A is the adjacency matrix of the voxel-level network. This is equivalent to the Ith diagonal element of the coarse-grained network.

In order to normalize the metric we also computed relative self-link weight by dividing the self-link by the sum of the other links the ROI has in the coarse-grained network:

$$c_{I_{rel}} = \frac{A_c(I, I)}{\sum_{I=1}^{N_c} A_c(I, J)}, \tag{7}$$

where A_c is the adjacency matrix of the coarse-grained network and N_c is the number of nodes in the coarse-grained network. The nominator equals the strength of node I.

3.4 Topological roles in the network

Here we followed a framework developed by Guimera et al. 2005b to classify the nodes into system-independent universal roles i.e. topological roles. The framework is based on the notion that in a network with a community structure, nodes that have similar topological roles also have similar topological properties such as centrality and distribution of links (Guimera et al. 2005a, Guimera et al. 2005b). The used topological properties reflect the node's role both in its community and in relation to the other communities.

3.4.1 Community detection

In their framework Guimera et al. 2005b used simulated annealing to detect communities in the network. Here we chose to use the Louvain algorithm that has been

described in more detail in Section 3.2.2. The coarse-grained network of each subject was used as a starting point and the Louvain algorithm was iterated 50 times for each subject. The best partition, *i.e.*, the partition with the highest modularity was chosen as the final community structure. While the exact algorithm differed from the original framework, both algorithms aim to maximize modularity and with enough iterations, the Louvain algorithm can be assumed to provide similar results.

3.4.2 Properties defining the topological role

Once the community structure of the network was defined, two relatively simple metrics were computed. Guimera et al. 2005b use network properties defined for unweighted networks. The coarse-grained networks used in this Thesis are weighted and as the weights carry important information, we wish to avoid binarizing and thresholding the network. Therefore, the measures used by Guimera et al. 2005b have been adapted for weighted networks by examining the node strength rather than degree.

Within-module strength

Within-module strength z measures the level of connectedness that a node has to the other nodes within its community. Mathematically, the within-module strength was computed as follows (adapted from Guimera et al. 2005b, Guimera et al. 2005a):

$$z_i = \frac{\kappa_i - \bar{\kappa_{s_i}}}{\sigma_{\kappa_{s_i}}}, \tag{8}$$

$$\kappa_i = \sum_{i' \in s_i} A_c(i, i'), \tag{9}$$

where A_c is the adjacency matrix of the coarse-grained network, s_i is the set of nodes in the same community as the node i, κ_i is the within-module strength of node i, $\bar{\kappa_{s_i}}$ the mean within-module strength of nodes in module s_i and $\sigma_{\kappa_{s_i}}$ is the standard deviation of the within-module strength of the nodes in module s_i. This can be viewed as a z-score as it is normalized by the mean and standard deviation of the within-module strength. Large values indicate that the node is well-connected within its community whereas small values show low level of connectivity.

Participation coefficient

The participation coefficient P measures the level of distribution of a node's links among all the communities in the network (adapted from Guimera et al. 2005b, Guimera et al. 2005a):

$$P_i = 1 - \sum_{s=1}^{N_M} \left(\frac{\kappa_{is}}{k_i} \right)^2, \tag{10}$$

where N_M is the total number of modules, κ_{is} is the total strength of links that node i has to the nodes in module s and k_i is the total strength of node i. Values close

to 1 indicate a uniform distribution of links among all communities whereas values close to 0 indicate majority of the links being within the node's own community.

3.4.3 Classification into topological roles

Within-module strength and the participation coefficient set a 2D space spanned by the different values these measures exhibit. This 2D space may be heuristically divided into subregions, each of which represents its own universal or topological role (see Fig. 3, for more details on the exact thresholding and division in the original framework see Guimera et al. 2005b). The space was divided into seven subregions representing four kinds of non-hub nodes and three kinds of hub nodes. The groups comprised ultra-peripheral nodes (R1), peripheral nodes (R2), non-hub connector nodes (R3), non-hub kinless nodes (R4), provincial hubs (R5), connector hubs (R6) and kinless hubs (R7) (see Fig. 3, Guimera et al. 2005b).

Instead of fixed heuristic thresholds we rather chose to limit the groups by percentiles of the data to make sure that the limits accounted for the characteristic scales of this data set. The division into hubs (R5, R6 and R7) and non-hubs (R1, R2, R3, R4) was done based on the within-module strength z. In this work a threshold of 45th percentile was used so that nodes with $z \geq$ 45th percentile were classified as hubs and nodes with $z <$ 45th percentile as non-hubs.

These two groups were then further divided based on their participation coefficients P ranging from the ultra-peripheral nodes and provincial hubs with a low participation coefficient to non-hub kinless nodes and kinless hubs with high participation coefficient. Within non-hubs, the thresholds were $P \leq$ 5th percentile for ultra-peripheral nodes, 5th percentile $< P \leq$ 60th percentile for peripheral nodes, 60th percentile $< P \leq$ 80th percentile for non-hub connectors and $P >$ 80th percentile for non-hub kinless nodes. Within hubs the thresholds were $P \leq$ 30th percentile for provincial hubs, 30th percentile $< P \leq$ 75th percentile for connector hubs and $P >$ 75th percentile for kinless hubs.

Guimera et al. 2005b use a global thresholding scheme in their work indicating that the same heuristic thresholds are applied on all nodes in the network. However, as discussed in Section 2.1.5, especially in brain networks it may be more interesting to examine the node's topological differences in relation to the other nodes in its community rather than in relation to the whole network (Chan et al. 2017). Therefore, we computed the topological role group assignments of nodes using both global percentile limits and community-wise percentile limits. These assignments will later be referred to as global and community-wise topological roles.

As a result each node got a class label indicating its topological role in the network at both the global and community level. Later, we examine the differences between hub and non-hub nodes as well as provincial and connector hubs. Also multi-class differences between all seven groups are briefly addressed.

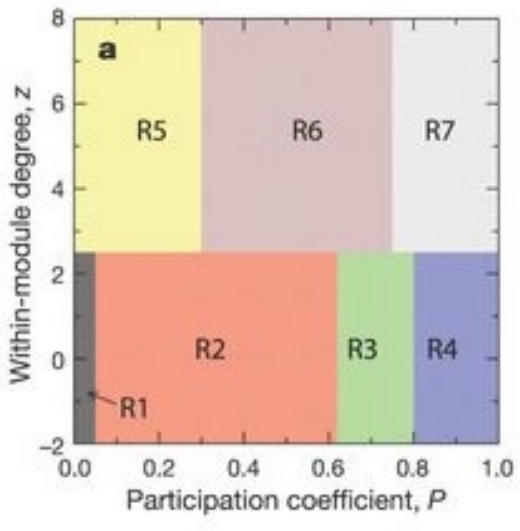

Figure 3: Topological role classes in the space spanned by participation coefficient P and within-module strength z. Adapted from Guimera et al. 2005b.

3.5 Topological role prediction using internal connectivity

3.5.1 Predictive models

Logistic ridge regression

Logistic regression (James et al. 2013) was used to perform two-class classification tasks. Logloss was chosen as the cost function and the model was fitted using the gradient descent algorithm. Step size was set to $\alpha = 0.00001$ and stopping criterion was defined as having less than 10^{-8} of a relative improvement in the cost function value between consecutive iterations. The maximum number of iterations was set to 10^7. The final model weight coefficients $\boldsymbol{w}$ were acquired as the values at last iteration before the convergence criterion was met. In addition to the stopping criterion, it was graphically confirmed that the cost function converged during training.

The probability of the observation belonging to group 1 was computed as

$$P(y = 1|\boldsymbol{w}, \boldsymbol{x}) = \frac{1}{1 + e^{w_0 + \sum_{i=1}^{d} w_i x_i}}, \tag{11}$$

where w_0 is the model coefficient for the intercept, w_i the model coefficient corresponding to the variable i, x_i the value of the variable i for observation $\boldsymbol{x}$ and d the dimensionality of the data.

For the final classification, a probability threshold of 0.5 was used so that observations with $P(y = 1|\boldsymbol{w}, \boldsymbol{x}) > 0.5$ were classified as class 1. The model performance was evaluated by 10-fold cross-validation where 20% of the training set was sampled to be used as validation set and the model of the fold was trained on the remaining 80% of the training data. The final performance was measured by average classification accuracy across the 10 folds.

The model was first trained using all five internal connectivity features: static spatial consistency, standard deviation of the within-ROI correlation distribution, spatiotemporal consistency, self-link weight, and relative self-link weight as well as ROI size. In order to examine the effect of ROI size, a second model was trained without ROI size and self-link weight which is directly constrained by ROI size.

Linear discriminant analysis

Linear discriminant analysis (LDA) was used to perform multi-class classification. The implementation of Python library scikit-learn (Pedregosa et al. 2011) was used to run the model fitting and predictions. Model training was performed using 80% of the whole sample and the model performance was evaluated as classification accuracy on the remaining 20% of the data. Similarly as with logistic regression, two models were trained with the first one including all five internal connectivity measures and ROI size and the second one excluding ROI size and self-link weight.

Baseline classifier

The model performance was compared to a baseline classifier where each observation was directly classified to the majority class of the training data set (Pedregosa et al. 2011). This method takes into account the distribution of the classes in the data set but does not take into account the values of model covariates. Therefore, it is an estimate of a sophisticated random guess.

3.5.2 Classification tasks

Classification to hubs and non-hubs

First performed classification task was separating hub nodes from non-hub nodes. To create a target variable, ROIs were divided into hubs and non-hubs so that groups 5, 6 and 7 were considered hubs and groups 1, 2, 3 and 4 were considered non-hubs (see Fig. 3). A logistic regression model was trained to perform the classification (see Section 3.5.1 for more details on model training).

Classification to provincial and connector hubs

In order to perform classification between provincial and connector hubs, the non-hub nodes of groups 1, 2, 3 and 4 were discarded. In addition, the group 7 of kinless hubs was also discarded in order to keep the sample sizes between groups reasonably even. The final classification was, therefore, performed between group 5 of provincial hubs and group 6 of connector hubs. A logistic regression model was trained and used for the classification task (see Section 3.5.1 for more details on model training).

Multi-class classification

For comparison, a model was also trained to perform a multi-class classification task where the seven original groups were directly used as the target variable. Here a

linear discriminant analysis (LDA) model was trained and the model performance was evaluated by multi-class classification accuracy (see Section 3.5.1 for more details on model training).

4 Results

4.1 Parcellations

The data-driven Louvain partition resulted in an individual parcellation for each subject. The average number of ROIs in these parcellations was 137.6 ± 5.62 (mean $\pm$ SD, min 123, max 146). The parcellation of an example subject is shown in Fig. 4A. The ROI sizes exhibit some variation across parcellations of individual subjects (Fig. 5). However, the number of ROIs and their size distribution can be considered reasonably similar across subjects and the results can, therefore, be regarded as comparable.

Using these subject-wise Louvain partitions as an input to meta-clustering resulted in a consensus partition with 129 ROIs (Fig. 4B). As this parcellation represents the agreement across subjects, this parcellation is shared across the whole subject population. The average size of a ROI was 183.3 ± 113.3 (mean $\pm SD$, min 16, max 542).

After applying the group-level mask, the Brainnetome atlas consisted of 246 ROIs with average size of 63.6 ± 33.4 (mean $\pm$ STD, min 3, max 168, see Fig. 4C).

The quality of the parcellations was first examined visually (see Fig. 4). Both data-driven parcellations suffer from fragmentation of larger ROIs into many smaller parts scattered across the brain making many of the ROIs non-contiguous. This problem appears to be more severe for the consensus partition than for the subject-wise Louvain partitions. Fragmentation is especially evident for the subcortical regions which suggests that it may also partly be explained by poor data quality. Subcortical regions are known to have a poorer signal-to-noise ratio than other brain regions (Glasser et al. 2016). The larger fragmentation of the consensus partition is also likely to be partly explained by the variation observed across subjects in both brain anatomy and the functional localization. Unlike the data-driven partitions, the Brainnetome atlas does not exhibit visible spatial fragmentation of ROIs.

These results show that the Brainnetome parcellation has less variable ROI size than the data-driven parcellations. The ROIs are also smaller on average which is a natural consequence of its larger number of ROIs. This discrepancy in the number of ROIs and ROI sizes may explain some of the varying patterns in computed measures and affect the comparability of results across different parcellations. We tried to increase the number of ROIs in the Louvain partition and consensus partition as well. However, decreasing the density threshold of the voxel-level adjacency matrix further caused the Louvain clusters to fragment into a couple of large ROIs and many very small ROIs of only a couple of voxels. Increasing the number of target clusters in the consensus partition resulted in either a few very large ROIs and many extremely small ROIs or relatively equal-sized but extremely fragmented ROIs depending on the network density used for the Louvain partitioning.

The criteria of grouping voxels together in the Louvain clustering is maximizing the modularity which implies stronger correlations between the voxels within a ROI than between voxels in different ROIs. In functional brain networks, the functional relationship between nodes is assumed to be expressed as a high correlation

coefficient. The Louvain algorithm treats the high correlations equally, independently of whether they are a product of neighboring voxels performing the same dynamics as a part of a brain region or whether they are a result of two far-away brain regions interacting through some of their voxels being functionally connected. Fragmented ROIs may actually consist of interacting voxels that belong to different brain regions. Constraining the voxel-level correlation matrices by neighborhood size (Craddock et al. 2012) or spatial distances between voxels (Wang et al. 2016) may help to avoid ROI fragmentation and increase ROI contiguity. It may also be interesting to examine approaches developed specifically for module detection in spatial networks (Expert et al. 2011).

The problems with increasing the number of ROIs in the consensus partition are not very surprising given that the framework has previously been used to find consensus partitions of considerably fewer nodes (Kujala et al. 2016).

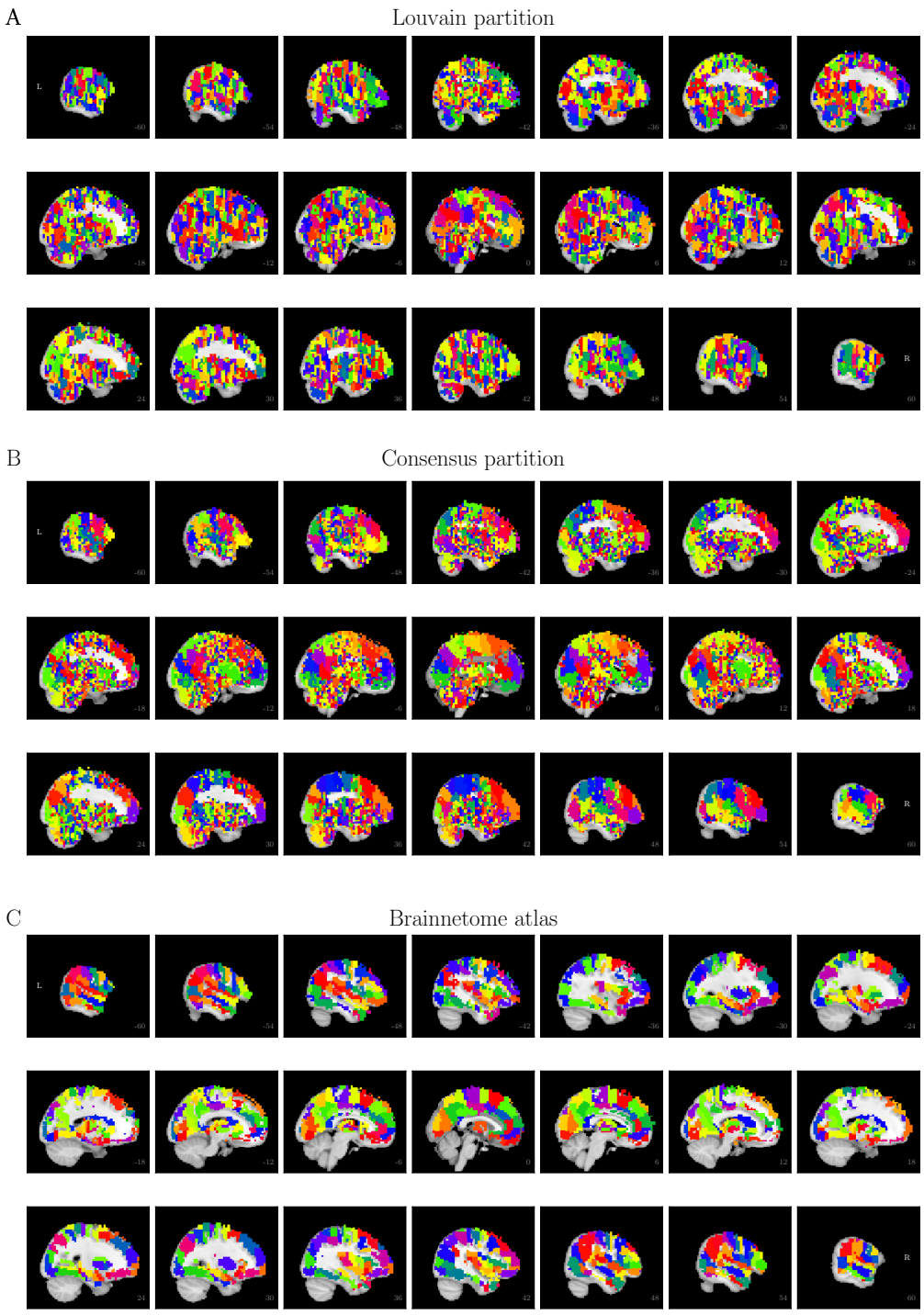

Figure 4: The parcellations used as node definitions of functional brain networks. A) The Louvain partition of an example subject shows that while there are some ROIs that appear spatially contiguous, there are also ROIs that are spatially scattered around the brain. Especially subcortical regions exhibit spatially scattered ROIs. B) The consensus partition shows that some parts of the brain exhibit shared group-level tendencies of larger spatially contiguous ROIs while some areas consist of spatially non-contiguous and scattered ROIs. This non-contiguity is observed especially in subcortical regions. C) The Brainnetome atlas exhibits more equally sized and spatially more contiguous ROIs than the data-driven parcellations.

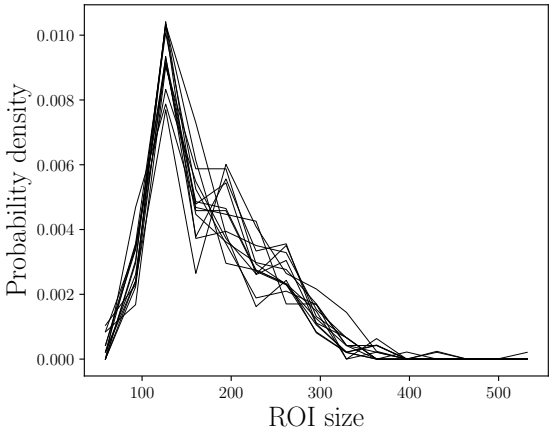

Figure 5: ROI size distributions of the subject-wise Louvain partitions of the 13 subjects that were examined in the study. The distributions are similar across subjects.

4.2 Internal connectivity

Internal connectivity was measured by five metrics: static spatial consistency, standard deviation of the within-ROI correlation distribution, spatiotemporal consistency, self-link weight and relative self-link weight (see Section 3.3 for detailed definitions). In addition, we compare the ROI size distributions pooled across subjects.

Static spatial consistency

Static spatial consistency peaks at relatively low values (Fig. 6A; mode of the distribution, Louvain partitions 0.029; consensus partition 0.029; Brainnetome 0.079). However, there are also ROIs with high static spatial consistency (Fig. 6A; maximum of the distribution, Louvain partitions 0.699; consensus partition 0.348; Brainnetome 0.522). The Brainnetome atlas exhibits more ROIs with higher values than the data-driven partitions. However, the Louvain partition has the largest maximum value of the static spatial consistency.

Static spatial consistency measures the average correlation inside a ROI. Both data-driven partitions show a visibly weaker static spatial consistency than the Brainnetome atlas. As the Louvain algorithm is expected to group together voxels that are densely interconnected, we expect to see many above-threshold links among these groups of voxels. The links that remain after thresholding are mostly strong links with a relatively high correlation value. Therefore, the low static spatial consistency values are rather surprising for the Louvain partition. On the other hand, the binarized and thresholded nature of the voxel-level adjacency matrix implies that the weight information is not available to Louvain algorithm and it treats all above-threshold links equally. This may explain why the Louvain communities do not result in high levels of static spatial consistency. The poor static spatial consistency of consensus partition may also be partly accounted for the large variation across Louvain partitions of different subjects. In addition, spatial fragmentation of ROIs may also partly account for the poor consistency of data-driven partitions as spatially adjacent voxels are more likely to be highly correlated.

However, it should be noted that the most spatially consistent ROIs in the Louvain partition are more spatially consistent than the most consistent ROIs in the Brainnetome atlas. The quality of the partitions and the validity of the internal connectivity assumptions is discussed in more detail in Section 5.1.

Standard deviation of the within-ROI correlation distribution

The standard deviation of the within-ROI correlation distribution exhibits a peak in the mid-range values between 0.05 and 0.35 with only a few ROIs showing a low or high value (Fig. 6B; mode of the distribution, Louvain partitions 0.167; consensus partition 0.144; Brainnetome 0.191). Brainnetome exhibits slightly wider distributions of within-ROI correlation than the other two parcellations while the within-ROI distributions of consensus partition tend to be the narrowest.

Spatiotemporal consistency

The distributions of spatiotemporal consistency (Fig. 6C) are relatively similar across parcellations and qualitatively similar to the results of our previous work (Ryyppö et al. in press). Nevertheless, all parcellations exhibit variation between ROIs which supports the notion that there are dynamical temporal changes in the levels of spatial consistency.

Self-link weight

The self-link weight peaks at very small values (Fig. 6D; mode of the distribution, Louvain partitions 86.1; consensus partition 28.7; Brainnetome 28.7) but the maximum values of the distributions are very large (Fig. 6D maximum of the distribution, Louvain partitions 2200; consensus partition 639; Brainnetome 2295). This is explained by the values being directly constrained by ROI size: the maximum number of links within a ROI is limited by the number of unique voxel pairs of the ROI. Therefore, comparison between parcellations may be biased by the differing ROI sizes.

Relative self-link weight

The relative self-link weight exhibits relatively large differences between the three parcellations. While maximum values are relatively similar (Fig. 6E; maximum of the distribution, Louvain partitions 0.859; consensus partition 0.641; Brainnetome 0.563), the modes of the distributions differ notably (Fig. 6E; mode of the distribution, Louvain partitions 0.577; consensus partition 0.067; Brainnetome 0.118).

The Louvain partition exhibits the highest level of relative self-link weight while the relative self-links of Brainnetome are the weakest. The Louvain partition is formed by Louvain clustering algorithm that aims to maximize modularity and as a result encourages voxel-level links within a ROI and discourages links between ROIs. Therefore, the algorithm is rather directly optimizing relative self-link weight making the observed result very logical. The consensus partition, however, exhibits only slightly higher values of relative self-link weight than Brainnetome. While the consensus partition is based on the individual Louvain partitions, optimizing the ROI assignment of each voxel across the subjects is sensitive to variation between subjects. This likely reduces the relative self-link weight in the consensus partition.

ROI size

ROI size distributions are described in more detail in Section 4.1. Here we visualize the ROI size distribution pooled across all subjects (Fig. 6F; mode of the distribution, Louvain partitions 130.4; consensus partition 203.2; Brainnetome 57.6). As discussed in Section 4.1, the ROI size in Brainnetome exhibits the least variation while the ROI size distribution of the consensus partition is the widest.

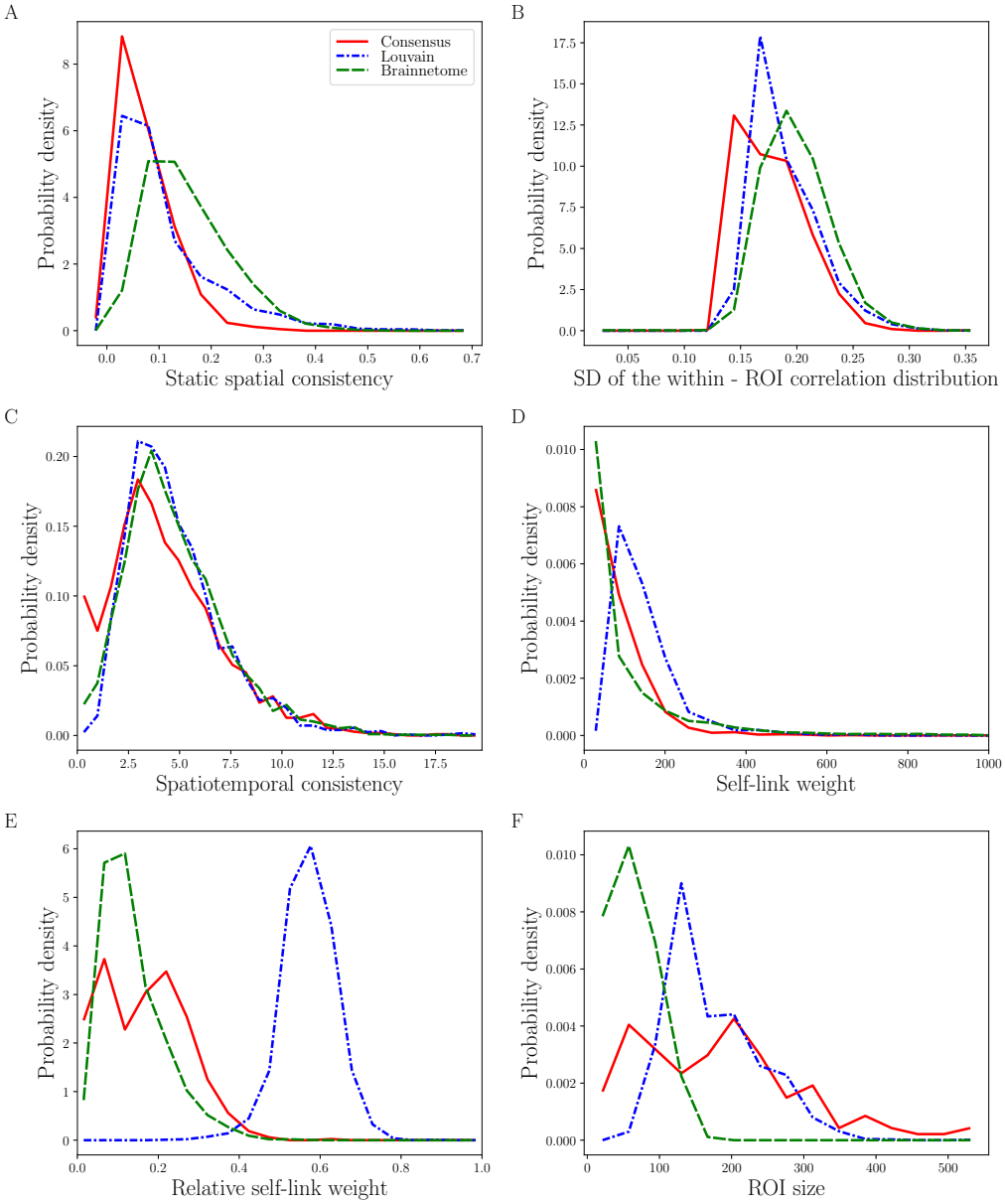

Figure 6: Internal connectivity features exhibit variation between parcellations and ROIs. A) Static spatial consistency distributions for the three examined parcellations. Static spatial consistency is considerably lower in the data-driven partitions than in the Brainnetome atlas. B) Distribution of standard deviation of within-ROI distribution visualized for different parcellations. The within-ROI correlation distributions are wider in the Brainnetome atlas and narrower in the Louvain partition. C) Spatiotemporal consistency distributions of the three examined parcellations are qualitatively similar. D) Self-link weight distributions of the three parcellations peak at low values while also exhibiting a long tail. The Louvain partition in general exhibits higher levels of self-link weight than Brainnetome atlas and consensus partition. E) Relative self-link weight of the three parcellations differs visibly. Louvain partition exhibits considerably higher relative self-link weight than other parcellations. F) ROI size distribution of different parcellations shows that the data-driven parcellations consist of larger ROIs than the Brainnetome atlas. All of the shown distributions are pooled across 13 subjects.

4.3 Topological roles

Topological roles were defined by computing two topological role metrics: within-module strength and participation coefficient. The ROIs were then classified into topological role classes based on their position in the two-dimensional space spanned by these two metrics (see Section 3.4.3 for details).

Within-module strength

The distributions of within-module strength were similar across partitions with the peak close to the value of zero (Fig. 7A; mode of the distribution, Louvain partitions -0.575; consensus partition -0.575; Brainnetome -0.575). This is likely explained by the normalized nature of the metric (see Section 3.4.2 for details). However, each parcellation also exhibits variation across ROIs making the metric able to capture the scale of topological differences between ROIs.

Participation coefficient

Participation coefficient exhibits differences between parcellations with a relatively large difference even in the modes of the distributions (Fig. 7B; mode of the distribution, Louvain partitions 0.575; consensus partition 0.880; Brainnetome 0.697). Brainnetome shows the widest distribution whereas the participation coefficient of the Louvain partition and the consensus partition exhibits a relatively narrow peak around the most typical values (Fig. 7B; SD of the distribution, Louvain partitions 0.103; consensus partition 0.105; Brainnetome 0.212). These differences could be explained by differences in the level of modularity of the brain network built from different parcellations. Especially in consensus partition, most nodes seem to have a very even distribution of links among the different modules which may raise questions on the mere existence of modules in the network. This supports the notion that ROI definitions have an important effect on the structure and characteristics of functional brain networks.

Classification into topological role groups

The two-dimensional space spanned by within-module strength and participation coefficient was used to classify the ROIs into seven topological role classes based on heuristically defined percentile thresholds. Two versions of the role classifications were computed one with the percentile thresholds defined locally within each module (shown in Fig. 8) and one with the thresholds defined globally from the whole network.

In the local topological role assignments the borders between classes are defined individually for each module and therefore we do not observe clear global borders in the assignments (Fig. 8). However, group-wise tendencies in the typical location and the amount of scatter are clearly visible.

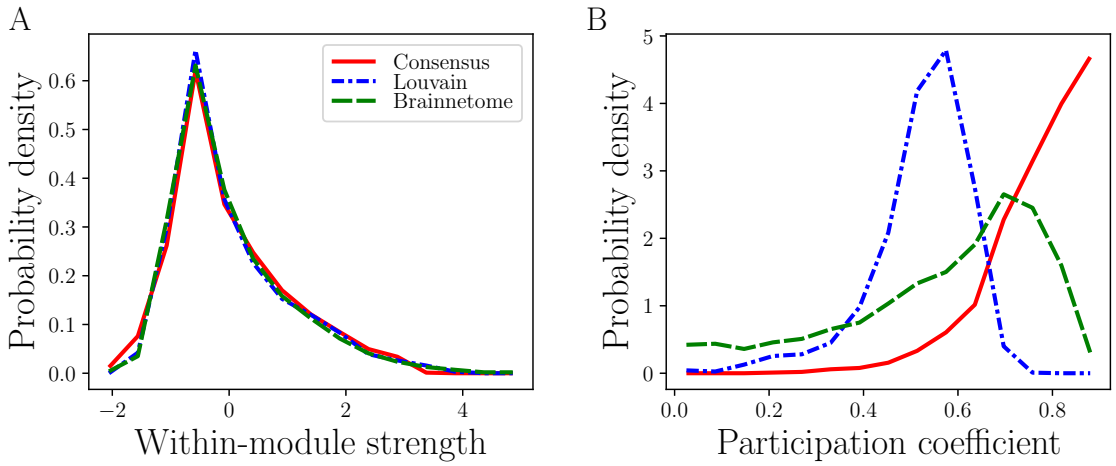

Figure 7: Topological role measures A) Within-module strength distributions of the three examined parcellations do not differ from each other considerably but values vary within parcellations for different ROIs. B) Participation coefficient shows differences across the three examined parcellations. The consensus partition shows the largest values while the Louvain partition exhibits a relatively narrow peak at lower values and the Brainnetome atlas exhibits the widest distribution. All of the shown distributions are pooled across 13 subjects.

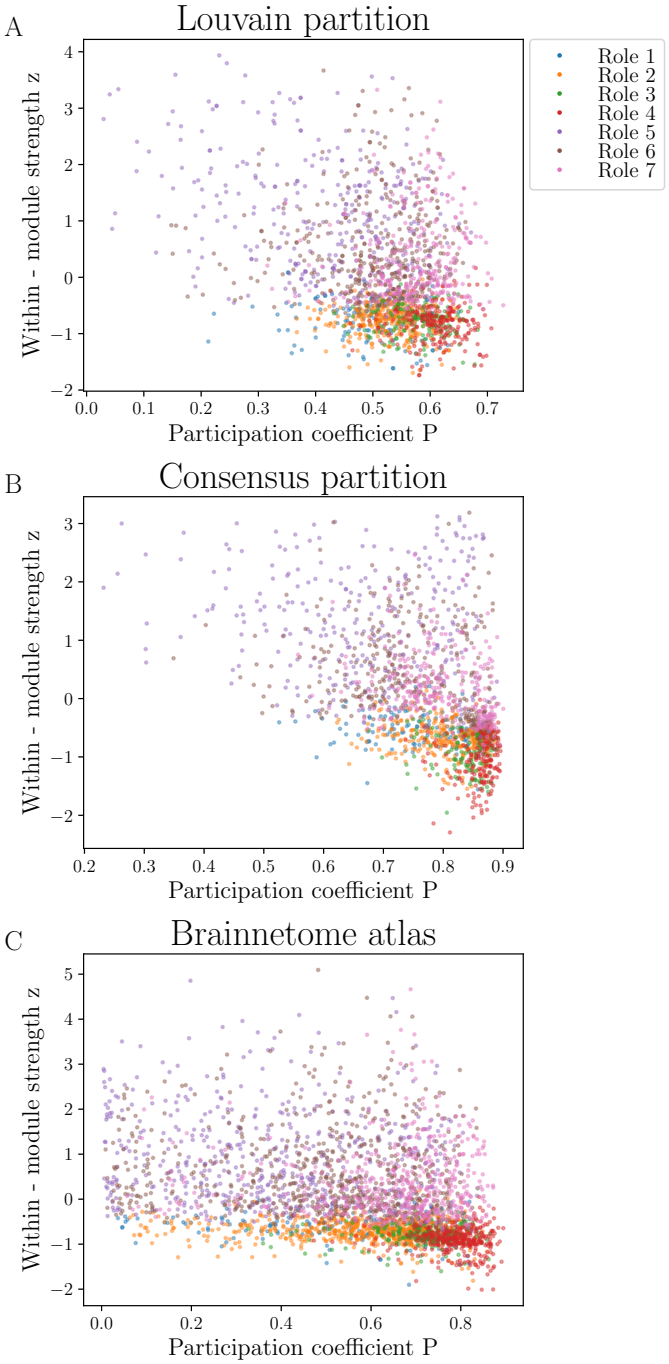

Figure 8: Each ROI visualized on a 2D plane set by within-module strength and the participation coefficient. Color shows the locally thresholded topological role assignments of ROIs. No clear borders between topological role classes are observed. However, the ROIs of the same topological role class tend to be located closer together than ROIs of different topological role classes. Therefore, the spatial distribution of topological role classes implies shared tendencies in the levels of within-module strength and the participation coefficient even across the different modules. A) Topological role assignments of ROIs in Louvain partition. B) Topological role assignments of ROIs in consensus partition. C) Topological role assignments of ROIs in Brainnetome atlas. All ROIs of all subjects are shown in the scatter plots.

4.4 Predicting topological roles using internal connectivity features

The internal connectivity features were used to predict the topological role class of the ROIs. The classifications were performed for each parcellation as well as for local and global topological role assignments. Numerical results are shown for all classification models while the visualizations of the underlying feature space and model coefficient values are presented only for our main results acquired for Louvain partition with local topological role assignments (for other visualizations, refer to Supplementary information).

4.4.1 Classification into hubs and non-hubs

Separation in the multidimensional feature space

The feature space spanned by the five internal connectivity measures and ROI size was visualized for visual inspection of the relationships in the data (see Fig. 9A for locally thresholded topological role assignments of the Louvain partition, see Supplementary information for other parcellations and globally thresholded topological roles). For the Louvain partition and the Brainnetome atlas, the separation of the two classes is mainly evident along the directions of the ROI-size-constrained metrics, *i.e.*, ROI size and self-link weight and their combinations with other variables. Some slight tendencies are visible also in other metrics such as the relative self-link weight. The consensus partition, on the other hand, exhibits a clearer separation also among the dimension of the relative self-link weight.

No large difference in separability was observed between local and global topological role classes in any of the parcellations. However, here we note that the shown scatter plot matrices do not capture all trends in the multidimensional feature space and separation may still be possible by a higher-dimensional hyperplane than the 2D planes visible in the scatter plot matrices.

Classification accuracy of the models

The training and test classification accuracies as well as the accuracies of the corresponding baseline classifiers are shown in Table 1 for models with the ROI-size-constrained internal connectivity measures included and in Table 2 for models without ROI-size-constrained measures. The models that contained ROI-size-constrained measures provided a considerable improvement in classification accuracy when comparing with the baseline classifier: in the Louvain partition, the classification accuracy improved from 54.29% to a test accuracy of 86.56% for the classification of local topological role classes. For other parcellations, the improvement was slightly smaller but yet considerable. This indicates that the internal connectivity features indeed exhibit differing patterns between hubs and non-hubs.

However, the classification accuracy was significantly reduced when excluding the measures constrained by ROI size. The test classification accuracy of local topological role classes in the Louvain partition dropped from 86.56% to 60.53% with

the exclusion of ROI size and self-link weight leaving only a marginal improvement compared to the baseline classifier accuracy of 54.29%. For the Brainnetome atlas, the results were qualitatively similar. However, the classification model for consensus partition maintained its classification accuracy considerably better: exclusion of ROI size and self-link weight lead only to a small reduction of accuracy from 80.90% to 76.64%.

This difference with the other parcellations is likely to be explained by the above mentioned separability along the dimension of relative self-link weight in the consensus partition (for visualization refer to Supplementary Information). Relative self-link weight is significantly correlated with ROI size in the consensus partition but not in the other partitions (Louvain partition $R = 0.03$, $p = 0.18$; consensus partition $R = 0.17$, $p \leq 10^{-5}$; Brainnetome atlas $R = 0.03$, $p = 0.06$). This indicates that the trends in internal connectivity features that separate hubs from non-hubs may in fact be largely driven by the dependence on ROI size.

Importance of different features in the predictions

This notion of the importance of the ROI size is supported by examination of the model coefficients that indicate the weight each feature carries in the final prediction. From the used definition of logistic class probability (see Equation 11) it follows that a large positive value of a coefficient indicates that a large value of a measure reduces the observation's probability of being a hub. As a result the measures that increase the probability of a ROI being a hub should have large negative coefficients.

For the Louvain partition, ROI size and self-link weight were the variables with the largest effect when included in the model and their large values increased the ROI's probability of being a hub (see Fig. 9B and supplementary information Fig. B1B). When excluding the ROI-size-constrained variables from the model, the relative self-link weight has little importance while static consistency, standard deviation of the within-ROI correlation distribution, and spatiotemporal consistency dominate the predictions (see Fig. 9C and Supplementary information Fig. B1C). These variables have an increasing effect on the hubness probability in general.

The consensus partition exhibits a slightly different trend of relative self-link weight getting a larger weight than ROI size (see Supplementary information Fig. B4B and B7B). When excluding the ROI-size-constrained variables, the ROI-size-dependent relative self-link weight keeps its importance (see Supplementary information Fig. B4C and B7C). Interestingly, large relative self-link decreases ROI's probability of being a hub when ROI size and self-link weight are included but increases it when the ROI-size-constrained variables are excluded. This could be explained by the fact that in the presence of other ROI-size-dependent variables, relative self-link weight balances the predictive over-fitting to these variables by fine-tuning the predictions towards the other direction whereas in their absence it takes larger responsibility for the large scale separation.

For the Brainnetome atlas, the most important coefficients are similar to the Louvain partition. The ROI size and self-link weight have the largest effect in increasing the hubness probability (see Supplementary information Fig. B10B

and B13B). When ROI-size-constrained variables are excluded, high values of static consistency, standard deviation of the within-ROI correlation distribution and spatiotemporal consistency increase a ROI's probability of being a hub while relative self-link weight has only a small effect (see Supplementary information Fig. B10C and B13C).

For classification of hubs and non-hubs, the model coefficient results remain qualitatively similar between local and global topological role assignments (refer to Fig. 9 and Supplementary information).

Internal connectivity differences between hubs and non-hubs

Having a large self-link weight strongly increases a ROI's probability of being a hub consistently in all of the models. The same applies to ROI size in most of the cases. Based on these results, it seems that hubs tend to be mostly larger and have a higher self-link weight than non-hubs.

When ROI size and self-link weight are excluded, high static spatial consistency mostly increases the hubness probability of a ROI. In the presence of ROI size and self-link weight, static spatial consistency exhibits more variable effects. However, the important role in the absence of ROI-size-constrained variables suggests that static spatial consistency tends to differ between hubs and non-hubs so that non-hubs in general tend to exhibit lower static spatial consistency.

High relative self-link weight mostly decreases the probability of hubness though this effect is usually rather small. The standard deviation of within-ROI correlation distribution mostly increases the probability of hubness. However, we note here that standard deviation of within-ROI distribution has only minor importance in most models.

High spatiotemporal consistency tends to increase a ROI's probability of being a hub but the effect is small in the majority of the models. The effects of the other internal connectivity measures are rather weak so it may not be meaningful to draw conclusions on their tendencies between hubs and non-hubs.

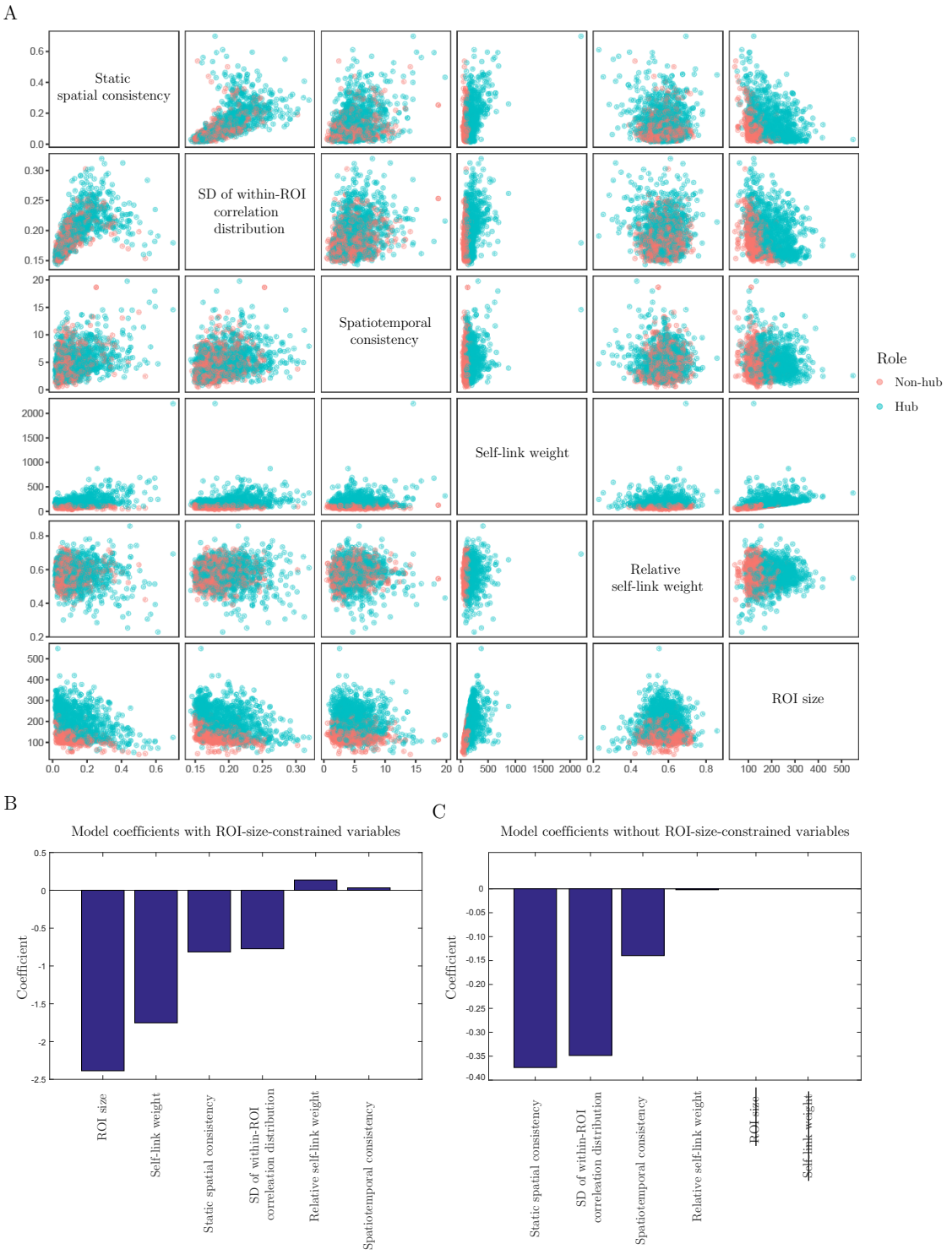

Figure 9: Prediction of the locally thresholded assignment to hubs and non-hubs in the Louvain partition. A) Scatter-plot matrix showing the visual separation of hub ROIs and non-hub ROIs in the feature space set by the internal connectivity measures. B) Model coefficients of the logistic regression model with ROI-size-constrained variables included. C) Model coefficients of the logistic regression model without ROI-size-constrained variables included. For globally thresholded topological role assignments and other parcellations refer to Supplementary Information.

4.4.2 Classification into provincial and connector hubs

Separation in the multidimensional feature space

The feature space spanned by the five internal connectivity measures and ROI size is presented as a scatter plot matrix (see Fig. 10A for locally thresholded topological role assignments of the Louvain partition, see Supplementary information for other parcellations and globally thresholded topological roles). All parcellations exhibit relatively little visual separation between provincial and connector hubs along the 2D planes visualized in the scatter plot matrix. In the consensus partition, some slight tendencies may be visible in static spatial consistency and ROI-size-dependent measures including ROI size, self-link weight, and relative self-link weight but no clear borders can be drawn. Results remain visually similar between local and global topological role classes.

Despite this lack of visual separability, we note that the classes may be separable along some higher-dimensional hyperplanes that take into account more features than these 2D representations of the data.

Classification accuracy of the models

Table 1 shows the training and test classification accuracies as well as the accuracies of the corresponding baseline classifiers for models with the ROI-size-constrained internal connectivity measures and Table 2 for models without ROI-size-constrained measures. From these results, it is evident that classifying ROIs between provincial and connector hubs is considerably easier for global than for local topological role assignments. This is visible in the larger predictive accuracy observed for the global assignments: for the Louvain partition the test classification accuracy was 83.00% for the global assignments but only 63.80% for the local assignments when ROI-size-constrained variables were included in the models. Both of these models, however, provided a relatively good improvement in comparison with the baseline classifier accuracy of 51.48% and 52.72%, respectively. Classification accuracies were slightly lower but acceptably good for the consensus partition but considerably lower for the Brainnetome atlas. For the Brainnetome atlas, the predictions for local topological role classes provided almost no improvement compared to the baseline classifier: test classification accuracy of the model was 56.65% while the baseline classifier achieved an accuracy of 55.50%.

Exclusion of the ROI-size-constrained variables (ROI size and self-link weight) did not reduce model performance considerably in most of the models. In the Louvain partition, the test classification accuracy of the local and global topological role assignment models were 63.80% and 83.00% with ROI-size-constrained variables and 64.28% and 79.70% without them, indicating very little change in the model performance. The difference for the classification of global topological role classes was slightly larger in the Brainnetome atlas with an improvement of accuracy from 60.85% to 66.54% by inclusion of ROI-size-constrained variables.

These results show that despite the lack of visual separability on 2D planes set by pairs of model variables, there seem to be patterns and relationships in the data that

separate provincial hubs from connector hubs. Including ROI size and self-link weight did not considerably improve results. Therefore, these separating patterns seem to be less likely to be accounted for by ROI size alone. However, the classifications of global topological classes were considerably more successful indicating that the good predictive accuracy may partly be explained by confounding factors such as community membership or location in the brain. Also, the variation in classification accuracy was rather large between parcellations.

Importance of different features in the predictions

Despite the fact that predictive accuracy does not reduce considerably by exclusion of ROI size and self-link weight, these two variables are the ones with the largest effect when included in the model for the Louvain partition (Fig. 10B). Having a strong self-link reduces a ROI's probability of being a connector hub whereas a large ROI size increases the probability. In global topological role classification, the other variables have only little importance (see Supplementary information Fig. B2B) whereas in the local role assignment classification the weights are distributed more equally (Fig. 10B).

When ROI size and self-link weight are excluded from the model, in the Louvain partition high values in most of the other internal connectivity features increase a ROI's probability of being a provincial hub (Fig. 10C). Especially static spatial consistency gets large importance in both global and local topological role models where large static spatial consistency decreases the probability of a ROI being a connector hub. In general, having a large relative self-link weight increases the probability of being a provincial hub. Standard deviation of the within-ROI correlation distribution has a large importance in increasing connector hub probability in the global topological class prediction (see Supplementary information Fig. B2B and C) whereas in local topological role classification it has very little weight (Fig. 10B and C). Spatiotemporal consistency has relatively little importance among the model coefficients.

For the consensus partition, on the other hand, the relative self-link weight has the largest importance in the global topological role classification independent of whether ROI-size-constrained measures are included (see Supplementary information Fig. B8B and C). In local topological role classes, the importance arises only when ROI size and self-link weight are excluded (see Supplementary information Fig. B5B and C). The standard deviation of within-ROI correlation distribution in general seems to increase the probability of ROI being a connector whereas static spatial consistency reduces the probability. Spatiotemporal consistency has a varying and non-consistent effect on the probability of a ROI being a connector hub.

In the Brainnetome atlas, the self-link weight and ROI size get a relatively large importance when included in the model (see Supplementary information Fig. B11B and B14B). The effects are opposite to each other with large self-link weight making a ROI more likely to be a provincial hub and large ROI size making the ROI more likely to be a connector hub. When excluding the ROI-size-constrained measures, static spatial consistency and relative self-link weight become the most influential

variables in the model (see Supplementary information Fig. B11C and B14C). Large static spatial consistency decreases the node's probability of being a connector hub. The relative self-link weight seems to have an opposite effect on the connector hub probability when examining global as opposed to local topological role assignments. Having a large relative self-link increases the probability of a node being a connector hub in the global sense but decreases the probability in the local role context. Here we need to note that the predictive power for Brainnetome atlas as very poor. Therefore, the coefficient values may not be indicative of real relationships but rather result of noise.

Internal connectivity differences between provincial and connector hubs

In general, ROIs with a large self-link weight are more likely to be provincial hubs than connector hubs. Large ROIs are more likely to be connector hubs in other parcellations except for the consensus partition. As a consequence, connector hubs tend to often be larger and exhibit weaker self-link than provincial hubs.

High static spatial consistency mostly increases the probability of a node being a provincial hub. Therefore, it seems that high static spatial consistency is more typical in provincial hubs while connector hubs have a lower static spatial consistency.

Other variables have a more varying effect depending on the parcellation and the local or global nature of the topological role assignments. Relative self-link weight mostly increases the likelihood of a ROI being provincial hub with some discrepancy in the Brainnetome models. Nevertheless, the general tendency points towards provincial hubs having on average higher relative self-link weight than connector hubs.

Spatiotemporal consistency has only a very weak effect, the direction of which is not consistent. The standard deviation of within-ROI correlation distribution has the most variable effect. Due to the generally weak nature of the model coefficients and the variability in their direction, spatiotemporal consistency and width of the within-ROI correlation distribution do not appear to be closely linked to the division between provincial and connector hubs.

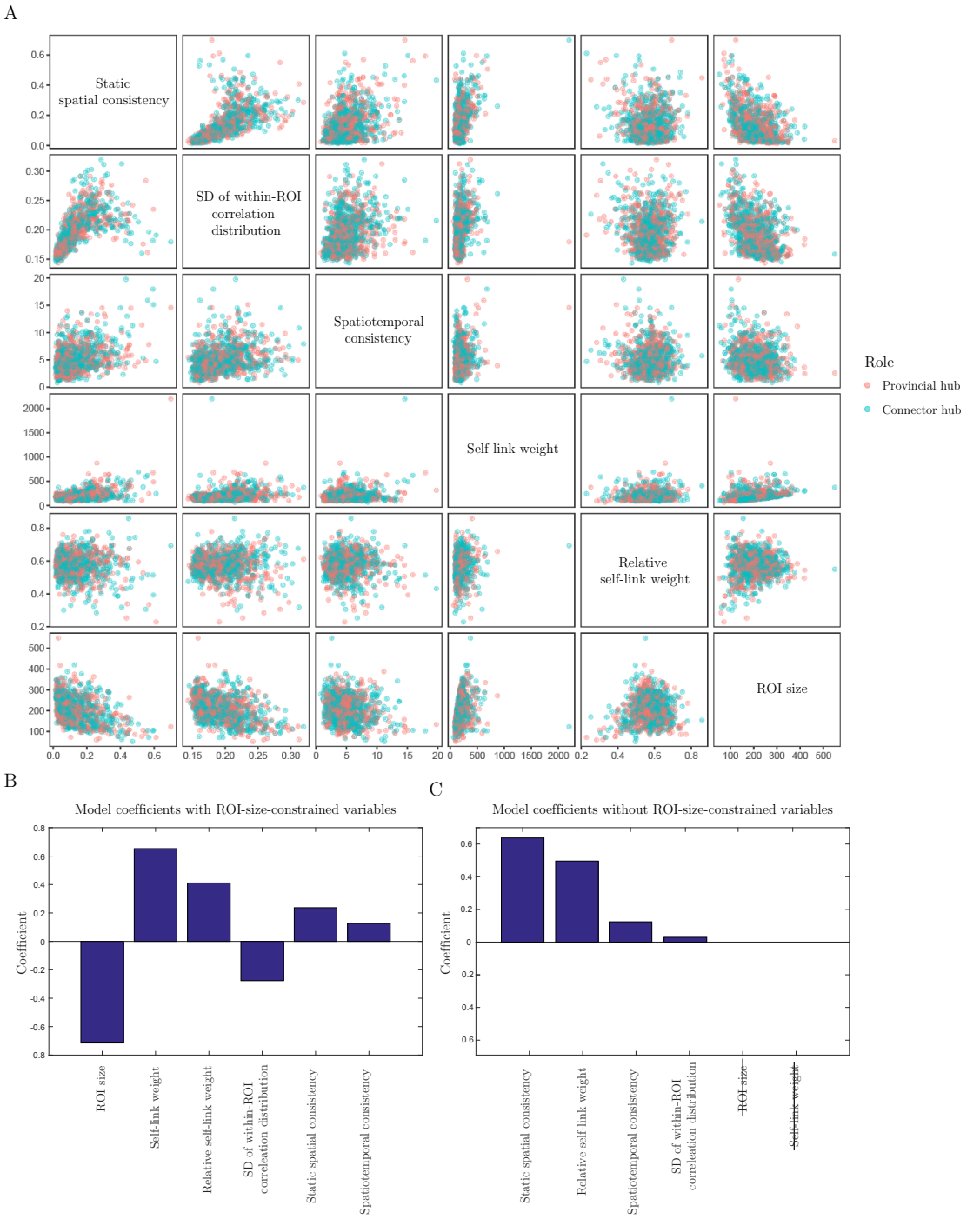

Figure 10: Prediction of the locally thresholded assignment to provincial hubs and connector hubs in the Louvain partition. A) Scatter-plot matrix showing the visual separation of provincial hubs and connector hubs in the feature space set by the internal connectivity measures. B) Model coefficients of the logistic regression model with ROI-size-constrained variables included. C) Model coefficients of the logistic regression model without ROI-size-constrained variables included. For globally thresholded topological role assignments and other parcellations refer to Supplementary Information.

4.4.3 Multi-class classification of topological role groups

Separation in the multidimensional feature space

The seven topological role classes are visualized in a scatter plot matrix showing a 2D representation of all pairs of variables (see Fig. 11 for locally thresholded topological role assignments of the Louvain partition, see Supplementary information for the other parcellations and globally thresholded topological roles). Separability of some classes seems rather high especially among the dimensions associated with ROI-size-constrained variables of ROI size and self-link weight. Some more abundant classes are likely easier to separate from each other than some of the less abundant classes with fewer observations. No large differences in the separability are visually observed between local and global topological role assignment classes nor between the different parcellations.

Classification accuracy of the models

When including also the ROI-size-constrained variables, internal connectivity features considerably improve the model performance in comparison with the baseline classifier for both local and global topological role assignments: for the Louvain partition the performance was improved to test classification accuracy of 50.47% for the global and 38.83% for the local classes while the corresponding accuracies of the baseline classifier were 23.01% and 20.10% respectively. Even the poorest results observed for the local topological role classes of the Brainnetome atlas provided an improvement from the baseline accuracy of 21.54% to the accuracy of 30.61%.

However, exclusion of the ROI-size-constrained variables lead to a notable reduction in the model classification accuracy: the accuracy of the local topological role model of Louvain dropped from 38.83% to 29.72%. Nevertheless, this is an improvement when comparing to the baseline classification accuracy of 20.10%. The global topological role classification of consensus partition maintained its good performance even when excluding ROI size and self-link weight: the accuracy was 47.11% in comparison with the original accuracy of 52.35% and baseline accuracy of 25.70%. The poorest results were observed for Brainnetome where the already weak accuracy of 30.61% was reduced to 27.38%. However, even this accuracy remains notably higher than the baseline accuracy of 21.54%.

The models with ROI-size-constrained measures included provided in general a good classification accuracy for a difficult multi-class classification problem of seven classes. Even though the exclusion of the ROI-size-constrained measures reduced the model performance, it remained on a reasonably good level when comparing to the baseline classifier.

Importance of different features in the predictions

As linear discriminant analysis consists of multiple linear separators between classes, we did not evaluate the weight of the variables in the predictions. These results serve mainly to show that internal connectivity features provide useful patterns and

relationships also for a more fine-grained separation.

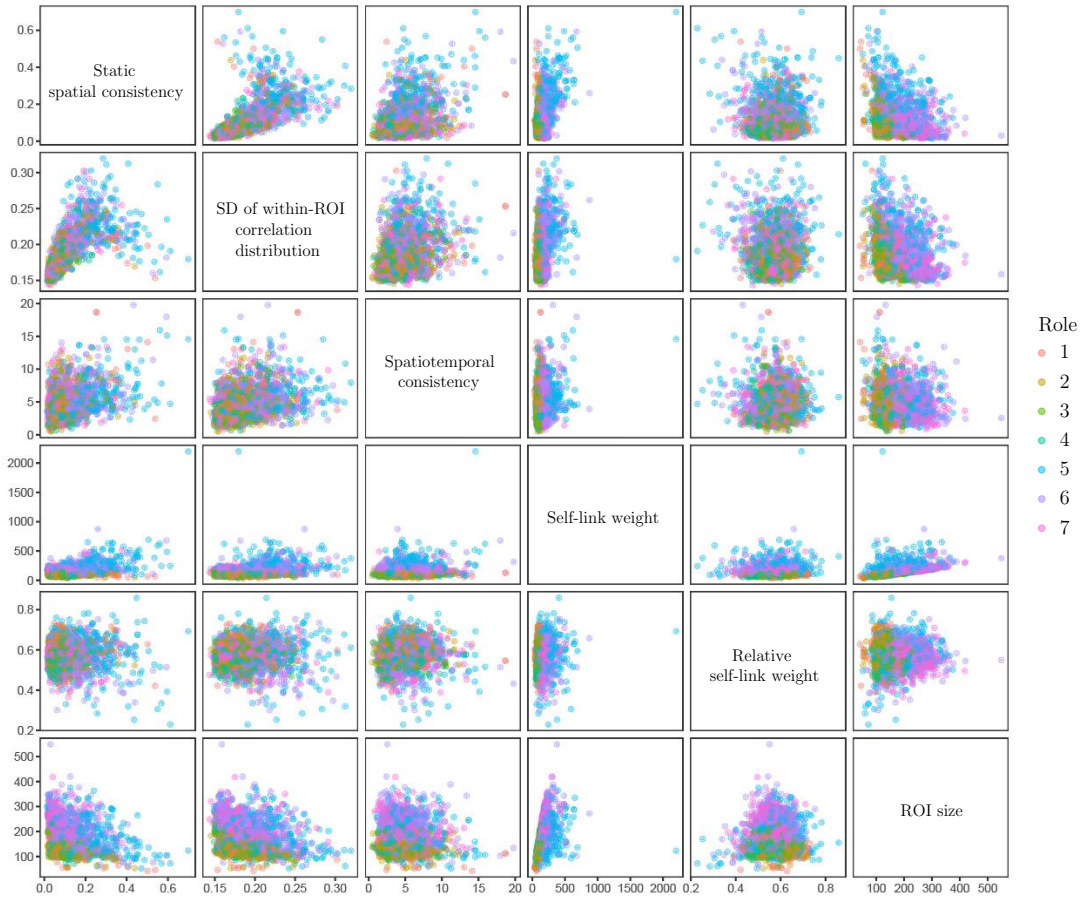

Figure 11: Prediction of the locally thresholded assignment to seven topological role classes in the Louvain partition. Scatter-plot matrix showing the visual separation of the seven role classes in the feature space set by the internal connectivity measures. For globally thresholded topological role assignments and other parcellations refer to Supplementary Information.

Table 1: Model performance with ROI size

Louvain partition			
Model accuracy	Training	Test	Baseline
Hub vs non-hub (local)	87.08%	86.56%	54.29%
Hub vs non-hub (global)	88.94%	87.19%	54.86%
Local vs connector hub (local)	66.07%	63.80%	52.72%
Local vs connector hub (global)	84.84%	83.00%	51.48%
Multi-class (local)	40.96%	38.83%	20.10%
Multi-class (global)	54.38%	50.47%	23.01%
Consensus partition			
Model accuracy	Training	Test	Baseline
Hub vs non-hub (local)	80.83%	80.90%	54.32%
Hub vs non-hub (global)	83.79%	84.39%	54.98%
Local vs connector hub (local)	66.47%	63.35%	52.22%
Local vs connector hub (global)	78.13%	76.58%	52.31%
Multi-class (local)	33.48%	34.30%	19.68%
Multi-class (global)	54.05%	52.35%	25.70%
Brainnetome atlas			
Model accuracy	Training	Test	Baseline
Hub vs non-hub (local)	75.98%	75.39%	54.57%
Hub vs non-hub (global)	74.43%	74.07%	55.01%
Local vs connector hub (local)	58.60%	56.65%	55.50%
Local vs connector hub (global)	67.47%	66.54%	50.20%
Multi-class (local)	28.36%	30.61%	21.54%
Multi-class (global)	36.10%	38.12%	23.45%

Table 2: Model performance without ROI size and self-link weight

Louvain partition			
Model accuracy	Training	Test	Baseline
Hub vs non-hub (local)	61.88%	60.53%	54.29%
Hub vs non-hub (global)	60.67%	59.58%	54.86%
Local vs connector hub (local)	65.50%	64.28%	52.72%
Local vs connector hub (global)	79.30%	79.70%	51.48%
Multi-class (local)	30.18%	29.72%	20.10%
Multi-class (global)	38.56%	34.59%	23.01%
Consensus partition			
Model accuracy	Training	Test	Baseline
Hub vs non-hub (local)	76.94%	76.64%	54.32%
Hub vs non-hub (global)	77.47%	77.08%	54.98%
Local vs connector hub (local)	62.44%	59.21%	52.22%
Local vs connector hub (global)	74.28%	72.76%	52.31%
Multi-class (local)	30.45%	31.23%	19.68%
Multi-class (global)	52.09%	47.11%	25.70%
Brainnetome atlas			
Model accuracy	Training	Test	Baseline
Hub vs non-hub (local)	63.34%	63.12%	54.57%
Hub vs non-hub (global)	64.2178	62.31%	55.01%
Local vs connector hub (local)	58.4848	55.66%	55.50%
Local vs connector hub (global)	61.26%	60.85%	50.20%
Multi-class (local)	24.47%	27.38%	21.54%
Multi-class (global)	32.02%	32.89%	23.45%

5 Discussion

5.1 Evaluation of the partitioning methods

When generating new parcellations, our first interest was estimating the quality of the acquired partition and consequently evaluating the appropriateness of the partitioning method for defining ROIs that can be used as nodes of functional brain networks. Goodness of partitions and their ROIs was based on visual inspection but also on examining static spatial consistency and relative self-link weight.

Visual inspection revealed that the data-driven partitions suffer from fragmentation of ROIs into many spatially separated subgroups of a few voxels that are scattered around the brain. This is problematic both from the neuroscientific and methodological point of view as ROIs are assumed to be functionally and neuronally uniform entities (Gordon et al. 2014, see Section 2.3.5 for details).

Both spatial consistency and relative self-link weight can be thought to measure different aspects of the internal connectivity assumptions. These assumptions should be fulfilled for a ROI to be well-defined. Static spatial consistency measures the functional homogeneity of a ROI which is one of the key assumptions when examining whether a ROI is well-defined. The low values exhibited especially by the data-driven partitions may indicate a serious concern about violating functional homogeneity assumptions. Therefore, based on static spatial consistency measure, the data-driven partitions as well as Brainnetome atlas are not especially well-defined.

In general these results on parcellation quality show that the goodness is very dependent on the measure of internal connectivity or functional homogeneity that is examined. The discrepancy between goodness measured by static spatial consistency and relative self-link weight may be caused by the fact that spatial consistency is sensitive to the average level of correlations whereas relative self-link weight is a product of searching for the strongest links and giving them equally much importance independent of the exact correlation values. These results could also change significantly if some other metrics of functional homogeneity were used.

The used internal connectivity metrics have been previously deployed to study networks built by averaging voxel-level signals across the ROI to define the links between ROIs (Stanley et al. 2013). In this case, functional homogeneity is a key assumption for the ROI signal to be representative of any real dynamics. However, coarse-grained networks are not subject to this type of averaging. Therefore, it remains an open question whether for example the similarity of connectivity profiles (Shen et al. 2013, Craddock et al. 2012) might be more appropriate to measure the internal connectivity assumptions of coarse-grained networks.

We also note that both of the used data-driven partition strategies only consider the static network structure estimated over the whole duration of the scan. As the interactions between ROIs and underlying voxels are dynamic in nature, it has been suggested that it may not be possible to find a static parcellation that shows high spatial consistency across the whole time course (Ryyppö et al. in press).

Based on these results, it appears that consensus partitioning may not be appropriate for parcellating the brain into a large number of ROIs. It should be rather used

to find larger scale group tendencies and their differences among smaller number of ROIs as has been done in previous work (Kujala et al. 2016). The Louvain partition at the level of single subject, on the other hand, shows more promising results. Further research should be conducted for example by applying spatial constraints to the correlation matrices or by otherwise accounting for the spatial coordinates. These modifications may help to avoid ROI fragmentation and also help to increase the static spatial consistency.

5.2 Internal connectivity differences between topological role classes

In the classification into hubs and non-hubs as well as in the classification into provincial and connector hubs, self-link weight, ROI size, and static spacial consistency were the most important factors in explaining the predictions. Other features had little and often quite variable effects even though sometimes slight tendencies were visible also in these features.

In the hub-non-hub framework, having a large self-link weight and high static spatial consistency in general increased a ROI's probability of being a hub. Hubs are central and well-connected nodes that typically have a large number of network neighbors. Therefore, these results are in agreement with earlier work that has demonstrated a link between high static spatial consistency and high node degree (Korhonen et al. 2017). Hub ROIs are thought to interact with many different neighbors which would require these brain regions to be highly active while signaling with many other brain regions. High activity has been suggested to result in higher regional homogeneity (Zang et al. 2004, Jiang et al. 2016) which also implies large functional homogeneity. Higher level of internal connectivity reflected in the stronger self-link and higher static spatial consistency could be explained by this higher level of activity through increased functional homogeneity.

A large ROI size also made a ROI more likely to be a hub. However, this effect is not very interesting from the internal connectivity point of view. It could rather be viewed as an confounding factor. A large size implies a larger spatial extent of the ROI and may, therefore, give a ROI an advantage of being able to form links to many different neighbors shadowing the actual effect of interesting internal connectivity features. This strengthens the notion that ROI size should be taken into account more actively when studying functional brain networks.

Relative self-link weight had a very small and variable effect across models. A wider within-ROI correlation distribution and higher spatiotemporal consistency somewhat increased the probability of a ROI being a hub. However, this effect was small and there was more variation among the different models. The larger width of the within-ROI correlation distribution may also be partly explained by higher static spatial consistency as the mean and standard deviation are known to often be correlated. The small effect of spatiotemporal consistency may be a result of the fact that the hub-non-hub framework does not account for temporal changes. This measure could have a larger importance for example in classifying ROIs into date and party hubs as this framework considers the temporal variation in the node's

behavior (Han et al. 2004, Agarwal et al. 2010).

In the provincial-connector hub framework, having a weaker self-link weight and low static spatial consistency increased the ROI's probability of being a connector hub. Provincial hubs have most of their links within their own community which means that these links are connected to a relatively homogeneous population of ROIs in the same community. Connector hubs, on the other hand, connect to a larger variety of different neighbors from different communities which may imply that their links are also more variable by nature. The lower internal connectivity of connector hubs may be explained by the fact that connector hubs need more variable neural mechanisms to cultivate these more varying links. This could potentially be achieved by the division of a ROI into multiple subpopulations of voxels that would be responsible for maintaining different links. Such a division would decrease the level of average internal connectivity.

Again, a larger ROI size made a ROI more likely to be a connector hub. Similarly to the predictions between hubs and non-hubs, this may be explained by the fact that a larger spatial extent makes a ROI physically close to a larger variety of other ROIs giving it an advantage in connecting to a large variety of neighbors in different parts of the brain. These more distant neighbors may be more likely to belong to different communities as brain networks are also spatially constrained networks.

A weak relative self-link mostly somewhat increases a ROI's probability of being a connector hub. Therefore, the effect of relative self-link weight is consistent with the effect of self-link weight although its effect is very small. The standard deviation of within-ROI correlation distribution and the spatiotemporal consistency had small and variable effects across the different models. If the connector hub ROI would consist of multiple subgroups of voxels as was hypothesized earlier, we could expect to see a wider distribution of within-ROI correlation values. Given this hypothesis it is interesting that the width of this distribution did not have more effects in the model. However, the small effect may again be partly explained by the low static spatial consistency as the mean and standard deviation of a distribution are often correlated. The provincial-connector hub framework does not account for temporal changes which could explain the small importance of spatiotemporal consistency in the predictions.

However, caution should be taken when interpreting these results as the effects and importance of different internal connectivity features are evaluated only based on their relative weight in the final prediction of the classification models. No statistical tests have been conducted to test for the differences between groups as the differences are likely to be a product of multiple features. Therefore, separation between groups should be rather thought of as a multidimensional hyperplane formed by a combination of features than single features alone. Some features might have had a different effect if included in the predictive model alone.

In addition, the importance of features has been evaluated qualitatively across different parcellations and between global and local topological role assignments by considering the direction and amplitude of the general tendencies. Therefore, some of the features that appear to have only a small or inconsistent importance across models may in fact play an important role in the predictions of some models. It is

typical that the groups are not separable along any single dimension alone but a separating hyperplane can be rather found as a combination of features in the high-dimensional feature space. Therefore, some of the features with small or inconsistent importance may exhibit small but significant differences between topological role classes especially when considered in the high-dimensional feature space together with other features.

5.3 Predicting the topological role from internal connectivity

In general, the logistic regression models that use internal connectivity features provide a considerable improvement in classification accuracy when comparing to the baseline classifier. Therefore, these results suggest that the data exhibits some differing patterns and relationships that can be used to separate topological role groups from each other.

Limitations of the predictive models

In the scope of this Thesis, only one type of model was trained per classification task: logistic regression was chosen for classification between hubs and non-hubs as well as provincial and connector hubs and Linear Discriminant Analysis was selected for multi-class classification. This choice was motivated by the aim of inference: the model coefficients of logistic regression provide visibility into the role each feature plays in the final prediction (James et al. 2013). Many more complex models may provide more accurate predictions but their results are not interpretable.

The choice of a low-complexity model may limit the predictive accuracy as logistic regression and LDA can both only capture trends that are linear by nature. Some of the scatter plot matrices may suggest there are also relationships that are not linear and the model complexity of logistic regression and LDA may be too low to accurately fit into the underlying data (see Fig. 9A, 10A, 11 and Supplementary information). However, the used models are less prone to over-fitting than some more complex alternatives (James et al. 2013). Notably, for all models of all parcellations, the training and testing accuracy are very similar indicating that the models have a good generalization behavior and do not suffer from over-fitting.

However, our feature space is rather low-dimensional which reduces the risk of over-fitting and might make it possible to use also more complex models without compromising generalization behavior. In the future it may be worth investigating whether the classification accuracy can be increased by use of more complex models.

Improving the characterization of internal connectivity

Classification accuracy may also be limited by the fact that the currently used five internal connectivity features and ROI size may not suffice in characterizing the richness of the internal connectivity patterns. Standard deviation of the within-ROI correlation distribution and static spatial consistency alone are a very coarse

description of the internal correlation structure. In future work, the characterization of internal connectivity could be broadened by more detailed metrics on the within-ROI correlation distribution such as skewness or kurtosis.

Spatiotemporal consistency attempts to capture temporal variation in internal connectivity by examining variation in the mean of the within-ROI correlation distribution. This variation could be measured in more detail by comparing the whole distribution across time windows for example by computing the Kullback-Leibler divergence between consecutive time windows.

It has also been hypothesized that ROIs may consist of multiple subregions that are correlated among themselves and weakly correlated or even anti-correlated with each other (Ryyppö et al. in press). This variation could potentially be characterized by measuring the module structure of the within-ROI voxel structure, for example by modularity or number of modules. Including a more rich description of the internal connectivity could help increase the classification accuracy and enable us to study the differences between topological role classes in even more detail.

Potential confounding factors

There are some potential confounding factors in the analysis. Many of the models relied on measures that are even directly constrained by ROI size. Many measures without this direct limiting relationship have been shown to be somewhat related to ROI size in our earlier work (Korhonen et al. 2017, Ryyppö et al. in press). This motivates the question on the extent to which these results can be accounted for a simple explanation such as ROI size. In order to rule out this possibility, we suggest this analysis to be repeated for a parcellation where ROIs are replaced by equal-sized spheres placed in the centroid of a ROI (see *e.g.* Power et al. 2011).

For model training the data is pooled across subjects and ROIs. Therefore, the classification accuracy may also vary across subjects and across ROIs. Effect of the subject identity was probed by including a subject effect into the logistic regression model. However, internal connectivity had a larger importance in explaining the topological role than subject identity. Nevertheless, it may be meaningful to examine differences in predictive accuracy between different subjects or ROIs in more detail.

Considerably higher classification accuracy was observed between provincial and connector hubs for global topological role assignments than for local ones. This raises the question whether this high accuracy could explained at least partly by confounding factors such as community membership or location in the brain. It may also be interesting to examine differences in accuracy of classifications between different communities and to examine the spatial distribution of classification accuracy across the brain.

Some of the definitions used in the analysis may also influence the predictive accuracy. The within-module strength and participation coefficient that underlie the topological role assignments are continuous by nature. In this Thesis, heuristic percentile thresholds were used to divide ROIs into topological role classes. However, these assignment limits are ultimately arbitrary. It could be useful to examine whether internal connectivity predicts the level of hubness as a continuous target

on the within-module strength scale or the level of connector nature of a hub as a continuous target along the participation coefficient value scale.

Accuracy differences between parcellations

Accuracy and model coefficients differ between different parcellations as well. The results for the consensus partition differ from the results for the Louvain partition and the Brainnetome atlas making it challenging to draw conclusions across partitions. Therefore, it seems that despite some shared tendencies and evident trends in the data, the relationship between hubness and internal connectivity is also dependent on the underlying parcellation. Some variation between parcellations may also be explained by the weak nature of the coefficients which may make their sign and mutual order more susceptible to noise.

These differences may also be partly explained by varying parcellation quality discussed in Section 4.1. Some of the differences are also likely to account for the distinctive structure of the estimated functional brain networks of the parcellations highlighting the importance of accurate node definition strategies. Our data-driven parcellations have not been extensively validated in earlier research so in the future it may be useful to repeat this analysis for some parcellations that have already been validated in more detail.

Accuracy differences between classification tasks

The results differed between classifications in the hub-non-hub framework in comparison with the provincial-connector hub framework. This appears to be at least partly explained by the fact that hubness seems to be somewhat trivially explained by ROI-size-related features whereas separation of provincial and connector hubs seems to rely on more complex combinations of underlying variables.

In addition, the sample size differed in the classification task between hubs and non-hubs as opposed to the classification task between provincial and connector hubs. Exclusion of non-hubs and kinless hubs from the latter classification task considerably reduced the sample size available for model training. This may also partly explain the differing classification accuracy.

Accuracy differences between role assignment methods

The results exhibit some variation in classification accuracy between local and global topological role assignments. For classification between hubs and non-hubs, there was no notable difference between the classification accuracies of local and global topological role classes. The classification into provincial and connector hubs, on the other hand, showed larger variability between local and global role assignments.

This is likely to be explained by the fact that the hubness assignments are more similar between local and global role classes than the assignments into provincial and connector hubs. For Louvain partitions, 94% of the ROIs had the same hub-non-hub assignments in local and global groupings, whereas only 74% of the provincial-

connector hub assignments were shared across the local and global groupings (for the consensus partition 92% and 66% and Brainnetome 94% and 71%, respectively).

5.4 Applications of the analysis

Internal connectivity provides interesting insights into the voxel-level neural activity while topological roles may provide information on the role and functional specialization of a brain region. Understanding the link between internal connectivity features and topological roles may help us understand the neural mechanisms that brain regions use to interact with each other and fulfill their functional role as a part of the functional brain network. This may very importantly increase our knowledge on brain function under different tasks.

Topological role assignments help us identify the most important nodes in functional brain networks. Removal of hub nodes with a distinct topological role has been demonstrated to have a different effect of network fragmentation and network functionality break-down in protein-protein networks in the context of date and party hubs (Han et al. 2004, Agarwal et al. 2010). Similarly, removal of provincial and connector hubs could be expected to have a different effect on the level of functionality of the remaining network. The varying effect of nodes in removal could be hypothesized to be indicative of their particular functional role in the original network. While these studied bioinformatics networks differ from functional brain networks, they nevertheless share many network characteristics. Therefore, it could be interesting to examine whether similar effects of role-dependent node removal apply to functional brain networks. These most important brain regions could then be chosen as target regions when studying for example connectivity differences between healthy and clinical populations. These insights could potentially be applied in automatic diagnostics of brain damage severity or in surgical planning in order to avoid the most important hubs in the brain. It could also help to localize brain regions among the damaged ones the connectivity of which is important and needs to be targeted in therapy such as transcranial magnetic stimulation (TMS).

Defining topological roles directly from the network structure requires rather heavy processing such as computing large correlation matrices or sorting large numbers of links while thresholding the networks. This makes fast estimation of topological roles difficult and limits their use in real time applications such as real-time fMRI (Christopher deCharms 2008). Processing necessary for defining internal connectivity is usually computationally less expensive and considerably faster. The observed link between topological roles and internal connectivity may allow for indirect prediction of a node's topological role from its internal connectivity patterns. As these internal connectivity patterns are faster to compute, they may allow us to extend the usability of topological role information to real-time applications. It has for example been suggested that real-time neuronal feedback through real-time fMRI may help to teach humans to control their neuronal activity (Christopher deCharms 2008). Therefore, real-time topological role estimation through internal connectivity features could be used for example in real-time fMRI therapy as feedback. This feedback loop could help to achieve brain activation that promotes the kind of topological roles

and network connectivity patterns that are typically exhibited by a healthy brain.

6 Conclusions

The data-driven ROI parcellations did not comply with all of the internal connectivity assumptions and the ROIs were not contiguous in the 3D space of the brain. This may be problematic for the ROI goodness and the neuroscientific interpretation of the ROIs. Therefore, we suggest that some modifications such as spatial constraints are needed before these node definition methods can be applied to further analysis.

When predicting topological roles of nodes in functional brain networks, internal connectivity features increased visibly the predictive accuracy in comparison to a baseline classifier. Therefore, these results demonstrate a link between internal connectivity and topological roles of nodes. Despite there being some differences in the effects of internal connectivity features across different models, there were also many general tendencies of internal connectivity feature differences between hubs and non-hubs as well as between provincial and connector hubs.

Having a strong self-link and a high static spatial consistency increased a ROI's probability of being a hub, implying that hubs on average have a higher level of internal connectivity than non-hubs. It is hypothesized that this may be due to the higher level of activation of hubs which results in higher functional homogeneity.

A weaker self-link weight and lower static spatial consistency, on the other hand, made a ROI more likely to be a connector hub indicating that connector hubs in general tend to have a weaker level of internal connectivity than provincial hubs. It is suggested that this may be due to the need for more variable neural mechanisms connector hubs use for cultivating connections to their more variable neighbors. We hypothesize that this may cause the ROI to be divided into multiple subpopulations of voxels that are responsible for forming different links. However, further characterization of internal connectivity and its modularity is needed to confirm this hypothesis.

Nevertheless, this analysis shows the important link between internal connectivity and topological roles of nodes and gives promise for increasing our understanding on the voxel-level neural mechanisms a ROI uses to fulfill its functional role in the brain network. In addition to important insights to brain function under different tasks, this understanding may be extendable to develop and enhance different diagnostic and therapy applications.

References

Agarwal, Sumeet, Deane, Charlotte M, Porter, Mason A, and Jones, Nick S (2010). "Revisiting date and party hubs: novel approaches to role assignment in protein interaction networks". In: *PLOS Computational Biology* 6.6, e1000817. DOI: 10.1371/journal.pcbi.1000817.

Alakörkkö, Tuomas, Saarimäki, Heini, Glerean, Enrico, Saramäki, Jari, and Korhonen, Onerva (2017). "Effects of spatial smoothing on functional brain networks". In: *European Journal of Neuroscience* 46.9, pp. 2471–2480. DOI: 10.1111/ejn.13717.

Alexander-Bloch, Aaron, Lambiotte, Renaud, Roberts, Ben, Giedd, Jay, Gogtay, Nitin, and Bullmore, Ed (2012). "The discovery of population differences in network community structure: new methods and applications to brain functional networks in schizophrenia". In: *NeuroImage* 59.4, pp. 3889–3900. DOI: 10.1016/j.neuroimage.2011.11.035.

Alexander-Bloch, Aaron F, Gogtay, Nitin, Meunier, David, Birn, Rasmus, Clasen, Liv, Lalonde, Francois, Lenroot, Rhoshel, Giedd, Jay, and Bullmore, Edward T (2010). "Disrupted modularity and local connectivity of brain functional networks in childhood-onset schizophrenia". In: *Frontiers in Systems Neuroscience* 4, p. 147. DOI: 10.3389/fnsys.2010.00147.

Alluri, Vinoo, Brattico, Elvira, Toiviainen, Petri, Burunat, Iballa, Bogert, Brigitte, Numminen, Jussi, and Kliuchko, Marina (2015). "Musical expertise modulates functional connectivity of limbic regions during continuous music listening." In: *Psychomusicology: Music, Mind, and Brain* 25.4, p. 443. DOI: 10.1037/pmu0000124.

Alluri, Vinoo, Toiviainen, Petri, Burunat, Iballa, Kliuchko, Marina, Vuust, Peter, and Brattico, Elvira (2017). "Connectivity patterns during music listening: Evidence for action-based processing in musicians". In: *Human Brain Mapping* 38.6, pp. 2955–2970. DOI: 10.1002/hbm.23565.

Bassett, Danielle S, Wymbs, Nicholas F, Porter, Mason A, Mucha, Peter J, Carlson, Jean M, and Grafton, Scott T (2011). "Dynamic reconfiguration of human brain networks during learning". In: *Proceedings of the National Academy of Sciences* 108.18, pp. 7641–7646. DOI: 10.1073/pnas.1018985108.

Bassett, Danielle S, Wymbs, Nicholas F, Rombach, M Puck, Porter, Mason A, Mucha, Peter J, and Grafton, Scott T (2013). "Task-based core-periphery organization of human brain dynamics". In: *PLOS Computational Biology* 9.9, e1003171. DOI: 10.1371/journal.pcbi.1003171.

Bassett, Danielle S and Sporns, Olaf (2017). "Network neuroscience". In: *Nature Neuroscience* 20.3, p. 353. DOI: 10.1038/nn.4502.

Bear, Mark F, Connors, Barry W, and Paradiso, Michael A (2007). *Neuroscience*. Vol. 3. Lippincott Williams & Wilkins. ISBN: 0-7817-6003-8.

Betzel, Richard F and Bassett, Danielle S (2017). "Multi-scale brain networks". In: *NeuroImage* 160, pp. 73–83. DOI: 10.1016/j.neuroimage.2016.11.006.

Blondel, Vincent D, Guillaume, Jean-Loup, Lambiotte, Renaud, and Lefebvre, Etienne (2008). "Fast unfolding of communities in large networks". In: *Jour-*

nal of Statistical Mechanics: Theory and Experiment 2008.10, P10008. DOI: 10.1088/1742-5468/2008/10/P10008.

Bullmore, Ed and Sporns, Olaf (2009). "Complex brain networks: graph theoretical analysis of structural and functional systems". In: *Nature Reviews Neuroscience* 10.3, p. 186. DOI: 10.1038/nrn2575.

Burunat, Iballa, Brattico, Elvira, Puoliväli, Tuomas, Ristaniemi, Tapani, Sams, Mikko, and Toiviainen, Petri (2015). "Action in perception: prominent visuo-motor functional symmetry in musicians during music listening". In: *PlOS One* 10.9, e0138238. DOI: 10.1371/journal.pone.0138238.

Chan, Micaela Y, Alhazmi, Fahd H, Park, Denise C, Savalia, Neil K, and Wig, Gagan S (2017). "Resting-state network topology differentiates task signals across the adult life span". In: *Journal of Neuroscience* 37.10, pp. 2734–2745. DOI: 10.1523/JNEUROSCI.2406-16.2017.

Chang, Wei-Tang, Nummenmaa, Aapo, Witzel, Thomas, Ahveninen, Jyrki, Huang, Samantha, Tsai, Kevin Wen-Kai, Chu, Ying-Hua, Polimeni, Jonathan R, Belliveau, John W, and Lin, Fa-Hsuan (2013). "Whole-head rapid fMRI acquisition using echo-shifted magnetic resonance inverse imaging". In: *NeuroImage* 78, pp. 325–338. DOI: 10.1016/j.neuroimage.2013.03.040.

Christopher deCharms, R (2008). "Applications of real-time fMRI". In: *Nature Reviews Neuroscience* 9.9, p. 720. DOI: 10.1038/nrn2414.

Colizza, Vittoria, Flammini, Alessandro, Serrano, M Angeles, and Vespignani, Alessandro (2006). "Detecting rich-club ordering in complex networks". In: *Nature Physics* 2.2, p. 110. DOI: 10.1038/nphys209.

Craddock, R Cameron, James, G Andrew, Holtzheimer, Paul E, Hu, Xiaoping P, and Mayberg, Helen S (2012). "A whole brain fMRI atlas generated via spatially constrained spectral clustering". In: *Human Brain Mapping* 33.8, pp. 1914–1928. DOI: 10.1002/hbm.21333.

Çukur, Tolga, Nishimoto, Shinji, Huth, Alexander G, and Gallant, Jack L (2013). "Attention during natural vision warps semantic representation across the human brain". In: *Nature Neuroscience* 16.6, p. 763. DOI: 10.1038/nn.3381.

Desikan, Rahul S, Ségonne, Florent, Fischl, Bruce, Quinn, Brian T, Dickerson, Bradford C, Blacker, Deborah, Buckner, Randy L, Dale, Anders M, Maguire, R Paul, Hyman, Bradley T, et al. (2006). "An automated labeling system for subdividing the human cerebral cortex on MRI scans into gyral based regions of interest". In: *NeuroImage* 31.3, pp. 968–980. DOI: 10.1016/j.neuroimage.2006.01.021.

Expert, Paul, Evans, Tim S, Blondel, Vincent D, and Lambiotte, Renaud (2011). "Uncovering space-independent communities in spatial networks". In: *Proceedings of the National Academy of Sciences* 108.19, pp. 7663–7668. DOI: 10.1073/pnas.1018962108.

Fan, Lingzhong, Li, Hai, Zhuo, Junjie, Zhang, Yu, Wang, Jiaojian, Chen, Liangfu, Yang, Zhengyi, Chu, Congying, Xie, Sangma, Laird, Angela R, et al. (2016). "The human brainnetome atlas: a new brain atlas based on connectional architecture". In: *Cerebral Cortex* 26.8, pp. 3508–3526. DOI: 10.1093/cercor/bhw157.

Fortunato, Santo (2010). "Community detection in graphs". In: *Physics Reports* 486.3, pp. 75–174. DOI: 10.1016/j.physrep.2009.11.002.

Friston, Karl J (1994). "Functional and effective connectivity in neuroimaging: a synthesis". In: *Human Brain Mapping* 2.1-2, pp. 56–78. DOI: 10.1002/hbm.460020107.

Friston, Karl J (2011). "Functional and effective connectivity: a review". In: *Brain Connectivity* 1.1, pp. 13–36. DOI: 10.1089/brain.2011.0008.

Girvan, Michelle and Newman, Mark EJ (2002). "Community structure in social and biological networks". In: *Proceedings of the National Academy of Sciences* 99.12, pp. 7821–7826. DOI: 10.1073/pnas.122653799.

Glasser, Matthew F, Coalson, Timothy S, Robinson, Emma C, Hacker, Carl D, Harwell, John, Yacoub, Essa, Ugurbil, Kamil, Andersson, Jesper, Beckmann, Christian F, Jenkinson, Mark, et al. (2016). "A multi-modal parcellation of human cerebral cortex". In: *Nature* 536.7615, pp. 171–178. DOI: 10.1038/nature18933.

Glerean, Enrico, Pan, Raj K, Salmi, Juha, Kujala, Rainer, Lahnakoski, Juha M, Roine, Ulrika, Nummenmaa, Lauri, Leppämäki, Sami, Nieminen-von Wendt, Taina, Tani, Pekka, et al. (2016). "Reorganization of functionally connected brain subnetworks in high-functioning autism". In: *Human Brain Mapping* 37.3, pp. 1066–1079. DOI: 10.1002/hbm.23084.

Gordon, Evan M, Laumann, Timothy O, Adeyemo, Babatunde, Huckins, Jeremy F, Kelley, William M, and Petersen, Steven E (2014). "Generation and evaluation of a cortical area parcellation from resting-state correlations". In: *Cerebral Cortex* 26.1, pp. 288–303. DOI: 10.1093/cercor/bhu239.

Göttlich, Martin, Ye, Zheng, Rodriguez-Fornells, Antoni, Münte, Thomas F, and Krämer, Ulrike M (2017). "Viewing socio-affective stimuli increases connectivity within an extended default mode network". In: *NeuroImage* 148, pp. 8–19. DOI: 10.1016/j.neuroimage.2016.12.044.

Guimera, Roger and Amaral, Luís A Nunes (2005a). "Cartography of complex networks: modules and universal roles". In: *Journal of Statistical Mechanics: Theory and Experiment* 2005.02, P02001. DOI: 10.1088/1742-5468/2005/02/P02001.

Guimera, Roger and Amaral, Luis A Nunes (2005b). "Functional cartography of complex metabolic networks". In: *Nature* 433.7028, p. 895. DOI: 10.1038/nature03288.

Guimera, Roger, Mossa, Stefano, Turtschi, Adrian, and Amaral, LA Nunes (2005c). "The worldwide air transportation network: Anomalous centrality, community structure, and cities' global roles". In: *Proceedings of the National Academy of Sciences* 102.22, pp. 7794–7799. DOI: 10.1073/pnas.0407994102.

Han, Jing-Dong J, Bertin, Nicolas, Tong, Hao, Goldberg, Debra S, et al. (2004). "Evidence for dynamically organized modularity in the yeast protein-protein interaction network". In: *Nature* 430.6995, p. 88. DOI: 10.1038/nature02555.

Handwerker, Daniel A, Gonzalez-Castillo, Javier, D'esposito, Mark, and Bandettini, Peter A (2012). "The continuing challenge of understanding and modeling hemodynamic variation in fMRI". In: *NeuroImage* 62.2, pp. 1017–1023. DOI: 10.1016/j.neuroimage.2012.02.015.

Harriger, Logan, van den Heuvel, Martijn P, and Sporns, Olaf (2012). "Rich club organization of macaque cerebral cortex and its role in network communication". In: *PlOS One* 7.9, e46497. DOI: 10.1371/journal.pone.0046497.

Hayasaka, Satoru and Laurienti, Paul J (2010). "Comparison of characteristics between region-and voxel-based network analyses in resting-state fMRI data". In: *NeuroImage* 50.2, pp. 499–508. DOI: 10.1016/j.neuroimage.2009.12.051.

Hebb, Donald O (1949). *The organization of behavior*. DOI: 10.1016/S0361-9230(99)00182-3.

Herculano-Houzel, Suzana (2009). "The human brain in numbers: a linearly scaled-up primate brain". In: *Frontiers in Human Neuroscience* 3. DOI: 10.3389/neuro.09.031.2009.

Holme, Petter (2005). "Core-periphery organization of complex networks". In: *Physical Review E* 72.4, p. 046111. DOI: 10.1103/PhysRevE.72.046111.

Holme, Petter and Saramäki, Jari (2012). "Temporal networks". In: *Physics Reports* 519.3, pp. 97–125. DOI: 10.1016/j.physrep.2012.03.001.

Huettel, Scott A, Song, Allen W, and McCarthy, Gregory (2004). *Functional magnetic resonance imaging*. Vol. 1. Sinauer Associates Sunderland. ISBN: 978-0-87893-288-7.

James, Gareth, Witten, Daniela, Hastie, Trevor, and Tibshirani, Robert (2013). *An Introduction to Statistical Learning*. Springer. ISBN: 978-1-4614-7137-0. DOI: 10.1007/978-1-4614-7138-7.

Jiang, Lili and Zuo, Xi-Nian (2016). "Regional homogeneity: a multimodal, multiscale neuroimaging marker of the human connectome". In: *The Neuroscientist* 22.5, pp. 486–505. DOI: 10.1177/1073858415595004.

Karypis, George and Kumar, Vipin (1998). "A fast and high quality multilevel scheme for partitioning irregular graphs". In: *SIAM Journal on Scientific Computing* 20.1, pp. 359–392. DOI: 10.1137/S1064827595287997.

Kiviniemi, Vesa, Kantola, Juha-Heikki, Jauhiainen, Jukka, Hyvärinen, Aapo, and Tervonen, Osmo (2003). "Independent component analysis of nondeterministic fMRI signal sources". In: *NeuroImage* 19.2, pp. 253–260. DOI: 10.1016/S1053-8119(03)00097-1.

Knoblauch, Kenneth, Ercsey-Ravasz, Mária, Kennedy, Henry, and Toroczkai, Zoltán (2016). "The brain in space". In: *Micro-, meso-and macro-connectomics of the brain*. Springer, pp. 45–74. DOI: 10.1007/978-3-319-27777-6_5.

Korhonen, Onerva, Saarimäki, Heini, Glerean, Enrico, Sams, Mikko, and Saramäki, Jari (2017). "Consistency of regions of interest as nodes of fMRI functional brain networks". In: *Network Neuroscience*. DOI: 10.1162/NETN_a_00013.

Kujala, Rainer, Glerean, Enrico, Pan, Raj Kumar, Jääskeläinen, Iiro P, Sams, Mikko, and Saramäki, Jari (2016). "Graph coarse-graining reveals differences in the module-level structure of functional brain networks". In: *European Journal of Neuroscience* 44.9, pp. 2673–2684. DOI: 10.1111/ejn.13392.

Lindquist, Martin A, Loh, Ji Meng, Atlas, Lauren Y, and Wager, Tor D (2009). "Modeling the hemodynamic response function in fMRI: efficiency, bias and mis-modeling". In: *NeuroImage* 45.1, S187–S198. DOI: 10.1016/j.neuroimage.2008.10.065.

Logothetis, Nikos K (2008). "What we can do and what we cannot do with fMRI". In: *Nature* 453.7197, pp. 869–878. DOI: 10.1038/nature06976.

Meunier, David, Lambiotte, Renaud, Fornito, Alex, Ersche, Karen, and Bullmore, Edward T (2009). "Hierarchical modularity in human brain functional networks". In: *Frontiers in Neuroinformatics* 3, p. 37. DOI: 10.3389/neuro.11.037.2009.

Mucha, Peter J, Richardson, Thomas, Macon, Kevin, Porter, Mason A, and Onnela, Jukka-Pekka (2010). "Community structure in time-dependent, multiscale, and multiplex networks". In: *Science* 328.5980, pp. 876–878. DOI: 10.1126/science.1184819.

Muldoon, Sarah Feldt and Bassett, Danielle S (2016). "Network and multilayer network approaches to understanding human brain dynamics". In: *Philosophy of Science* 83.5, pp. 710–720. DOI: 10.1086/687857.

Newman, Mark (2010). *Networks: an introduction*. Oxford University Press. ISBN: 978-0-19-920665-0.

Olesen, Jens M, Bascompte, Jordi, Dupont, Yoko L, and Jordano, Pedro (2007). "The modularity of pollination networks". In: *Proceedings of the National Academy of Sciences* 104.50, pp. 19891–19896. DOI: 10.1073/pnas.0706375104.

Papo, David, Zanin, Massimiliano, Martínez, Johann H, and Buldú, Javier M (2016). "Beware of the small-world neuroscientist!" In: *Frontiers in Human Neuroscience* 10, p. 96. DOI: 10.3389/fnhum.2016.00096.

Pedregosa, F., Varoquaux, G., Gramfort, A., Michel, V., Thirion, B., Grisel, O., Blondel, M., Prettenhofer, P., Weiss, R., Dubourg, V., Vanderplas, J., Passos, A., Cournapeau, D., Brucher, M., Perrot, M., and Duchesnay, E. (2011). "Scikit-learn: Machine Learning in Python". In: *Journal of Machine Learning Research* 12, pp. 2825–2830.

Power, Jonathan D, Cohen, Alexander L, Nelson, Steven M, Wig, Gagan S, Barnes, Kelly Anne, Church, Jessica A, Vogel, Alecia C, Laumann, Timothy O, Miezin, Fran M, Schlaggar, Bradley L, et al. (2011). "Functional network organization of the human brain". In: *Neuron* 72.4, pp. 665–678. DOI: 10.1016/j.neuron.2011.09.006.

Power, Jonathan D, Barnes, Kelly A, Snyder, Abraham Z, Schlaggar, Bradley L, and Petersen, Steven E (2012). "Spurious but systematic correlations in functional connectivity MRI networks arise from subject motion". In: *NeuroImage* 59.3, pp. 2142–2154. DOI: 10.1016/j.neuroimage.2011.10.018.

Power, Jonathan D, Schlaggar, Bradley L, Lessov-Schlaggar, Christina N, and Petersen, Steven E (2013). "Evidence for hubs in human functional brain networks". In: *Neuron* 79.4, pp. 798–813. DOI: 10.1016/j.neuron.2013.07.035.

Rubinov, Mikail and Sporns, Olaf (2010). "Complex network measures of brain connectivity: uses and interpretations". In: *NeuroImage* 52.3, pp. 1059–1069. DOI: 10.1016/j.neuroimage.2009.10.003.

Ryyppö, Elisa, Glerean, Enrico, Brattico, Elvira, Saramäki, Jari, and Korhonen, Onerva (in press). "Regions of Interest as Nodes of Dynamic Functional Brain Networks". In: *Network Neuroscience* 0.ja, pp. 1–36. DOI: 10.1162/NETN_a_00047.

Schwarz, Adam J and McGonigle, John (2011). "Negative edges and soft thresholding in complex network analysis of resting state functional connectivity data". In: *NeuroImage* 55.3, pp. 1132–1146. DOI: 10.1016/j.neuroimage.2010.12.047.

Shehzad, Zarrar, Kelly, AM Clare, Reiss, Philip T, Gee, Dylan G, Gotimer, Kristin, Uddin, Lucina Q, Lee, Sang Han, Margulies, Daniel S, Roy, Amy Krain, Biswal, Bharat B, et al. (2009). "The resting brain: unconstrained yet reliable". In: *Cerebral Cortex* 19.10, pp. 2209–2229. DOI: 10.1093/cercor/bhn256.

Shen, Xilin, Tokoglu, Fuyuze, Papademetris, Xenios, and Constable, R Todd (2013). "Groupwise whole-brain parcellation from resting-state fMRI data for network node identification". In: *NeuroImage* 82, pp. 403–415. DOI: 10.1016/j.neuroimage.2013.05.081.

Smith, Stephen M, Miller, Karla L, Salimi-Khorshidi, Gholamreza, Webster, Matthew, Beckmann, Christian F, Nichols, Thomas E, Ramsey, Joseph D, and Woolrich, Mark W (2011). "Network modelling methods for FMRI". In: *NeuroImage* 54.2, pp. 875–891. DOI: 10.1016/j.neuroimage.2010.08.063.

Sporns, Olaf (2013). "Network attributes for segregation and integration in the human brain". In: *Current Opinion in Neurobiology* 23.2, pp. 162–171. DOI: 10.1016/j.conb.2012.11.015.

Sporns, Olaf, Chialvo, Dante R, Kaiser, Marcus, and Hilgetag, Claus C (2004). "Organization, development and function of complex brain networks". In: *Trends in Cognitive Sciences* 8.9, pp. 418–425. DOI: 10.1016/j.tics.2004.07.008.

Sporns, Olaf, Tononi, Giulio, and Kötter, Rolf (2005). "The human connectome: a structural description of the human brain". In: *PLOS Computational Biology* 1.4, e42. DOI: 10.1371/journal.pcbi.0010042.

Stanley, Matthew Lawrence, Moussa, Malaak Nasser, Paolini, Brielle, Lyday, Robert Gray, Burdette, Jonathan H, and Laurienti, Paul J (2013). "Defining nodes in complex brain networks". In: *Frontiers in Computational Neuroscience* 7, p. 169. DOI: 10.3389/fncom.2013.00169.

Strehl, Alexander and Ghosh, Joydeep (2002). "Cluster ensembles—a knowledge reuse framework for combining multiple partitions". In: *Journal of Machine Learning Research* 3.Dec, pp. 583–617.

Thirion, Bertrand, Flandin, Guillaume, Pinel, Philippe, Roche, Alexis, Ciuciu, Philippe, and Poline, Jean-Baptiste (2006). "Dealing with the shortcomings of spatial normalization: Multi-subject parcellation of fMRI datasets". In: *Human Brain Mapping* 27.8, pp. 678–693. DOI: 10.1002/hbm.20210.

Tian, Lixia, Jiang, Tianzi, Liang, Meng, Li, Xiaobo, He, Yong, Wang, Kun, Cao, Bingli, and Jiang, Tao (2007). "Stabilities of negative correlations between blood oxygen level-dependent signals associated with sensory and motor cortices". In: *Human Brain Mapping* 28.7, pp. 681–690. DOI: 10.1002/hbm.20300.

Tononi, Giulio, Sporns, Olaf, and Edelman, Gerald M (1994). "A measure for brain complexity: relating functional segregation and integration in the nervous system". In: *Proceedings of the National Academy of Sciences* 91.11, pp. 5033–5037. DOI: 10.1073/pnas.91.11.5033.

Tzourio-Mazoyer, Nathalie, Landeau, Brigitte, Papathanassiou, Dimitri, Crivello, Fabrice, Etard, Olivier, Delcroix, Nicolas, Mazoyer, Bernard, and Joliot, Marc

(2002). "Automated anatomical labeling of activations in SPM using a macroscopic anatomical parcellation of the MNI MRI single-subject brain". In: *NeuroImage* 15.1, pp. 273–289. DOI: 10.1006/nimg.2001.0978.

Van den Heuvel, Martijn P and Sporns, Olaf (2011). "Rich-club organization of the human connectome". In: *Journal of Neuroscience* 31.44, pp. 15775–15786. DOI: 10.1523/JNEUROSCI.3539-11.2011.

Van den Heuvel, Martijn P and Sporns, Olaf (2013). "Network hubs in the human brain". In: *Trends in Cognitive Sciences* 17.12, pp. 683–696. DOI: 10.1016/j.tics.2013.09.012.

Wang, Jing and Wang, Haixian (2016). "A supervoxel-based method for groupwise whole brain parcellation with resting-state fMRI data". In: *Frontiers in Human Neuroscience* 10, p. 659. DOI: 10.3389/fnhum.2016.00659.

Wang, Jinhui, Wang, Liang, Zang, Yufeng, Yang, Hong, Tang, Hehan, Gong, Qiyong, Chen, Zhang, Zhu, Chaozhe, and He, Yong (2009). "Parcellation-dependent small-world brain functional networks: a resting-state fMRI study". In: *Human Brain Mapping* 30.5, pp. 1511–1523. DOI: 10.1002/hbm.20623.

White, John G, Southgate, Eileen, Thomson, J Nichol, and Brenner, Sydney (1986). "The structure of the nervous system of the nematode Caenorhabditis elegans: the mind of a worm". In: *Philosophical Transactions of the Royal Society B* 314, pp. 1–340. DOI: 10.1098/rstb.1986.0056.

Wig, Gagan S, Schlaggar, Bradley L, and Petersen, Steven E (2011). "Concepts and principles in the analysis of brain networks". In: *Annals of the New York Academy of Sciences* 1224.1, pp. 126–146. DOI: 10.1111/j.1749-6632.2010.05947.x.

Wig, Gagan S, Laumann, Timothy O, and Petersen, Steven E (2014). "An approach for parcellating human cortical areas using resting-state correlations". In: *NeuroImage* 93, pp. 276–291. DOI: 10.1016/j.neuroimage.2013.07.035.

Zalesky, Andrew, Fornito, Alex, Harding, Ian H, Cocchi, Luca, Yücel, Murat, Pantelis, Christos, and Bullmore, Edward T (2010). "Whole-brain anatomical networks: does the choice of nodes matter?" In: *NeuroImage* 50.3, pp. 970–983. DOI: 10.1016/j.neuroimage.2009.12.027.

Zang, Yufeng, Jiang, Tianzi, Lu, Yingli, He, Yong, and Tian, Lixia (2004). "Regional homogeneity approach to fMRI data analysis". In: *NeuroImage* 22.1, pp. 394–400. DOI: 10.1016/j.neuroimage.2003.12.030.

Zhang, Xiao, Martin, Travis, and Newman, Mark EJ (2015). "Identification of core-periphery structure in networks". In: *Physical Review E* 91.3, p. 032803. DOI: 10.1103/PhysRevE.91.032803.

A Acknowledgements

I acknowledge the computational resources provided by the Aalto Science-IT project. I wish to thank Rainer Kujala for the use of tools provided as part of Brainnets toolbox (available at https://github.com/rmkujala/brainnets). In addition, I acknowledge the preprocessing tools provided as a part of Bramila Pipeline (version 2.0, available at https://version400.aalto.fi/gitlab/BML/bramila) and FSL software (version 5.0.9 https://www.fmrib.ox.ac.uk).

For the data set used in this Thesis, I am grateful to Elvira Brattico for providing the studied fMRI data set. The data collection was financially supported by the Danish National Research Foundation (project DNRF 117). In addition, I thank Brigitte Bogert, Benjamin Gold, Marina Kliuchko, David Ellison, Taru Numminen-Kontti, Mikko Heimälä, Jyrki Mäkelä, Marita Kattelus, and Toni Auranen for their contribution in data collection. I wish also to acknowledge the help of Petri Toiviainen, Vinoo Alluri, and Iballa Burunat in providing the studied data set.

B Supplementary Information

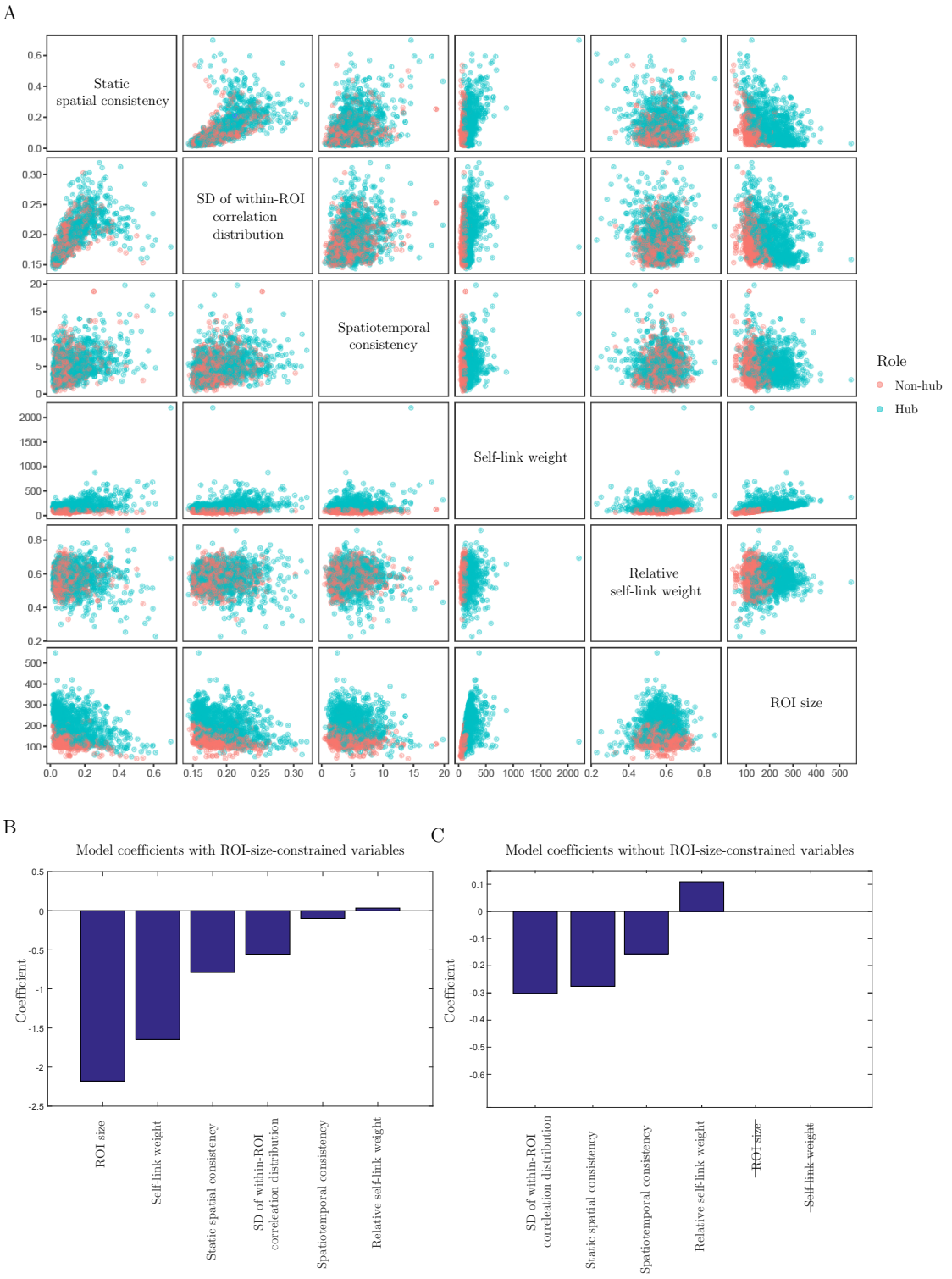

Figure B1: Prediction of the globally thresholded assignment to hub ROIs and non-hub ROIs in the Louvain partition. A) Scatter-plot matrix showing the visual separation of hubs and non-hubs in the feature space set by the internal connectivity measures. B) Model coefficients of the logistic regression model with ROI-size-constrained variables included. C) Model coefficients of the logistic regression model without ROI-size-constrained variables included.

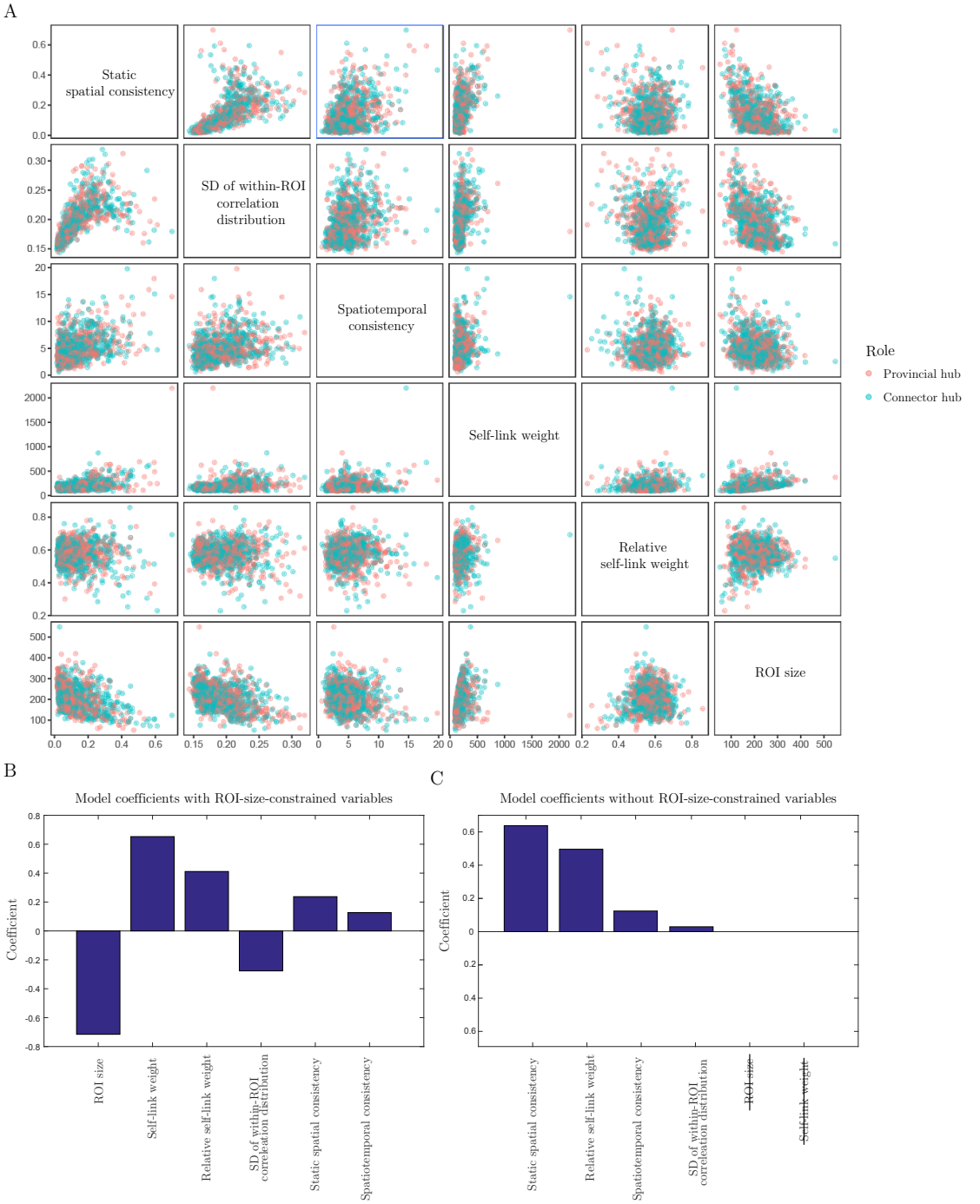

Figure B2: Prediction of the globally thresholded assignment to provincial hubs and connector hubs in the Louvain partition. A) Scatter-plot matrix showing the visual separation of provincial hubs and connector hubs in the feature space set by the internal connectivity measures. B) Model coefficients of the logistic regression model with ROI-size-constrained variables included. C) Model coefficients of the logistic regression model without ROI-size-constrained variables included.

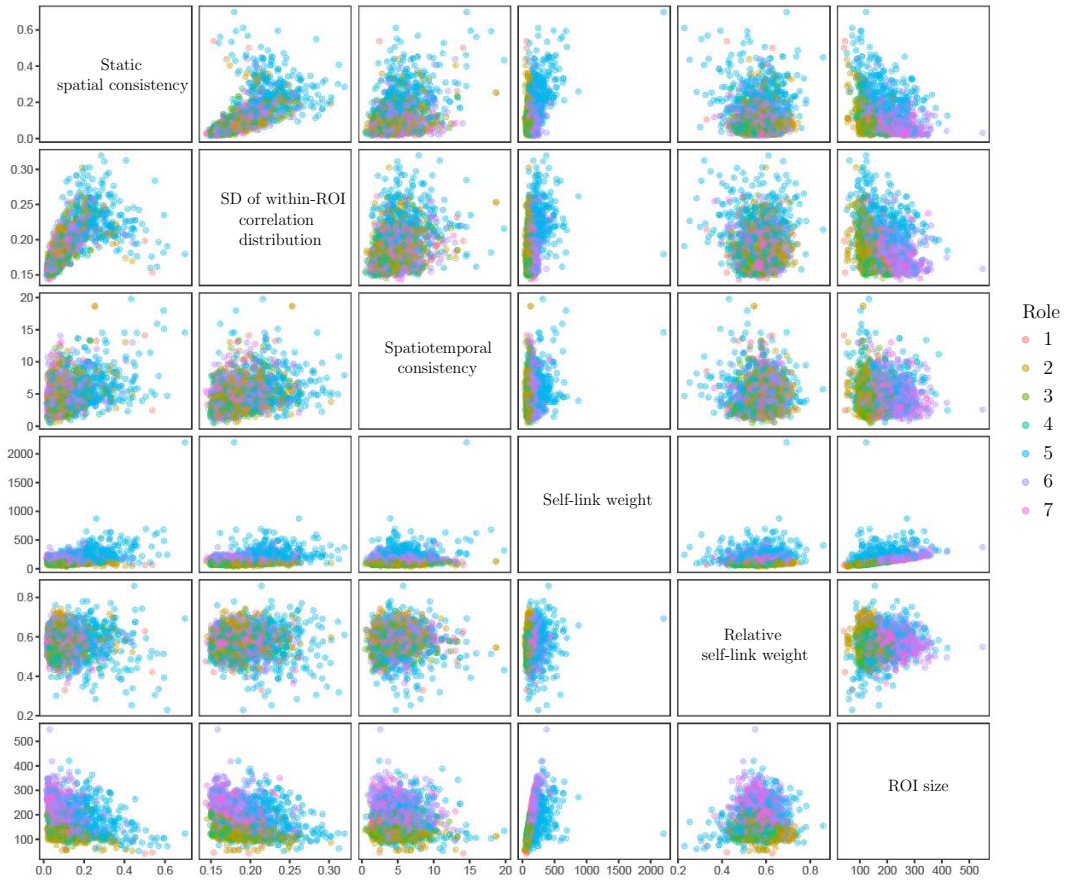

Figure B3: Prediction of the globally thresholded assignment to seven topological role classes in the Louvain partition. Scatter-plot matrix showing the visual separation of the seven classes in the feature space set by the internal connectivity measures.

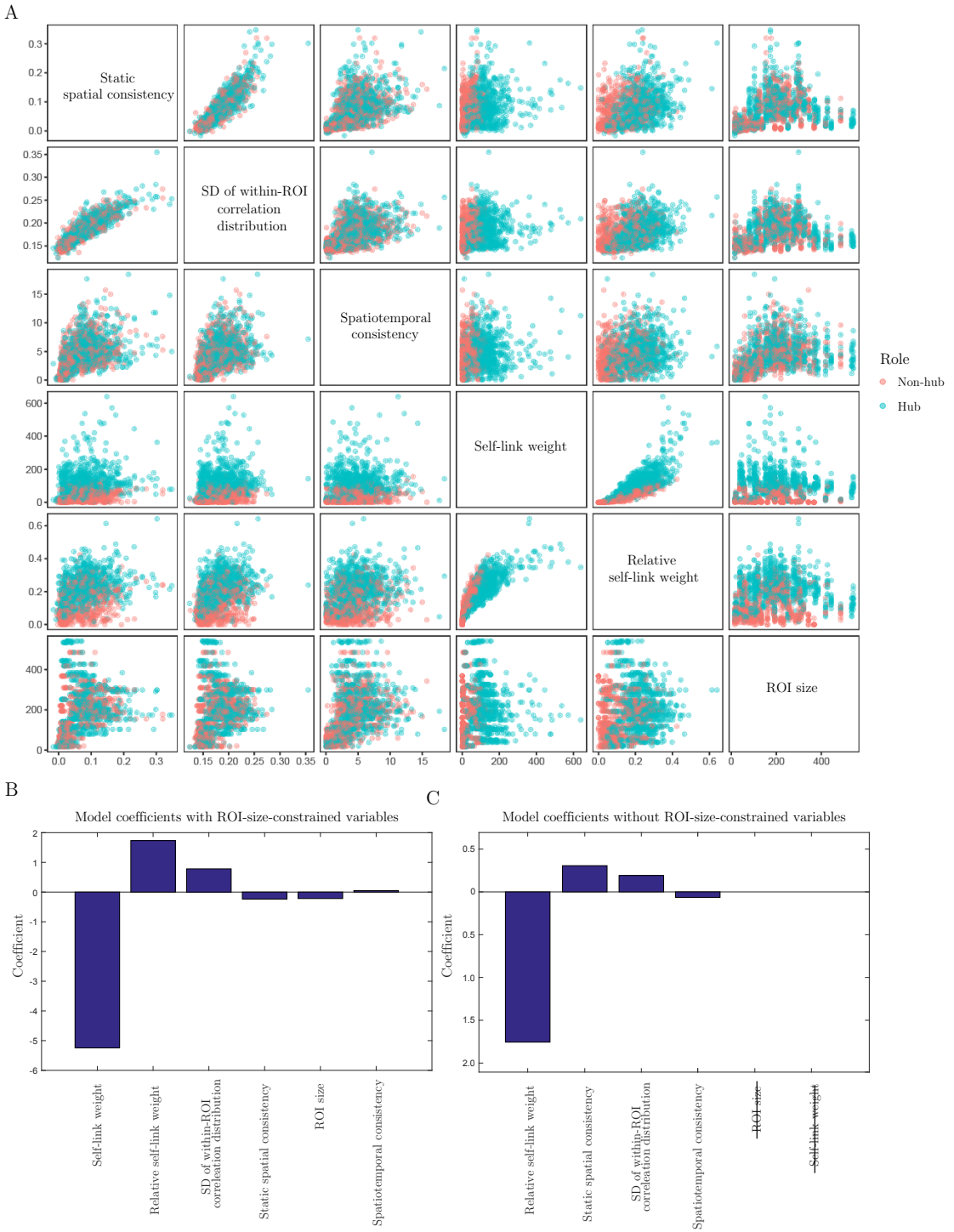

Figure B4: Prediction of the locally thresholded assignment to hub ROIs and non-hub ROIs in the consensus partition. A) Scatter-plot matrix showing the visual separation of hubs and non-hubs in the feature space set by the internal connectivity measures. B) Model coefficients of the logistic regression model with ROI-size-constrained variables included. C) Model coefficients of the logistic regression model without ROI-size-constrained variables included.

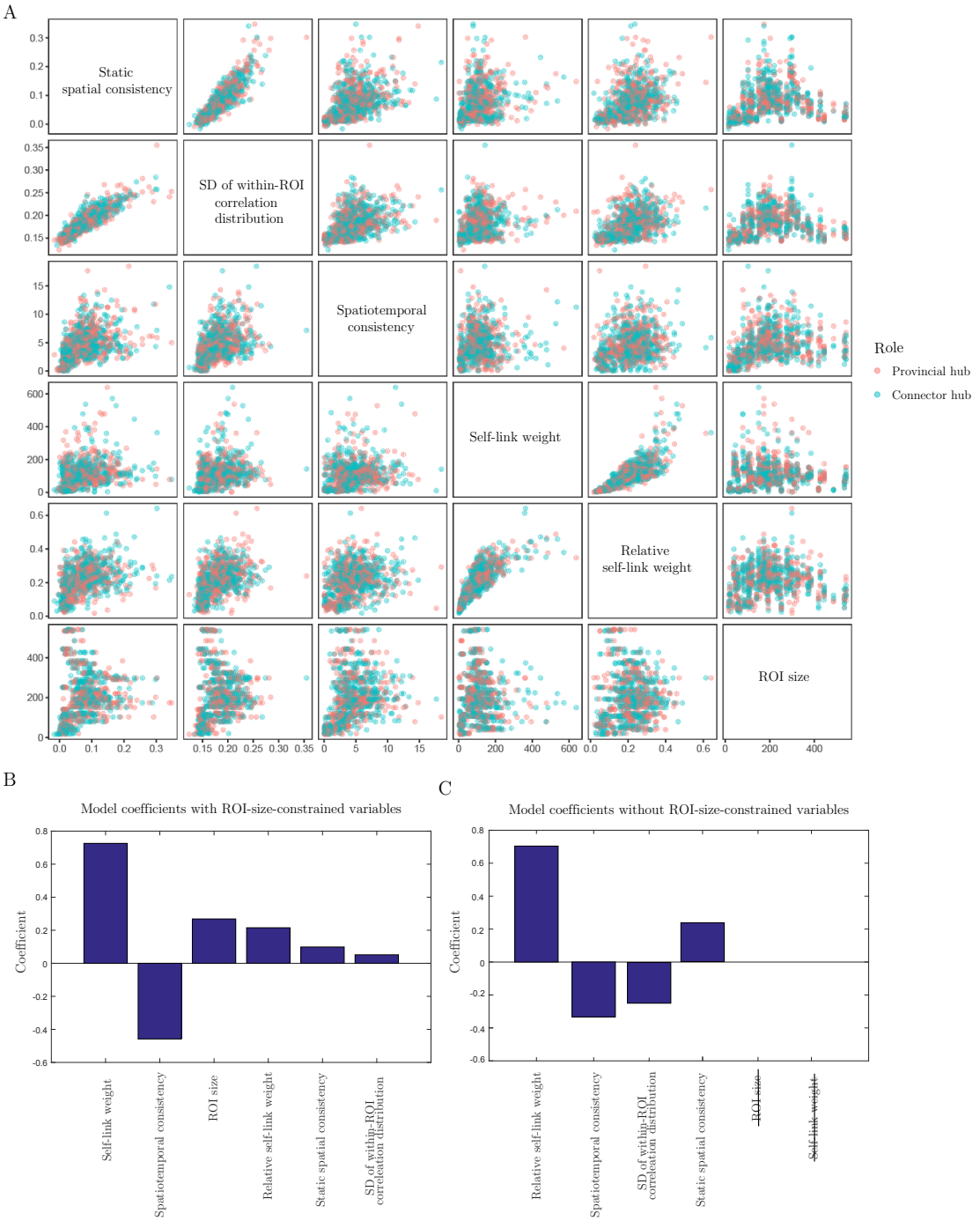

Figure B5: Prediction of the locally thresholded assignment to provincial hubs and connector hubs in the consensus partition. A) Scatter-plot matrix showing the visual separation of provincial hubs and connector hubs in the feature space set by the internal connectivity measures. B) Model coefficients of the logistic regression model with ROI-size-constrained variables included. C) Model coefficients of the logistic regression model without ROI-size-constrained variables included.

Figure B6: Prediction of the locally thresholded assignment to seven topological role classes in the consensus partition. Scatter-plot matrix showing the visual separation of the seven classes in the feature space set by the internal connectivity measures.

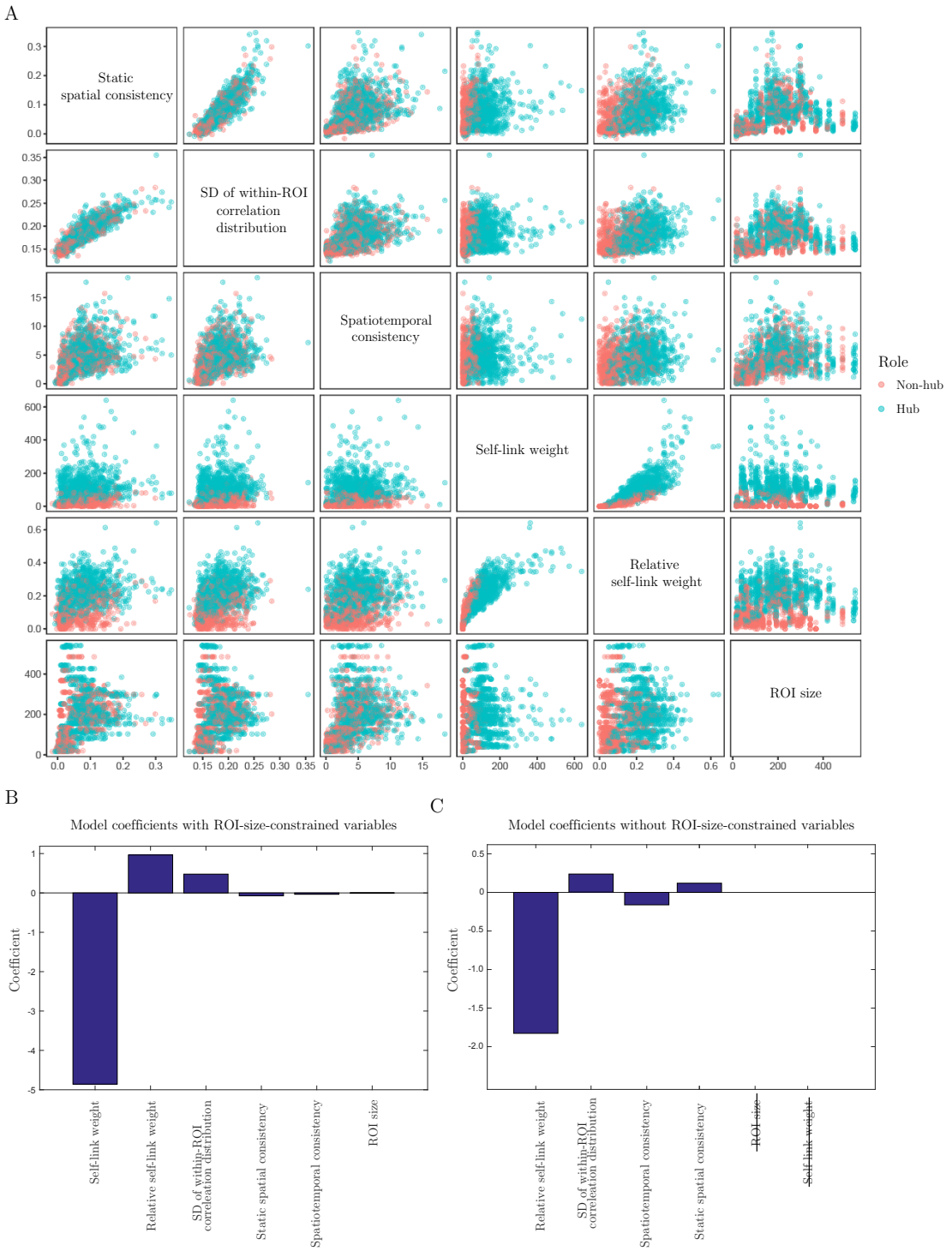

Figure B7: Prediction of the globally thresholded assignment to hub ROIs and non-hub ROIs in the consensus partition. A) Scatter-plot matrix showing the visual separation of hubs and non-hubs in the feature space set by the internal connectivity measures. B) Model coefficients of the logistic regression model with ROI-size-constrained variables included. C) Model coefficients of the logistic regression model without ROI-size-constrained variables included.

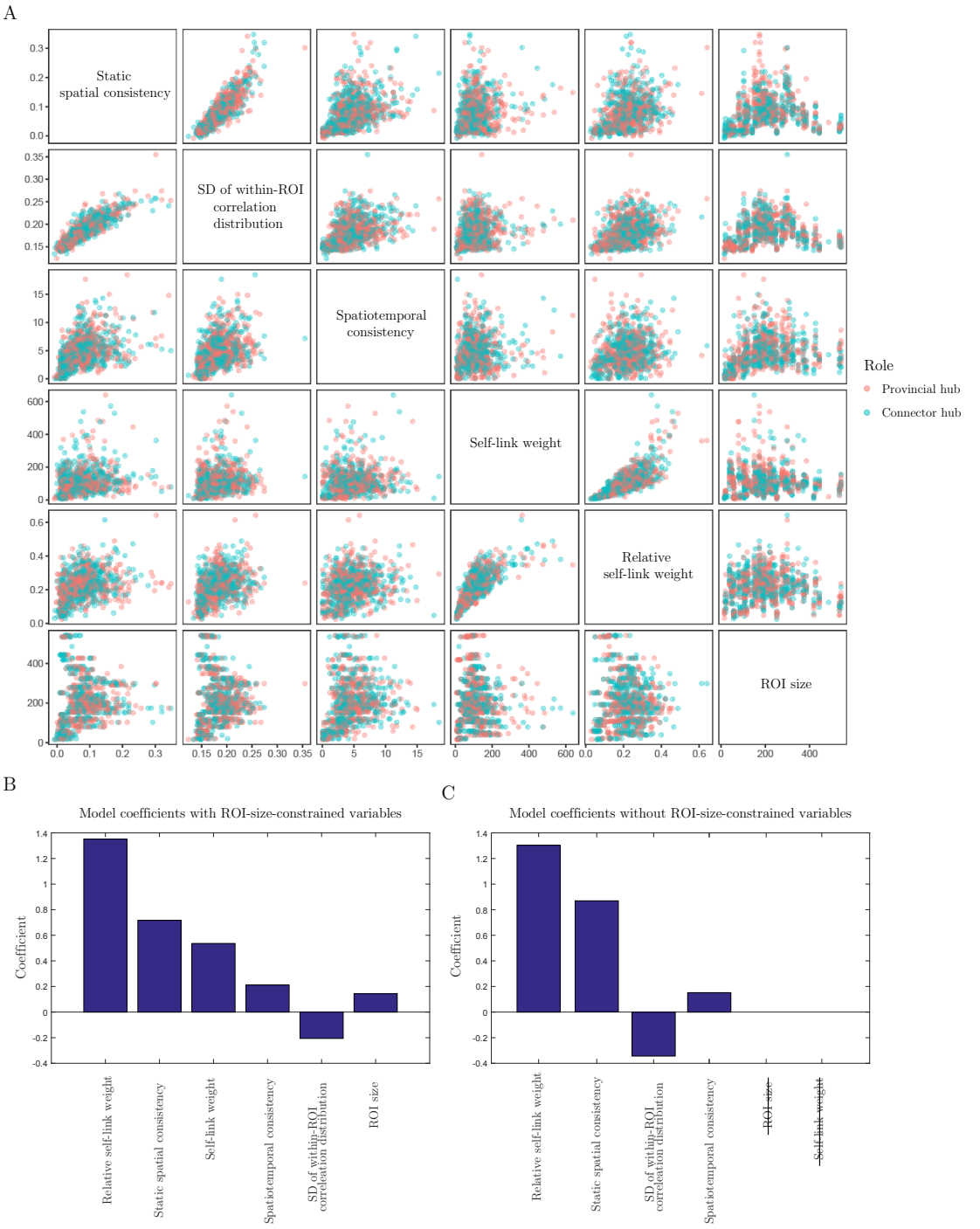

Figure B8: Prediction of the globally thresholded assignment to provincial hubs and connector hubs in the consensus partition. A) Scatter-plot matrix showing the visual separation of provincial hubs and connector hubs in the feature space set by the internal connectivity measures. B) Model coefficients of the logistic regression model with ROI-size-constrained variables included. C) Model coefficients of the logistic regression model without ROI-size-constrained variables included.

Figure B9: Prediction of the globally thresholded assignment to seven topological role classes in the consensus partition. Scatter-plot matrix showing the visual separation of the seven classes in the feature space set by the internal connectivity measures.

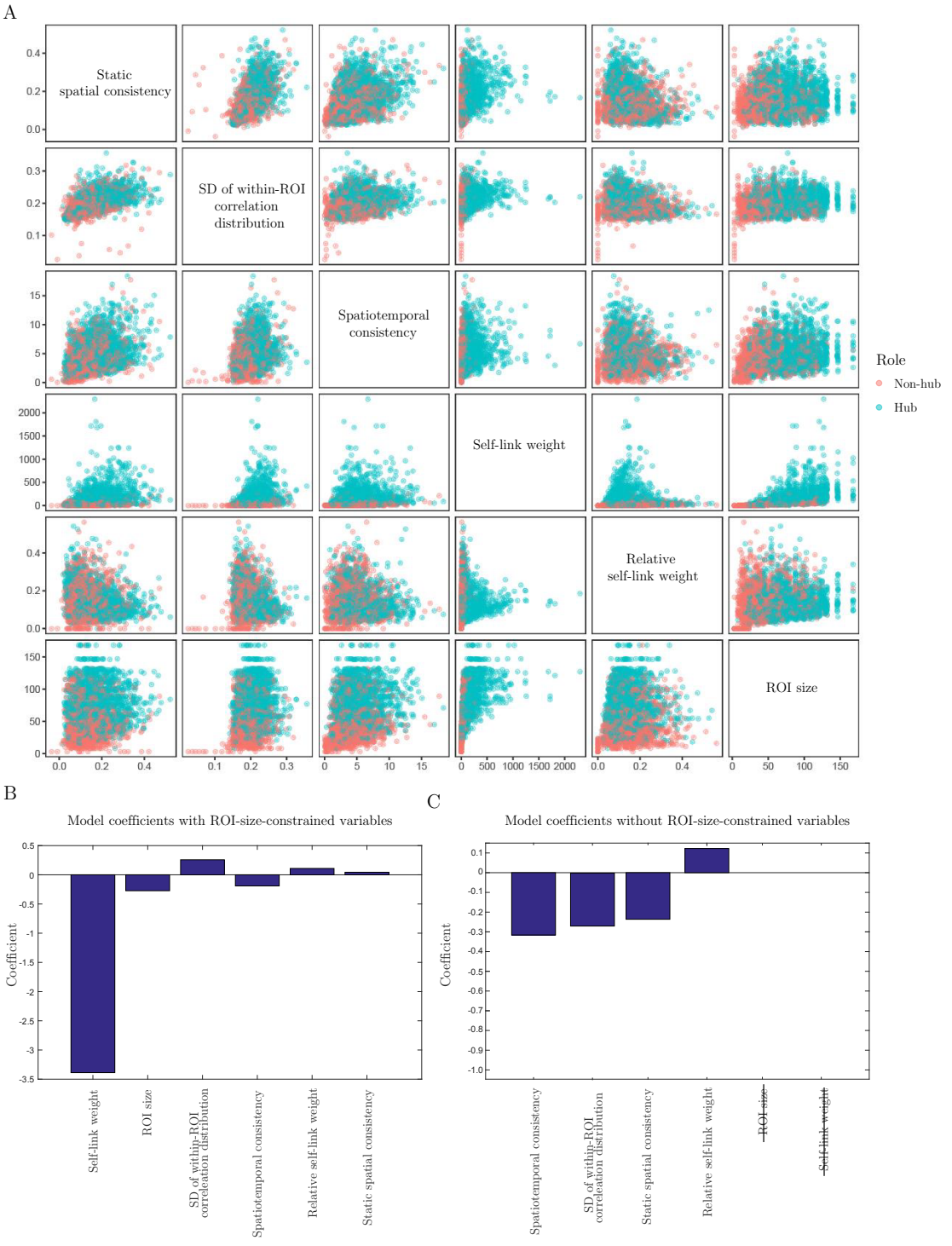

Figure B10: Prediction of the locally thresholded assignment to hub ROIs and non-hub ROIs in the Brainnetome atlas. A) Scatter-plot matrix showing the visual separation of hubs and non-hubs in the feature space set by the internal connectivity measures. B) Model coefficients of the logistic regression model with ROI-size-constrained variables included. C) Model coefficients of the logistic regression model without ROI-size-constrained variables included.

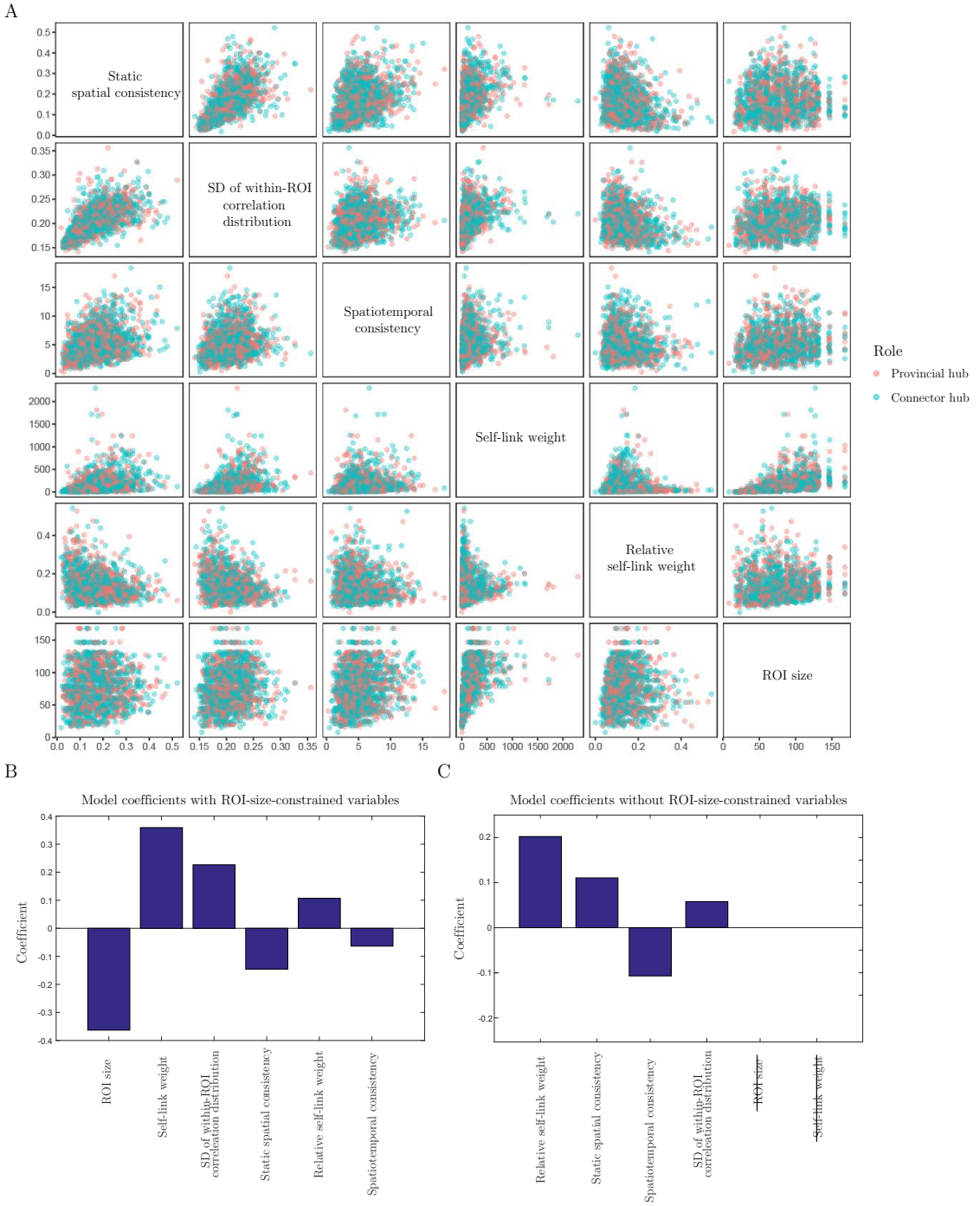

Figure B11: Prediction of the locally thresholded assignment to provincial hubs and connector hubs in the Brainnetome atlas. A) Scatter-plot matrix showing the visual separation of provincial hubs and connector hubs in the feature space set by the internal connectivity measures. B) Model coefficients of the logistic regression model with ROI-size-constrained variables included. C) Model coefficients of the logistic regression model without ROI-size-constrained variables included.

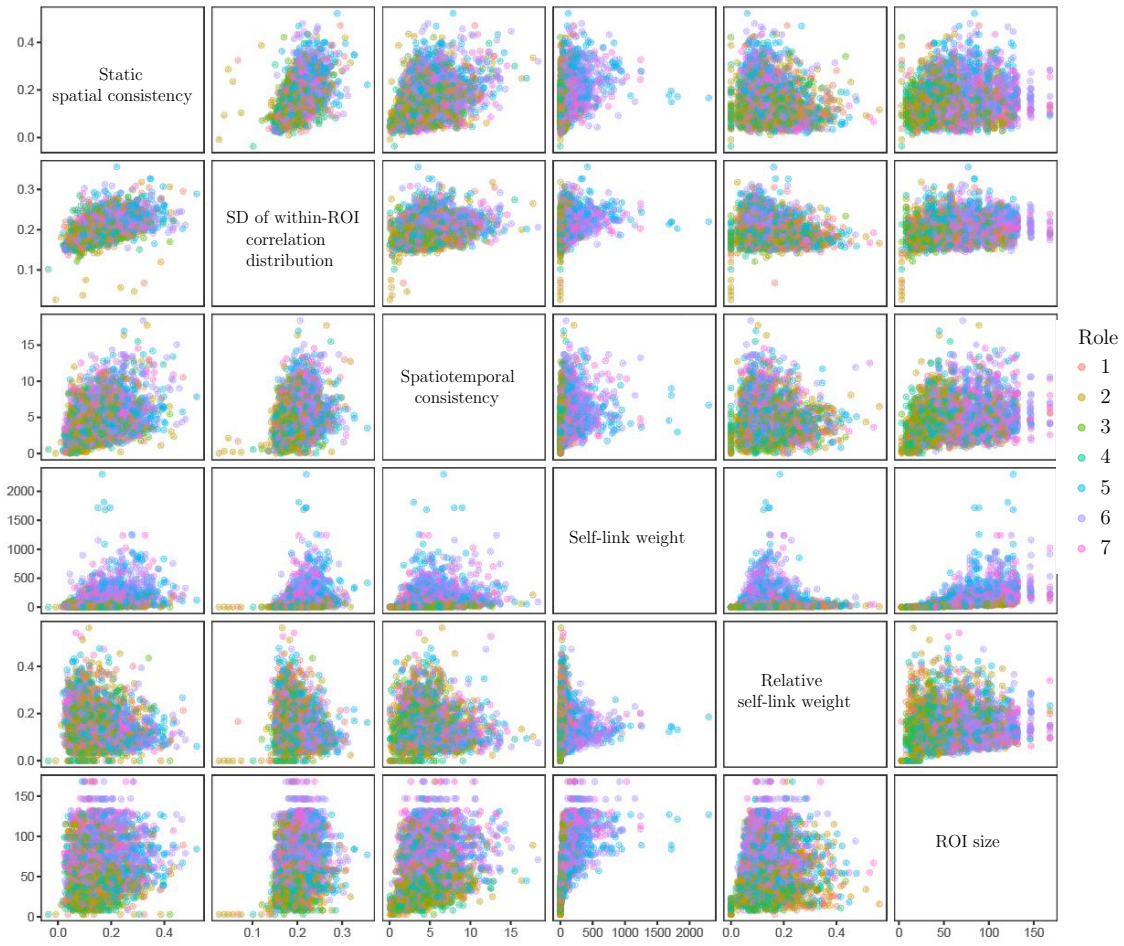

Figure B12: Prediction of the locally thresholded assignment to seven topological role classes in the Brainnetome atlas. Scatter-plot matrix showing the visual separation of the seven classes in the feature space set by the internal connectivity measures.

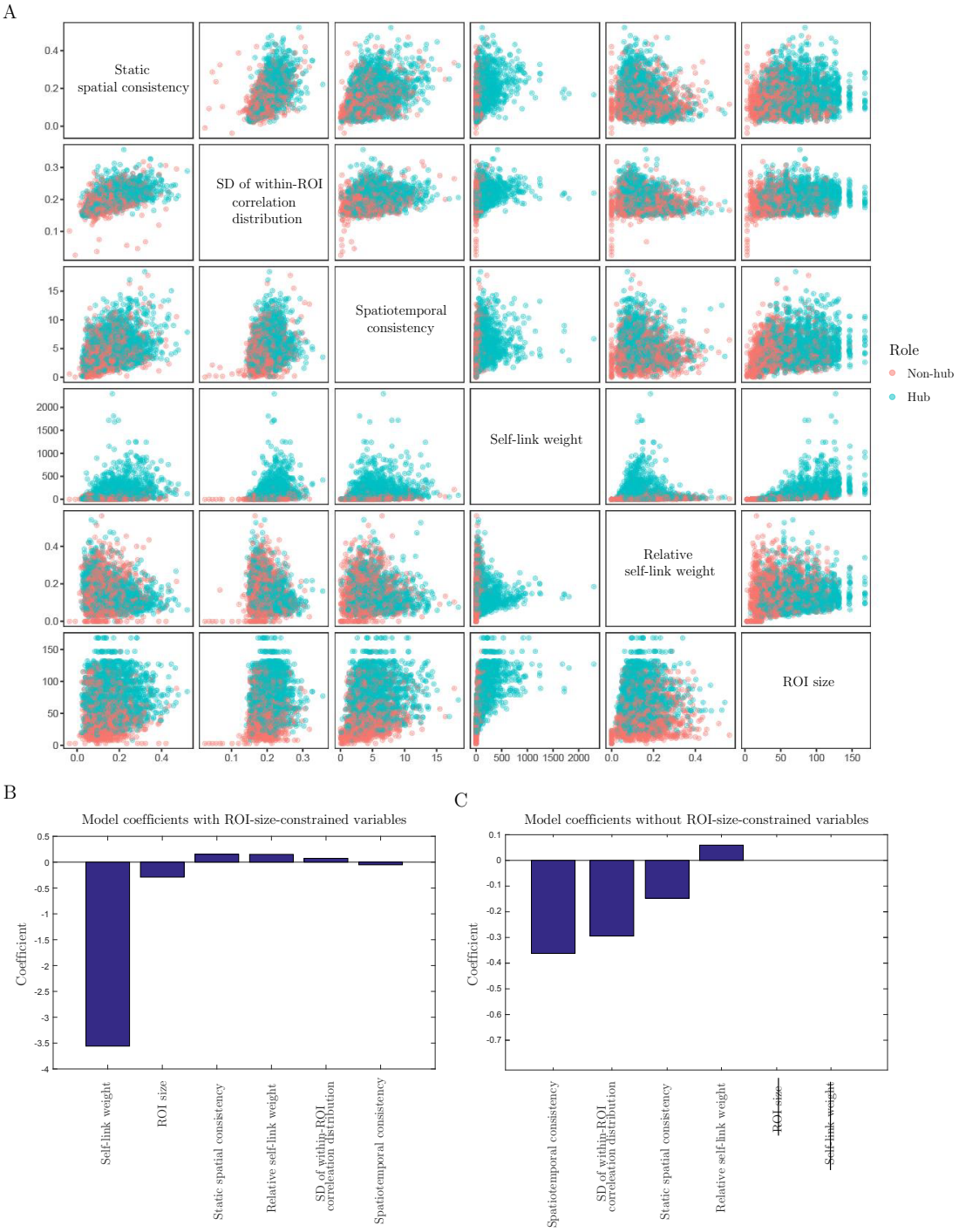

Figure B13: Prediction of the globally thresholded assignment to hub ROIs and non-hub ROIs in the Brainnetome atlas. A) Scatter-plot matrix showing the visual separation of hubs and non-hubs in the feature space set by the internal connectivity measures. B) Model coefficients of the logistic regression model with ROI-size-constrained variables included. C) Model coefficients of the logistic regression model without ROI-size-constrained variables included.

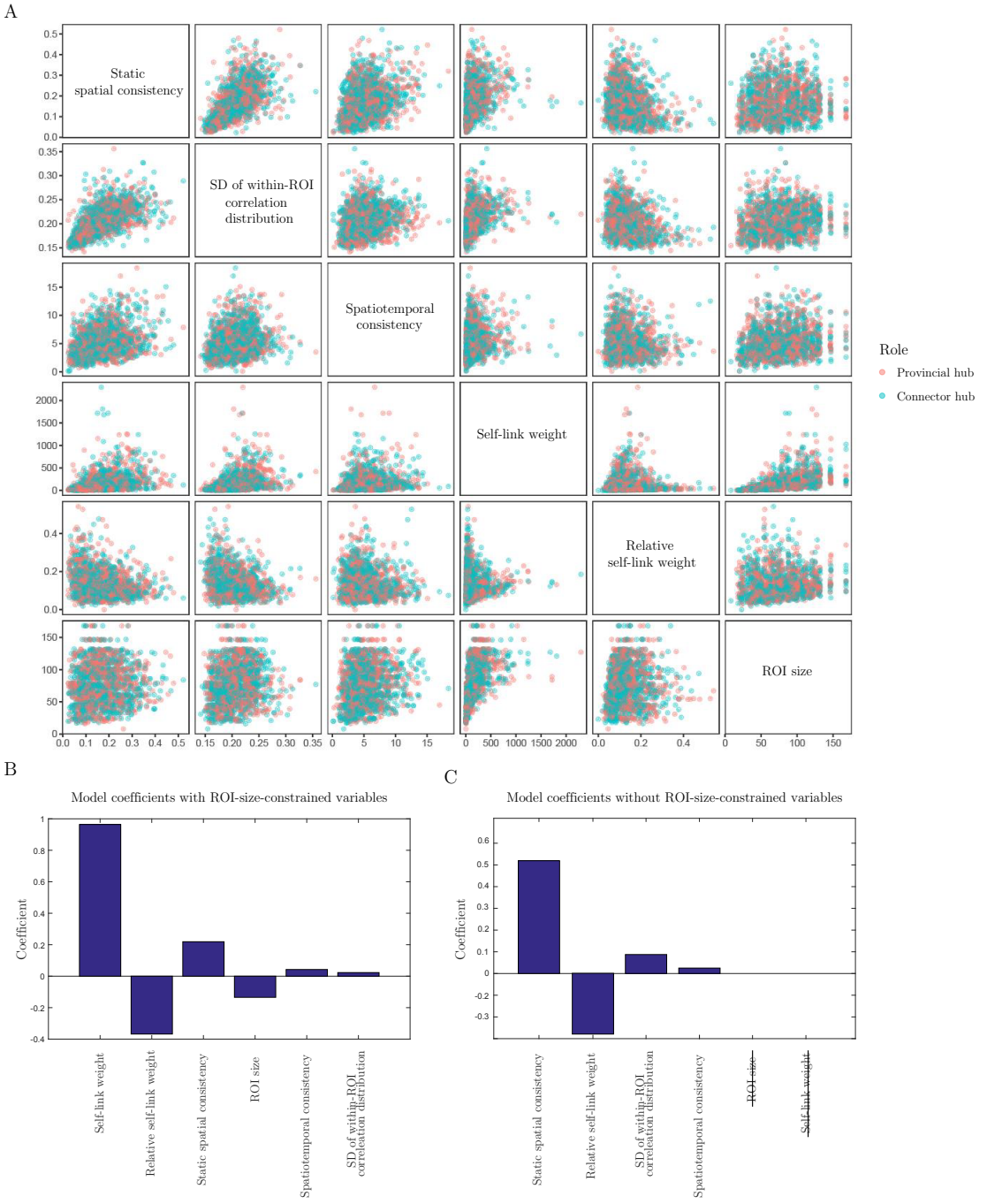

Figure B14: Prediction of the globally thresholded assignment to provincial hubs and connector hubs in the Brainnetome atlas. A) Scatter-plot matrix showing the visual separation of provincial hubs and connector hubs in the feature space set by the internal connectivity measures. B) Model coefficients of the logistic regression model with ROI-size-constrained variables included. C) Model coefficients of the logistic regression model without ROI-size-constrained variables included.

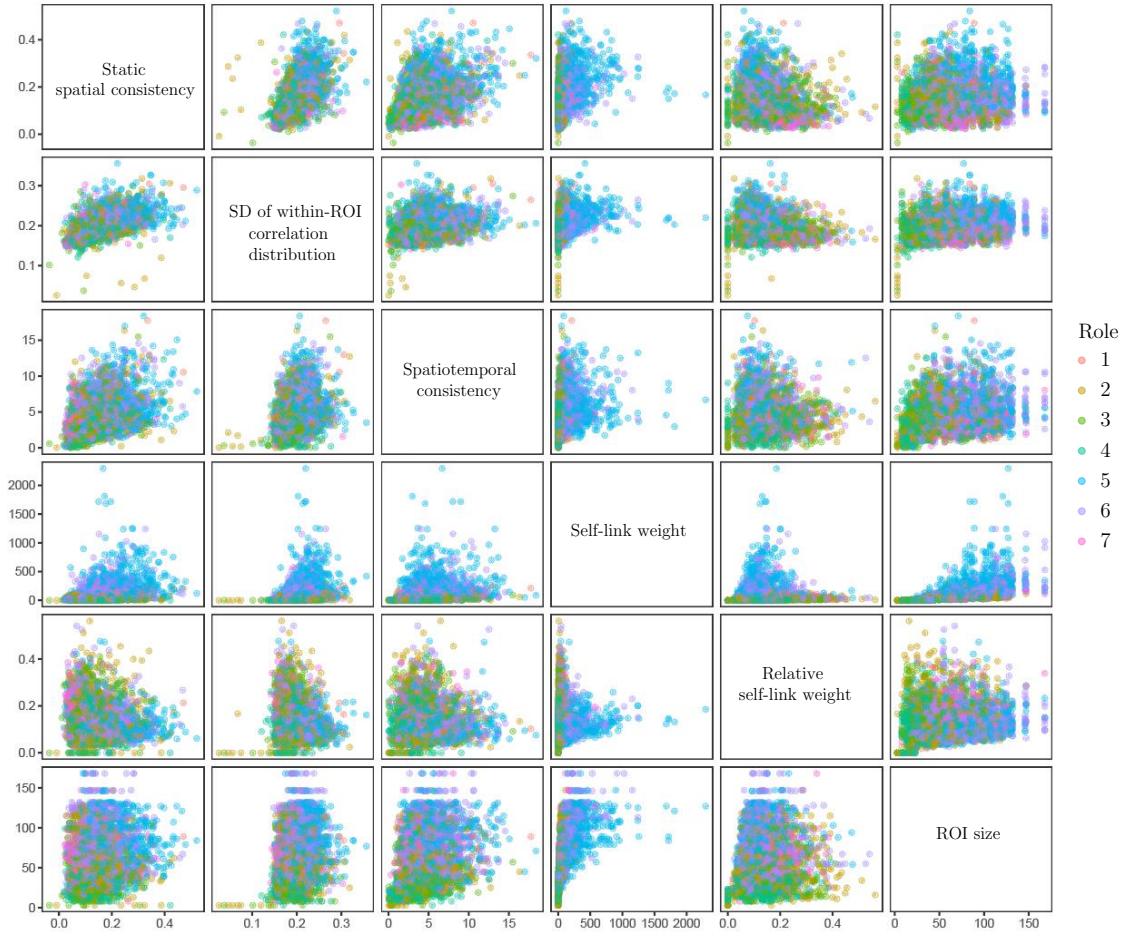

Figure B15: Prediction of the globally thresholded assignment to seven topological role classes in the Brainnetome atlas. Scatter-plot matrix showing the visual separation of the seven classes in the feature space set by the internal connectivity measures.